

Univerzita Karlova v Praze  
Matematicko-fyzikální fakulta

Disertační práce

2010

Mgr. Juraj Nožár



Univerzita Karlova v Praze  
Matematicko-fyzikální fakulta

# DISERTAČNÍ PRÁCE



Juraj NOŽÁR

## Transport náboje v molekulárních systémech a vliv příměsí

Katedra makromolekulární fyziky  
Ústav makromolekulární chemie, AV ČR, v.v.i.

Vedoucí disertační práce: Prof. RNDr. Stanislav NEŠPŮREK, DrSc.

Studijní program: Fyzika

Studijní obor: F4 Biofyzika, chemická a makromolekulární fyzika

Praha 2010





## Acknowledgements

My thanks and gratitude belongs to my supervisor, Prof. RNDr. Stanislav Nešpůrek, DrSc., for his helpful advices and guidance in my scientific work. During all my studies he encouraged me in developing my own thoughts.

Further thanks from me come to my colleagues and collaborators: Sergii Pochevailov, Ph.D. of IMC, AS CR, v.v.i., for his help with the measurements of the phtahlocyanines and sensors; Anna Kochalska of IMC, AS CR, v.v.i., for her cooperation and patience during degradation studies; Miroslav Menšík, Ph.D. of IMC, AS CR, v.v.i., for his helpful advices, discussions and help with theoretical problems; RNDr. Miroslav Pospíšil, Ph.D. and RNDr. Petr Kovář, Ph.D. of MFF UK for their assistance with molecular dynamics simulations; Mgr. Jakub Šebera, Ph.D. of IMC, AS CR, v.v.i., for his advices and supervision of my work.

The access to the MetaCentrum supercomputing facilities provided under the research intent MSM6383917201 is highly appreciated, since most of my simulations were run on their clusters.



Prohlašuji, že jsem tuto disertační práci vypracoval samostatně a výhradně s použitím citovaných pramenů, literatury a dalších odborných zdrojů.

Beru na vědomí, že se na moji práci vztahují práva a povinnosti vyplývající ze zákona č. 121/2000 Sb., autorského zákona v platném znění, zejména skutečnost, že Univerzita Karlova v Praze má právo na uzavření licenční smlouvy o užití této práce jako školního díla podle § 60 odst. 1 autorského zákona.

V Praze dne .....



**Název práce:** Transport náboje v molekulárních systémech a vliv příměsí

**Autor:** Juraj Nožár

**Katedra:** Katedra makromolekulární fyziky

**Vedoucí disertační práce:** Prof. RNDr. Stanislav NEŠPŮREK, DrSc.,  
Ústav makromolekulární chemie, AV ČR, v.v.i.

**Abstrakt** Táto práca sa zaoberá štyrmi základnými aspektami prenosu nosiča náboja: (1) hĺbka potenciálovej jamy vytvorenej okolo nosiča náboja, ktorý je lokalizovaný na polymérnom reťazci (tzv. polarónová väzbová energia). (2) Rozsah delokalizácie nosiča náboja a vplyv stérických efektov. (3) Pohyblivosť nosiča náboja na reťazci. (4) Vplyv prenosu nosiča náboja na stabilitu polymérneho reťazca. Ako modelový materiál boli použité polysilánové reťazce. Všetky vlastnosti boli študované prostredníctvom teoretických metód kvantovej chémie a molekulárnej dynamiky, ktoré umožnili sledovať mechanizmus prenosu na úrovni redistribúcie spinovej a elektrónovej hustoty, zmeny vibračných módov a dynamiky geometrie reťazcov. Porovnanie teoretických a experimentálnych výsledkov ukázalo veľmi dobrú zhodu vo všetkých oblastiach.

**Klíčová slova** Polarón, polarónová väzbová energia, pohyblivosť na reťazci, polysilány, kvantová chémia, molekulárna dynamika

**Title:** Charge carrier transport in molecular systems and influence of the additives

**Author:** Juraj Nožár

**Katedra:** Department of Macromolecular Physics

**Supervisor:** Prof. RNDr. Stanislav NEŠPŮREK, DrSc., Institute of Macromolecular Chemistry, AS CR, v.v.i.

**Abstract** This thesis concerns with 4 basic aspects of the charge carrier transport: (1) depth of the potential well formed around the charge carrier when localized on a polymer chain; i.e. so called polaron binding energy. (2) Extent of the charge carrier delocalization over the polymer chain and influence of steric effects on this value. (3) Intrachain mobility of the charge carrier. (4) Effect of charge carrier transfer on the chain stability. Polysilanes, which are well known for their semi-conducting properties, were chosen as model material for investigation. Outlined properties were studied by means of quantum chemistry and molecular dynamics, which allowed us to investigate the process of the charge carrier transfer in great detail. Theoretical results were then compared to the experiments with very good agreement.

**Keywords** Polaron, polaron binding energy, intrachain mobility, polysilanes, quantum chemistry, molecular dynamics.



# Contents

|          |  |           |
|----------|--|-----------|
| <b>1</b> | <b>Introduction</b>                                  | <b>13</b> |
| <b>2</b> | <b>Theoretical background</b>                        | <b>17</b> |
| 2.1      | Charge carriers in molecular systems . . . . .       | 17        |
| 2.1.1    | Electronic states of the molecular systems . . . . . | 18        |
| 2.1.2    | Conjugated polymers . . . . .                        | 20        |
| 2.1.3    | Charge carrier transport in molecules . . . . .      | 22        |
| 2.2      | Quasiparticles in molecular systems . . . . .        | 28        |
| 2.2.1    | Molecular crystals . . . . .                         | 30        |
| 2.2.2    | Polymers . . . . .                                   | 31        |
| 2.3      | Degradation of polymers . . . . .                    | 34        |
| 2.4      | Phthalocyanines . . . . .                            | 36        |
| 2.5      | Theoretical computing . . . . .                      | 37        |
| 2.5.1    | Quantum mechanics . . . . .                          | 37        |
|          | Basis sets . . . . .                                 | 38        |
|          | Methods . . . . .                                    | 39        |
|          | Basis set superposition error (BSSE) . . . . .       | 43        |
| 2.5.2    | Molecular mechanics and dynamics . . . . .           | 44        |
|          | Forcefield . . . . .                                 | 44        |
|          | Molecular mechanics . . . . .                        | 46        |
|          | Molecular dynamics . . . . .                         | 48        |
| <b>3</b> | <b>Thesis aims</b>                                   | <b>51</b> |
| <b>4</b> | <b>Computational methods</b>                         | <b>53</b> |
| 4.1      | Quantum mechanics . . . . .                          | 53        |
| 4.1.1    | Potential energy surface scan . . . . .              | 53        |
| 4.1.2    | Stabilization energies . . . . .                     | 55        |
| 4.1.3    | Deformation energy . . . . .                         | 56        |
| 4.1.4    | Electron-phonon term . . . . .                       | 57        |
| 4.1.5    | Polaron binding energy . . . . .                     | 58        |

|          |  |           |
|----------|--|-----------|
| 4.2      | Molecular mechanics and dynamics . . . . .               | 58        |
| 4.3      | Charge carrier mobility . . . . .                        | 59        |
| 4.3.1    | Electronic coupling . . . . .                            | 59        |
| 4.3.2    | Dynamic electron-phonon term . . . . .                   | 61        |
| 4.3.3    | Reorganization energy . . . . .                          | 62        |
| 4.3.4    | Effective distance between jumping sites . . . . .       | 63        |
| <b>5</b> | <b>Investigated molecules</b>                            | <b>65</b> |
| 5.1      | Sigma conjugated polymers . . . . .                      | 65        |
| 5.1.1    | PMPSi . . . . .  | 65        |
|          | Structure . . . . .                                      | 66        |
|          | Infrared spectra . . . . .                               | 68        |
|          | UV-VIS spectra . . . . .                                 | 70        |
|          | HOMO-LUMO Gaps . . . . .                                 | 71        |
|          | Distribution of states and orbitals . . . . .            | 72        |
| 5.1.2    | PBMSi . . . . .  | 75        |
|          | Structure . . . . .                                      | 75        |
|          | Infrared spectra . . . . .                               | 76        |
|          | Distribution of states and orbitals . . . . .            | 77        |
| 5.1.3    | Summary and Discussion . . . . .                         | 77        |
| 5.2      | Phthalocyanines . . . . .                                | 80        |
| 5.2.1    | Structures . . . . .                                     | 80        |
| 5.3      | Degradation additives . . . . .                          | 81        |
| 5.3.1    | Structures . . . . .                                     | 81        |
| <b>6</b> | <b>Results and Discussion</b>                            | <b>83</b> |
| 6.1      | Polarons in polysilylenes . . . . .                      | 84        |
| 6.1.1    | PMPSi . . . . .  | 84        |
| 6.1.2    | PBMSi . . . . .  | 90        |
| 6.1.3    | Summary and Discussion . . . . .                         | 92        |
| 6.2      | Polaron delocalization length . . . . .                  | 94        |
| 6.2.1    | Influence of conformational deformations on Si-backbone  | 95        |
| 6.2.2    | Localization-time evolution . . . . .                    | 97        |
|          | Short-term . . . . .                                     | 97        |
|          | Long-term . . . . .                                      | 102       |
| 6.2.3    | Summary and Discussion . . . . .                         | 102       |
| 6.3      | Charge carrier mobility in polysilylenes chain . . . . . | 104       |
| 6.3.1    | Hole mobility . . . . .                                  | 105       |
| 6.3.2    | Summary and discussion . . . . .                         | 107       |
| 6.4      | Polysilanes degradation . . . . .                        | 109       |
| 6.4.1    | Model 1 . . . . .  | 113       |



|  |            |
|--|------------|
| <i>CONTENTS</i>  | 11         |
| 6.4.2 Model 2 . . . . .                                  | 114        |
| 6.4.3 Experimental results . . . . .                     | 115        |
| 6.4.4 Chain length after degradation . . . . .           | 117        |
| Absorbance change . . . . .                              | 117        |
| Blue-shift . . . . .                                     | 118        |
| 6.4.5 Summary and Discussion . . . . .                   | 119        |
| 6.5 NO <sub>2</sub> sensors . . . . .                    | 120        |
| 6.5.1 Interaction with NO <sub>2</sub> . . . . .         | 121        |
| 6.5.2 Summary and Discussion . . . . .                   | 128        |
| <b>Summary and Outlook</b>                               | <b>129</b> |
| <b>References</b>  | <b>133</b> |
| <b>List of tables</b>                                    | <b>140</b> |
| <b>Nomenclature</b>                                      | <b>143</b> |
| <b>List of publications and conference contributions</b> | <b>145</b> |
| <b>7 Appendices</b>                                      | <b>149</b> |
| 7.1 Dynamic electron-phonon term . . . . .               | 149        |
| 7.2 Electron coupling input file . . . . .               | 152        |
| 7.3 Deformation energy input file . . . . .              | 157        |



# Chapter 1

## Introduction

Charge carrier transport in molecular systems is of extreme importance in the field of conductive and semiconductive polymers, fotovoltaics, photo- and electro-luminiscence, photochromism, photolithography and many others. However, even though the need for the precise knowledge of the transport mechanisms is great, the progress is not satisfactory by this time. The reason for this is that the transport of the charge carrier in molecular systems are of different nature, compared to the metal-like materials:

1. *Purity of the material* - Molecular materials can be very rarely considered pure in the sense of inorganic conductors and semiconductors. At most times, the sample will contain molecules of different lengths, residues of the synthesis process, crystalline structure is not present or is only short range, intramolecular geometries are deformed as a result of steric effects and thermodynamic laws.
2. *Conduction band* - Weak intermolecular interactions result in the narrow conduction band, which causes lower mobilities of the charge carriers in the system.
3. *Charge carriers* - In inorganic materials conductivity is usually provided by electrons. On the other hand in molecular systems the conductivity is influenced by electrons, holes or even ions. Different transport mechanism applies to each of these charge carrier types. From this point of view, molecular materials are more complicated.
4. *Transport model* - Conduction band structure and intermolecular packing result in different model of the charge carrier transport. While in the inorganic materials, coherent transport takes place, in the molecular systems also hopping model has to be taken into consideration. In fact, it is prevailing mechanism.

From the differences presented above, one can see that the conductive and semiconductive molecular materials require different scientific methods than their inorganic counter-parts. The studies of the electronic properties of the molecular materials can be distinguished into two main approaches: The *bulk properties* were only studied in the origins of the research in this area. Macroscopic sample is inspected in order to create large scale devices (photovoltaic panels, organic displays, photoluminescence diodes, etc.). Mostly, intermolecular processes are targeted by the research and material properties can be strongly affected by the sample preparation (crystallinity, orientation of the molecules, etc.). The second approach aims for the processes, which take place on a single molecule (polaron formation, excitation mechanism, relaxation of the system, transfer of the charge carrier between different conjugated groups of a single molecule, etc.) and results in a field of studies known as *Molecular electronics*. These properties can be modified by the change of the molecular structure (selection of the molecular system, side groups, steric effects, length of the polymer, etc.). Possibility to provide these studies first emerged in theoretical fields of the physics, via modeling engines, which solve the problems through *Quantum chemical calculations* or *Molecular mechanical* methods. However, experimental methods achieved amazing progress within last decade and now allow to measure properties on single molecule.

In order to fully describe processes in conductive molecular systems we need to combine both approaches, thus, the workflow of such an experiment can look like the following:

1. *Charge generation* - At the beginning of each charge carrier transport, charge generation process must take place. In molecular systems this can be achieved by photoexcitation, thermal excitation, injection and several others.
2. *Response of the molecule to the charge carrier occurrence* - Presence of the excess charge carrier on a site may significantly alter some of the properties of the resident molecule.
3. *Intramolecular transport* - Since molecules can be quite large, intramolecular transport between different conjugated groups of the system can play an important role.
4. *Intermolecular transport* - Transport between neighbouring sites (chains) is basic pre-requisite of bulk conductivity or semiconductivity.
5. *Bulk transport* - At this point, a transport model needs to be applied to the system. Since the molecular matter rarely forms pure crystal

structure, usually statistical methods have to be applied in order to achieve meaningful results. Different models can be needed for different temperatures (e.g. increase in temperature shifts charge carrier transport from coherent to the hopping model) and different sample preparation methods (preparation method can significantly alter long-range orientation of the molecules).

In this thesis, I have compiled the results of my work during my PhD. studies. Thesis first provides theoretical background of the field of study (Ch. 2) and then on the basis of the current problems we have formulated the research aims (Ch. 3). Molecules under study are summarized in Chapter 5 and methods used for the examination are described in the Chapter 4. I have been mostly interested in the problems of *Response of the molecule to the charge carrier presence* (Section 6.1 and 6.2), *Intramolecular transport* (Section 6.3) and *Intermolecular transport* (Section 6.4 and 6.5). Overall summary of the results is given in Chapter 6.5.2.



# Chapter 2

## Theoretical background

This chapter will provide brief introduction to contemporary state of physics in the field of charge carrier transport phenomenon in molecular systems. These are believed to be prospective materials for future nano-scaled electronic devices with lower manufacturing costs than silicon based devices.

### 2.1 Charge carriers in molecular systems

Molecular materials are no longer considered to be electrically insulating. There are various ways in which they can conduct electric current:

1. Conduction through dispersed conductive filler in *composites* - Molecular material serves as an insulating matrix, in which conductive particles are dispersed. Conductivity is non-linear function of the filler concentration and at point of *percolation threshold* it changes dramatically as filler particles form macroscopic pathway for the charge carriers.
2. Ionic conduction in *polymer electrolytes* - Charge carriers are ionic species (molecules or atoms) which can move through volume in the material. These are highly sensitive to pressure (as its increase “squeezes out” the free volume in the material and thus restricts the movement of the ionic particles) and humidity (which affects ion separation).
3. Intrinsic conduction in *conjugated polymers* - Charge carriers originate from molecules own electronic structure and charge transport is provided by electrons or holes.

In this thesis, I was concerned only with *intrinsic charge carriers* in conjugated systems. Charge carrier transport in such molecular systems is closely related to the electronic structure of the system. Thus, detailed review

of electronic levels in organic materials is provided in the part 2.1.1. In part 2.1.2 is given characterization of the conjugated molecules based on the knowledge of the electronic states. Last part (2.1.3) contains theoretical treatment for the carrier transport within single molecule.

### 2.1.1 Electronic states of the molecular systems

Structure of the electronic states in molecular semiconductors usually significantly differs from the states, that can be found in the inorganic semiconductors. Overlap between orbitals of neighboring molecules is very small due to greater distances (0.5 - 1.0 nm), thus, each molecule preserves most of its individuality. Therefore, electron diagram lacks wide valence and conduction band. Typical width of these bands varies between 0.01 and 0.04 eV.

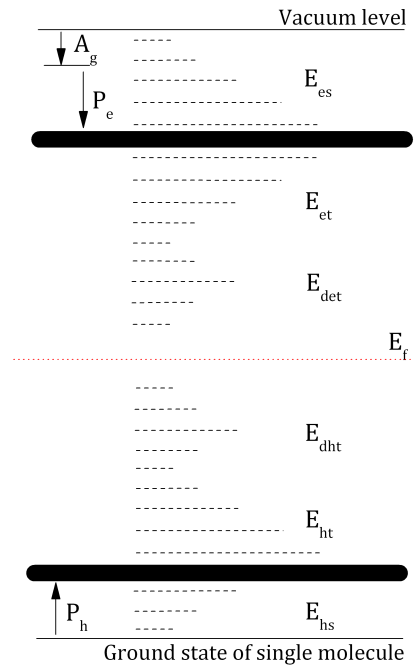


Figure 2.1: Electronic states in molecular material differ from those, that can be found in single molecule. Valence band ( $E_v$ ) is shifted by the value of the *hole polarization energy*  $P_h$  and conduction band ( $E_c$ ) is shifted by the energy of *electron polarization*  $P_e$ . Other symbols have following meaning:  $A_g$  is electron affinity of a single molecule,  $E_f$  is Fermi level,  $E_{et}$  and  $E_{det}$  are shallow and deep traps for electrons, respectively,  $E_{ht}$  and  $E_{dht}$  are shallow and deep traps for holes, respectively.  $E_{es}$  and  $E_{hs}$  are scattering centers for electrons and holes, respectively.



Fig. 2.1 shows schematic diagram of the electronic states of a molecular semiconductor. Note, that *valence band* and *conduction band* are shifted by the polarization energies of hole ( $P_h$ ) and electron ( $P_e$ ), respectively. This energy comes from the fact that excess charge carrier introduced into the material will cause redistribution of the electron density on the resident molecule and on the closest neighbors. Since this effect is mostly caused by Coulombic interaction, it can be calculated as ion (the excess charge carrier)-dipole (dipole induced by the excess charge carrier) interaction (first term in Eq. 2.1) and dipole-dipole interaction<sup>1</sup>:

$$P = - \sum_{i=1}^{N-1} \frac{\alpha e^2}{2r_i^4} + \sum_{i,k} \frac{\alpha^2 e^2}{r_i^3 r_k^3} [\vec{r}_i \vec{r}_k - 3r_{ik}^{-2} (\vec{r}_i \vec{r}_{ik}) (\vec{r}_k \vec{r}_{ik})], \quad (2.1)$$

where  $\vec{r}_{ik}$  is distance between interacting molecules  $i$  and  $k$ ,  $\alpha$  is polarizability and  $e$  is elementary charge. This equation is an approximation in the sense that it omits interactions of higher multipoles.

As written above, distances between the molecules in the molecular semiconductors are big compared to those in inorganic semiconductors. Also bonding energies are smaller. The result of this configuration is that the intermolecular distance varies and creates local areas of higher and lower density which act as shallow traps ( $E_{et}$  and  $E_{ht}$  in Fig. 2.1) and scattering centers ( $E_{es}$  and  $E_{hs}$  in Fig. 2.1). In general, these imperfections form quasi-continuum of states and can be treated by statistical methods. Since the distribution of these states is given as a result of number of random processes, it is convenient to anticipate gaussian distribution:

$$h_i(E) = \frac{(N_t)_i}{\sigma_i \sqrt{2\pi}} \exp \left\{ -\frac{[E - (E_t)_i]^2}{2\sigma_i^2} \right\}, \quad (2.2)$$

where  $i$  denotes holes or electrons,  $(N_t)_i$  is total concentration of local states and  $(E_t)_i$  is energetic depth of the maximum of the distribution,  $\sigma_i$  is half-width of the distribution. One can see from Eq. 2.2 that local states are symmetric around conduction band for electrons and around valence band for holes.

Deep traps are formed by impurities which has greater electron affinity or lower ionization potential than polymer matrix. Also, if the impurity is of significantly different size, it can create deep trap as the local density (and thus polarization energy) will be altered substantially.

Electronic state diagram shown in the Fig. 2.1 remains valid also in the case of long polymer chains. Movement of the charge carrier on such a

---

<sup>1</sup>Interaction of induced dipoles has opposite sign, since it partially compensates ion-dipole term; see second term in Eq. 2.1.

molecule can play significant role in overall mobility and charge conductivity in bulk sample. Since interatomic distances within the molecule are dictated by covalent bonds, they cannot vary significantly. Variance in local density and polarizability is in this case caused by the flexibility of such chain and geometry imperfections (valence bond rotations, bond angles, dihedral angles, etc.). Deep traps can be caused by cross-linking, unsaturated bonds, impurities, short chains, etc.

### 2.1.2 Conjugated polymers

As mentioned above, one of the mechanisms, which can explain charge carrier transport, is electron delocalization emerging from chemical nature of the system. Conduction band is created from orbitals neighbor atoms which can share electrons among each other. Even though this mechanism is somewhat similar to inorganic materials, substantial differences exist between one another. The most important comes from nature of bonding between sites, long range ordering, and dimensionality of the ordering.

Structure of the inorganic semiconductors is determined by strong covalent bonds between atoms in the crystal lattice. On the other hand, in the polymer materials, the intermolecular interactions originate from weak van der Waals and London type interactions. Therefore the intermolecular distances are greater and overlap of molecular orbitals is small. While inorganic crystalline semiconductors possess 3D long-range periodicity, polymers have only 1D periodicity (or periodicity in other dimensions is of different origin than covalent).

The mechanism of conduction is determined by long-range order (supramolecular structure in case of organic semiconductors), since the charge carriers are transported over distances usually much greater than single repeating unit. Conjugated polymers show various types of supramolecular ordering, e.g.  $\pi$ -stacking, polycrystalline structures with crystalline domains (polymer chains folded in lamellar order) separated by amorphous domains or orientation order by hydrogen bonds.

On the other hand, transfer within single molecule is governed by the conjugation of the electron system. Charge carrier can almost freely move along the conjugated parts. The first known conductive polymers were  $\pi$ -conjugated systems. Their delocalization originates from alternating single and multiple bonds (lone pairs, radicals or carbenium ions may be part of the delocalized system also). It was found that in the first approximation, activation energy of these molecules decreases with chain prolongation and

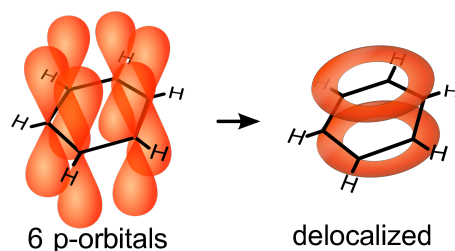


Figure 2.2: Schematic example of  $\pi$ -conjugated molecule. 6 separate p-orbitals in benzen overlap and form continual rings above and bellow the molecular plane.

follows formula:

$$E_A = \frac{19(N + 1)}{N^2}, \quad (2.3)$$

where  $E_A$  is activation energy and  $N$  is number of monomer units in the conjugated system.

$$E_T = k_B T, \quad (2.4)$$

According to this formula, activation energy was expected to decrease with increasing length of the conjugated system and at a certain length (approx. 1000 units) reach the value of thermal energy given by Eq. 2.4 (where  $k$  is Boltzmann constant and  $T$  is temperature in Kelvins). At this length, the charge carriers would be excited to the conductive band solely by the thermal excitation and polymer should expose metal-like conductivity. However, it was observed that this is not the case, because it is thermodynamically impossible to create ideal polymer chain of such length. In the real polymer chain several defects will always emerge:

1. Lengths of the single and multiple bonds are not the same. This alternating stabilizes the polymer but decreases electron delocalization.
2. Rotation of the chain around bonds lowers the conjugation.
3. Steric effects can disturb ideal periodicity of molecule (e.g. can interfere with co-planarity of the side-chains in poly-(fenylacetylene))

The measure of  $\pi$ -delocalization is given by ratio

$$\beta_{C-C} / \beta_{C=C}, \quad (2.5)$$

where  $\beta_{C=C}$  is the overlap integral between two p-orbitals located on the neighbor carbon-atoms, which are double bonded and  $\beta_{C-C}$  is the overlap integral between two p-orbitals located on the neighbor carbon-atoms which are single bonded. The higher the ratio is, the better delocalization.

Very strong dependence exist between local deformations of the molecule and conductivity. (Venkataraman *et al.*, 2006) measured dependence of the conductivity on the twist angle between phenyls in a biphenyl structure. They found that conductance decreases with the increasing twist angle and follows cosine-square relation predicted for transport through  $\pi$ -conjugated biphenyl systems (Woitellier *et al.*, 1989).

Later, it was found that conjugation and electron delocalization exists also in purely  $\sigma$ -bonded systems, i.e.  $\sigma$ -conjugation. For example, in methane, the bonding electrons are shared by all five atoms equally. Pervasive existence of delocalization is implicit in molecular orbital theory. Stronger  $\sigma$ -conjugation however exists in the molecules, which backbone is constituted of silicon atoms (i.e. polysilylenes). This comes from the fact, that  $\sigma$ -orbitals of the silicon atoms are larger and greater overlap between them is possible. The measure of  $\sigma$ -delocalization is given by ratio

$$\beta_{vic}/\beta_{gem}, \quad (2.6)$$

where  $\beta_{vic}$  is the electron overlap between two hybridized  $sp^3$  orbitals located on the neighbor atoms and  $\beta_{gem}$  is the overlap integral between two  $sp^3$  orbitals located on the same atom. The higher the ratio is, the better delocalization.

### 2.1.3 Charge carrier transport in molecules

Intra-chain charge carrier transport in polymers is complicated phenomenon, which can be treated by the tight-binding approximation. In this model a chain is represented by a sequence of  $N$  sites, which corresponds to the repeating units. Tight-binding approximation then takes into consideration only transfer of the charge carrier between neighboring sites. Hamiltonian for such model is shown in Eq. 2.7:

$$H = \sum_{n=1}^N [\epsilon_n a_n^\dagger a_n - b_{n,n+1} (a_{n+1}^\dagger a_n + a_n^\dagger a_{n+1})] \quad (2.7)$$

where  $a_n$  and  $a_n^\dagger$  are annihilation and creation operators of a charge carrier at  $n^{th}$  site,  $\epsilon_n$  is the energy of a charge carrier localized at this site and  $b_{n,n+1}$  is transfer integral between the sites  $n$  and  $n+1$ . Both quantities  $\epsilon_n$  and

$b_{n,n+1}$  are influenced by the random structure of the polymer chain and its surrounding.

Using the Hamiltonian 2.7 and wave function

$$|\psi(t)\rangle = \sum_{n=1}^N c_n(t) |n\rangle \quad (2.8)$$

where  $|n\rangle$  is a state located at  $n^{\text{th}}$  site; the time-dependant Schrödinger equation can be written in the form

$$H |\psi(t)\rangle = i\hbar \frac{\partial}{\partial t} |\psi(t)\rangle \quad (2.9)$$

This equation can be solved either by means of the direct numerical integration (Toman *et al.*, 2006) or using stationary states  $|\psi_n\rangle$ , which are solutions of the time-independent Schrödinger equation

$$H |\psi_n\rangle = E_n |\psi_n\rangle \quad (2.10)$$

The solution of the Eq. 2.9 is then given by the relation

$$H |\psi(t)\rangle = \sum_{n=1}^N k_n e^{\frac{-iE_n t}{\hbar}} |\psi_n\rangle \quad (2.11)$$

in which the time-independent coefficients  $k_n$  can be found from the initial conditions  $c_0 t = 0 = 1$  and  $c_i(t = 0) = 0$  for any  $i \neq 0$ .

As mentioned before, the quantities  $\epsilon_n$  and  $b_{n,n+1}$  are strongly influenced by the surroundings and random deformations on the molecular chain. Influence of this dispersion was extensively studied in (Toman *et al.*, 2006) and (Toman *et al.*, 2009), where the distribution was controlled by addition of polar molecules. These were randomly oriented in the vicinity of the polymer chain and thus causing broadening of the distribution of states. It was shown that increase of the distribution hinders intra- and inter-chain mobility.

At high temperature (including room temperature), the charge carriers in polymers are localized at individual molecules and the hopping transport mechanism is prevailing. It can be described by Marcus theory (Marcus, 1993). The rate of a self-exchange process is given as

$$k_{et} = \frac{4\pi^2}{\hbar} \frac{1}{\sqrt{4\pi\lambda k_B T}} t^2 \exp\left(-\frac{(\lambda + \Delta G^0)^2}{4k_B T}\right), \quad (2.12)$$

where  $h$  is Planck constant,  $k_B$  is Boltzmann constant,  $T$  is thermodynamic temperature,  $\Delta G^0$  is the free energy difference between the initial and final

site,  $\lambda$  is reorganization energy (see Eq. 2.13) and  $t$  is electronic coupling (see Eq. 2.16).

Reorganization energy in Eq. 2.12 represents energy, which is needed for relaxation, when charge carrier jumps from a molecule A to a molecule B (see Fig. 2.3). Charge carrier localized on the site A affects its equilibrium geometry and vibration modes (see section 2.2) while site B is in its neutral state. After the carrier jump the roles of sites will exchange and each site will relax to the opposite state. Thus reorganization energy can be written as sum of two terms

$$\lambda = \lambda_A + \lambda_B, \quad (2.13)$$

where  $\lambda_A$  is energy needed for the relaxation of the site A from charged to neutral state and  $\lambda_B$  is energy needed for relaxation of the site B from neutral to charged state. In the simplest approximation these two terms can be expressed as follows:

$$\lambda_A = E_n^{(A)}(q_+) - E_n^{(A)}(q_n) \quad (2.14)$$

$$\lambda_B = E_+^{(B)}(q_n) - E_+^{(B)}(q_+) \quad (2.15)$$

where  $E_n^{(A)}(q_+)$  is the total electronic energy of the site A in the neutral state and in the charged geometry,  $E_n^{(A)}(q_n)$  is electronic the total energy of the site A in the neutral state and in the neutral geometry,  $E_+^{(B)}(q_+)$  is the total electronic energy of the site B in the charged state and in the charged geometry and  $E_+^{(B)}(q_n)$  is the total electronic energy of the site B in the charged state and in the neutral geometry (see Fig. 2.3). Note, that both  $\lambda_A$  and  $\lambda_B$  are always positive values since they are given as difference of energy of non-relaxed state and relaxed state. Computational details will be given in section 4.3.

The electronic coupling  $t$  from Eq. 2.12 represents the ease of the charge carrier jump between sites A and B and can be expressed by formula

$$t = \frac{H_{AB} - S_{AB}(H_{AA} + H_{BB})/2}{1 - S_{AB}^2}, \quad (2.16)$$

where  $H_{AB}$  is the charge-transfer integral,  $S_{AB}$  the spatial overlap, and  $H_{AA}$  and  $H_{BB}$  the site energies.

With  $\lambda$  and  $t$ , one can calculate  $k_{et}$  according to Eq. 2.12. According to the Einstein-Smoluchowski equation (Eq. 2.17, (Atkins, 1994)) diffusion coefficient  $D$  of the charge carrier can be calculated, where  $L$  is the effective

distance between the jumping sites. Its actual value depends on the examined model; e.g.

1. *Center-to-center distance of monomer units* - when investigating intramolecular movement of the charge carrier on a polymer chain with none polaron formation (or polaron localized on single monomer) (Toman *et al.*, 2006)
2. *Center-to-center distance of molecules in the molecular crystal* - model of jumps between adjacent molecules, when polaron is localized on single molecule (approximation of small polaron) (Weng *et al.*, 2009)
3. *Average chain distance* - investigation of 3D mobility in bulk polymer material (inter-molecular mobility) (Toman *et al.*, 2009)
4. *Center-to-center polaron distance* - model in which polaron does not spread over the whole polymer chain and thus adjacent parts of the same polymer chain represent jumping sites (see sections 6.2 and 6.3).

Knowledge of the diffusion coefficient  $D$  allows us to calculate the drift mobility of the charge carrier from Einstein relation (Atkins, 1994), according to Eq. 2.18, where  $e$  is the elementary charge.

$$D = \frac{L^2 k_{et}}{2} \quad (2.17)$$

$$\mu = \frac{eD}{k_B T} \quad (2.18)$$

Eq. 2.17 is valid for 3-dimensional system. Transition from 3D to 1D can be done by multiplicative factor 1/3: we will derive this conclusion in case of isotropic environment where motions along different axes are not correlated. In this case, mean-square of the total traveled distance  $(\Delta l)^2$  is given by expression

$$(\Delta l)_{3D}^2 = (\Delta x)^2 + (\Delta y)^2 + (\Delta z)^2, \quad (2.19)$$

where  $(\Delta i)^2$  are mean-square traveled distances in direction of axes  $x$ ,  $y$  and  $z$ . In isotropic environment, the mean-square traveled distances will be approx. equal to each other:

$$(\Delta x)^2 \approx (\Delta y)^2 \approx (\Delta z)^2, \quad (2.20)$$

thus, if two dimensions are inaccessible (e.g.,  $y$  and  $z$ ), overall mean-square traveled distance will be:

$$(\Delta l)_{1D}^2 = \frac{(\Delta l)_{3D}^2}{3} = (\Delta x)^2 \quad (2.21)$$

Note, that this term does not take scattering centers into consideration, since they behave as barriers in the 1D wire (thus model can be used only for small charge carrier concentration, where influence of barriers created by localized charge carriers can be neglected).

When time-dependence of mean-square traveled distance is known, then frequency dependant mobility can be evaluated from Kubo formula (Kubo, 1957) which was simplified into the form (Scher & Lax, 1973)

$$\mu(\omega \rightarrow 0) = \frac{-e\omega^2}{2k_B T} \text{Re} \left[ \int_0^\infty (\Delta l)^2(t) \exp(-i\omega t) dt \right] \quad (2.22)$$

where  $t$  is time and  $\omega = 2\pi f$  is frequency of an external field. For the diffusive motion, which is expected in the long time limit due to the destructive interference even in the non-dissipative model, we get  $(\Delta l)^2(t) \propto t$ . In this case the Kubo formula can be rewritten to the form of the Einstein relation (see Eq. 2.18):

$$\mu(\omega \rightarrow 0) = \frac{e}{2k_B T} \frac{(\Delta l)^2(t)}{t} \quad (2.23)$$



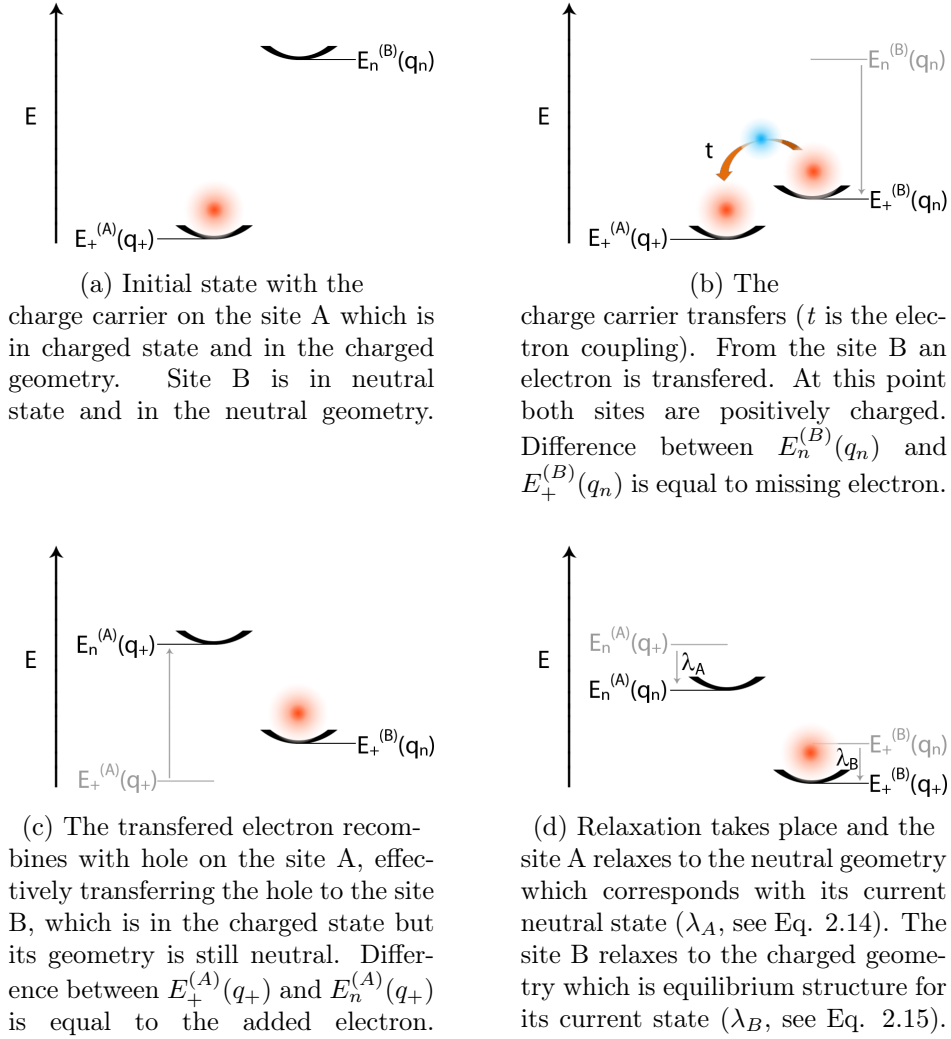


Figure 2.3: When charge carrier transfers from A to B, both sites undergo changes. These transformations require energy, which subsequently affects the rate of self-exchange (see Eq. 2.12). The example shown in this figure schematically shows the energy changes when a hole is transferred.

## 2.2 Quasiparticles in molecular systems

Presence of a charge carrier in the molecular system is usually accompanied by creation of a quasiparticle - it can be roughly defined as combination of a particle and its influence on the local environment. There are many quasiparticles that can emerge in polymers and molecular crystals:

1. *Electron hole* - Empty electronic state left by removed electron.
2. *Phonon* - Quantization of the modes of lattice vibrations.
3. *Exciton* - Molecular excited state; molecular geometry has adapted to excess of energy received in excitation process and to the new electron configuration.
4. *Excimer* - Excited dimer. Excitation energy is shared among two neighbor molecules of the same nature.
5. *Exciplex* - Excited dimer complex. Excitation energy is shared among two neighbor molecules of a different nature (e.g. electron donor and acceptor).
6. *Polaron* - Charge carrier clothed in a cloud of geometry (both intra- and inter-molecular) deformations and electronic polarization effects.

In this thesis, I have been solely concerned with the problems of the *polaron* formation in molecular materials, which is substantial for the process of the charge mobility: Polaron-like particles in organic molecular crystals were extensively studied by (Silinsh & Capek, 1994). Fig. 2.4 schematically shows hierarchy of interaction time scales for different processes which take place in the presence of an excess charge carrier:

1. *Electronic polaron* - The fastest process, which causes reorganization of the electron clouds in the molecules conjugated parts. Its relaxation time corresponds with the speed of the electron processes (e.g. excitation of an electron is of range  $10^{-16} - 10^{-15}$  seconds) and its energy is of level 1.0 – 1.5 eV.
2. *Molecular polaron* - Corresponds with the relaxation of vibration modes on the resident molecule. Normal vibronic modes will alter its vibration frequencies and equilibrium positions in response to the presence of the excess charge. Relaxation time correlates with the vibration frequencies of different parts of the molecule (e.g. period of stretching vibration of the C-H bond is about  $10^{-14}$  seconds which is the fastest vibration motion).

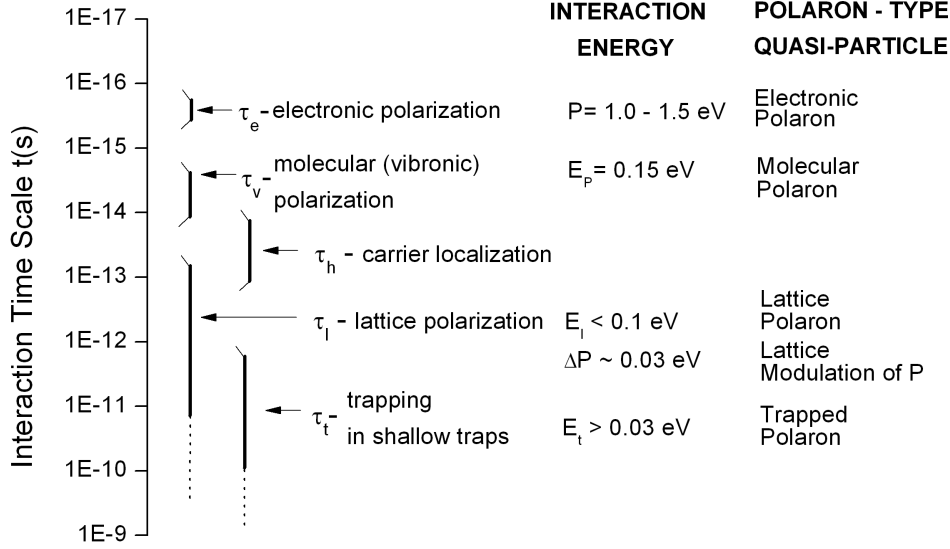


Figure 2.4: Presence of an unbalanced charge carrier will cause several processes to take place, thus different kinds of polarons can be formed. These will establish new equilibrium in the system. Reproduced from (Silinsh & Capek, 1994)

3. *Lattice polaron* - Charge carrier does not only affect the resident molecule but through the coulombic interaction it alters intermolecular distances (lattice dimensions in the case of crystalline material). Relaxation times correspond with the lattice phonons. The *lattice modulation*  $\Delta P$ , which reflects the local density variations and distortions of the lattice, will always exist in the real samples.
4. *Trapped polaron* - Polaron quasiparticle can be trapped in the shallow traps formed by impurities or *lattice modulations*.

Approximate interaction energies can be estimated from uncertainty relation

$$\tau_{int} = \hbar / \Delta E_{int}, \quad (2.24)$$

where  $\tau_{int}$  is the interaction time,  $\hbar$  is the reduced Planck constant and  $\Delta E_{int}$  is the interaction energy.

Processes shown in Fig. 2.4 have their corresponding energies and relaxation times. Thus generally: longer the charge carrier is localized on the site the deeper well around it is created (therefore, quasiparticles are rarely formed in inorganic semiconductors, since the localization time of the charge

carriers in such materials is very short). On the other hand: deeper the potential well is, the longer the quasiparticle is trapped in it. Thus, we can see that polaron is *auto-consistent state*. The depth of the formed trap is one of the most important features of the polarons and it significantly affects the mobility via following relation:

$$\mu(T, \vec{E} \rightarrow 0) = \mu_0 \exp \left[ -\frac{E_p}{2k_B T} - \frac{4}{9} \frac{\sigma^2}{(k_B T)^2} \right], \quad (2.25)$$

where  $\vec{E}$  is electric field,  $T$  is thermodynamic temperature,  $\sigma$  is dispersion of states,  $\mu_0$  is mobility at zero temperature and  $E_p$  is the depth of formed trap, which is throughout the literature and in this thesis called *polaron energy*.

In general, all types of polaron can be present in the molecular material. However, two distinct situations occur based on the prevailing long-range orientation of molecules: *crystalline* (or polycrystalline) and *amorphous* structure. Both materials differ by the magnitude of relaxation processes which take place. In real samples both states are usually mixed, but for the sake of simplicity I will discuss them separately.

### 2.2.1 Molecular crystals

Polaron formation has been first studied in the molecular crystals, where the problem is simplified by existing symmetry. Silinsh et al. (Silinsh & Capek, 1994; Silinsh, 1980) has introduced and developed the model of *nearly small molecular* (vibronic) *polaron* (MP), formed by the interactions of an excess charge carrier localized on a molecule with the IR-active vibrations of the resident molecule and the nearest-neighbor molecules. The presence of the excess charge results in a position changing of equilibrium configurations of the nuclei (schematic illustration in Fig. 2.7). The formation energy of the MP in anthracene and tetracene is about 0.15 eV; 60 % of the value comes from the formation of ionic state of the charged molecule and the rest results from interactions with surrounding molecules. The polarization of lattice vibrations is not included.

Fig. 2.5 shows the changes, which take place in a molecular crystal under the influence of an excess charge carrier (in this case excess electron denoted as  $e^-$ ). Once the electron is placed within the lattice, the quick electronic relaxation shifts the electron clouds localized on the neighbor molecules. Due to the Coulombic interaction delocalized  $\pi$  electrons tend to shift away from excess negative charge. Afterwards vibronic relaxation occurs. Since the oriented molecular crystal is stiff, the change of the intermolecular distances is rather negligible (this is denoted in the Fig. 2.5 by the unchanged lattice

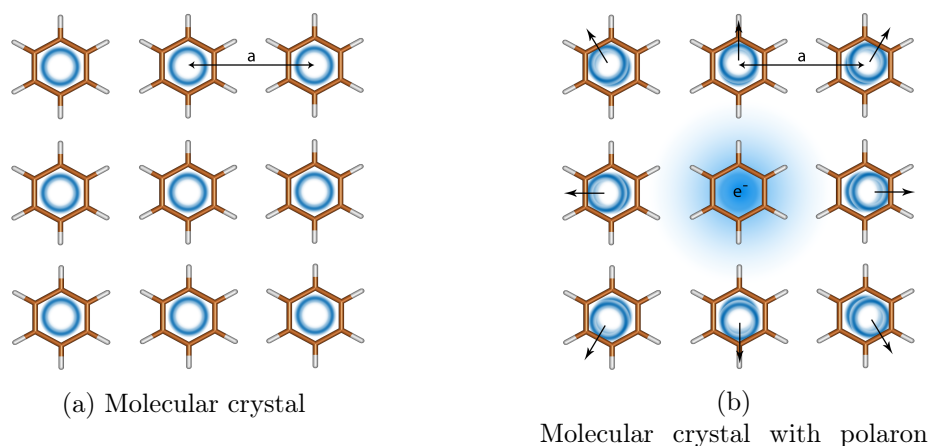


Figure 2.5: Polaron formed in the molecular crystal. In figure (a) is illustrative molecular crystal composed of benzenes with lattice constant  $a$ . Figure (b) shows the response of the system to the presence of excess electron  $e^-$ .

constant  $a$ ).

### 2.2.2 Polymers

Processes of the polaron creation in polymer material significantly differ from those which take place in the molecular crystal. Complexity of this issue has caused that our understanding of its formation (mostly its quantitative aspects) falls behind the knowledge about the situation in the periodic conditions of crystalline material. Macromolecules, differ from molecular crystals in the following main aspects:

1. *Flexibility* - Long polymer chains are more flexible, thus their geometry can significantly alter upon interaction with the excess charge carrier.
2. *Non-periodicity* - Absence of the long range periodic orientation results in requirement of usage of sophisticated statistical methods when treated theoretically.

Following from the differences (mostly flexibility of the polymer chain), one can assume that deformation of the skeleton will take place in relaxation processes. Indeed, this is the case in polymer molecule. Upon localization of the excess charge on the molecule, fast electron relaxation takes place. However, afterwards the long-range geometry itself is altered what will lead to a new electron distribution, shifted vibronic frequencies and equilibrium positions. Fig. 2.7 schematically depicts the relaxation process that take

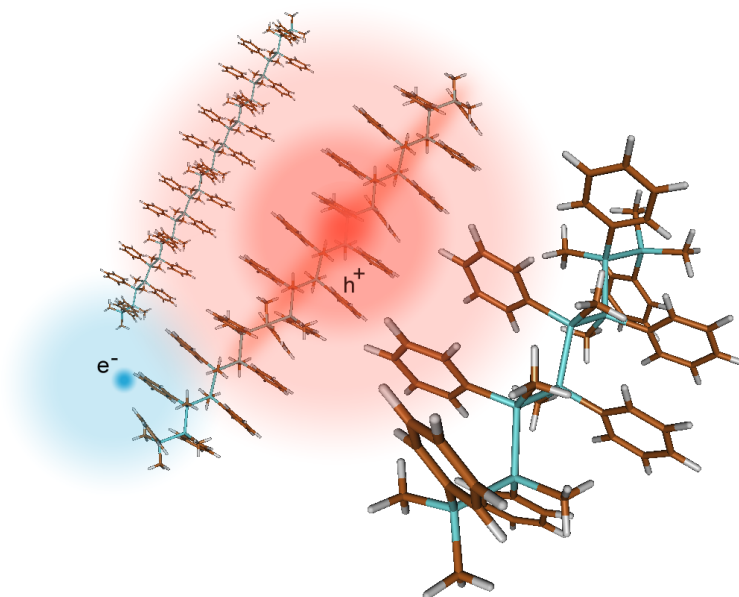


Figure 2.6: Presence of the delocalized hole on the polymer chain will affect geometry of the resident molecule and its closest neighbors. In the figure  $h^+$  denotes hole and  $e^-$  electron

place in the presence of an excess charge carrier and leads to the formation of a polaron (note, that this process is also valid for the molecular crystals, however one should understand, that long-range geometry does not change significantly in the periodic lattice). Following stages can be identified in the process:

1. *Ground neutral state*  $M_0$  - When none excess charge carrier is present on the molecule or it is not in the vicinity, then molecule is in its ground state. Equilibrium position of a vibronic motion is  $q_0$  and vibration frequency is  $\omega_0$ .
2. *Hot state*  $(M_0h)^+$  - Transfer of excess charge is fast process (at the time scale of electron processes, see section 2.2, Fig. 2.4). Thus, at the moment of the charge carrier transfer onto a molecule, its geometry remains same as in the *Ground neutral state* with unperturbed equilibrium position ( $q_0$ ) and vibration frequency ( $\omega_0$ ).
3. *Relaxation process* - Presence of the excess charge alters electron distribution, equilibrium positions ( $q_0 \rightarrow q_p$ ) and vibronic frequencies ( $\omega_0 \rightarrow \omega_p$ ). Magnitude of these processes depends on the localization time of the charge carrier.

4. *Relaxed positive state  $M^+$*  - If the localization time of the charge carrier is sufficiently long, then the molecule relaxes to a new equilibrium positions ( $q_p$ ) and vibronic frequencies ( $\omega_p$ ).

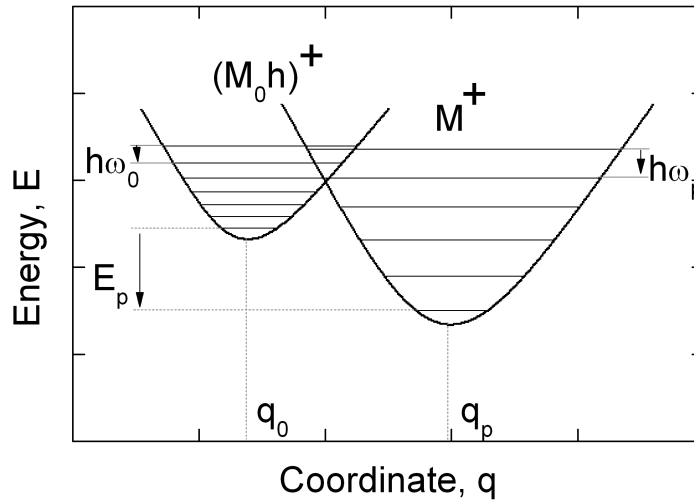


Figure 2.7: Schematic vibronic relaxation which takes place upon localization of an excess charge (in this case positive, represented by an electron hole  $h^+$ ) at a molecule

Fig. 2.7 also indicates the energy of the trap created by this process,  $E_p$ . Note, that it is a combination of the deformation (as a result of the  $q_0 \rightarrow q_p$  shift), electron redistribution (not shown in Fig. 2.7) and vibronic relaxation ( $\omega_0 \rightarrow \omega_p$  shift).

Several experimental methods were used to measure the polaron energy. Nespurek et. al. developed a method for the determination of the polaron binding energy from the temperature and voltage dependencies of charge carrier mobility. The principle of the method can be found in (Nespurek *et al.*, 2001). The obtained value of the polaron binding energy for PMPSi was  $E_p = 0.2$  eV. Also it was estimated as  $E_p = 0.16$  eV (Bässler *et al.*, 1994) by the linear extrapolation of the temperature dependence of the activation energy of the charge carrier mobility to zero temperature. However, the dependence is not generally linear and, therefore, the  $E_p$  value is rough estimation only. Reasoning can be also based on the value of  $E_p = 0.08$  eV by Pan et al (Lujun *et al.*, 1999) presented for excitons. Regarding to the fact that in the molecular crystals, the defects of the same feature form about 3 times deeper traps for charge carriers than for singlet excitons (Silinsh, 1980), one can write for the charge-polaron binding energy  $E_p = 0.24$  eV.

## 2.3 Degradation of polymers

Poly(organylsilanes) have many interesting properties. One of them is their non-stability under UV illumination. While, it can be limiting in some areas of use, it can also be promising in another (e.g. photolithography (Hayase, 2003)). Polysilanes, when exposed to UV light, decompose to species having disparate properties in comparison with those of non-degraded material. Even though there are many materials available for the photolithographic process, polysilylenes stand out in large scale integrated circuit manufacturing: silicon atoms included in the polymer chain are not recognized as impurities in silicon devices. Thus, while other metal atoms can cause contamination problems, silicon atoms bound to silicon wafer firmly. Therefore, there are not empty spaces in-between the photoactive layer and substrate which could result in short or cold junctions.

UV illumination of polysilylenes results in several processes and numbers of different species are formed. One can mention photobleaching, photocrosslinking, bond scission, formation of metastable states like dangling bonds, conformational transformations, weak bonds, etc. Naito (Naito, 2002) found two types of dangling bonds and described their annealing behavior of wells potential configuration diagram. Similar were observations of (Sharma *et al.*, 2007), based on the results of degradation in varying media. It resulted in the model, based on the existence of two types of segments in the main chain, which is in good agreement with the calculations of (Takeda *et al.*, 1994), reporting two types of photo created metastable weak bond states. Important property from the point of polysilane degradation is that the above mentioned species are not stable and for low light intensities transform themselves back, thus forming non-degraded polymer chain. It is valid also for short intense light pulses. The degradation starts during long time illumination by an intense light. The energy is mainly concentrated in short segments where photodegradation begins (Meszároš *et al.*, 2003) and where polysiloxanes species Si–O–Si on air, or carbosilanes Si–CH<sub>2</sub>–Si species in vacuo are formed (Kricheldorf *et al.*, 1996). For lithographic applications, among others, the efficiency of the degradation plays important role. In case of polysilylenes, the speed of the degradation has to be improved as much as possible.

After the illumination, an electron is excited to anti-bonding state and hole moves along the chain with the mobility  $10^{-2} \text{ cm}^2 \text{ V}^{-1} \text{ s}^{-1}$  for poly[methyl (phenyl) silylene] (PMPSi), as it follows from microwave measurements (Nespurek *et al.*, 2000). The electron can recombine with the hole or move to the side (phenyl) group which acts, for PMPSi, as an electron acceptor (see Fig. 2.8). The back transfer of the electron to the main chain can occur



in time of microseconds ( $36 \mu\text{s}$  for PMPSi (Nespurek & Eckhardt, 2001)). During this or shorter times the degradation can take place. High efficiency photodegradation needs longer absence of an electron from the polysilane chain. This is possible to realize using a strong acceptor as an additive. Electron from the side group can be transferred to the additive molecule and form anion radical. If the anion radical is unstable, the back transfer to the chain is impossible and a Si–Si bond scission is more probable (Kani *et al.*, 1998). Therefore, to increase the photodegradation efficiency the additive must fulfill two important rules; (1) to be an electron acceptor (in respect to the given polymer) (2) with non-stable anion-radical.

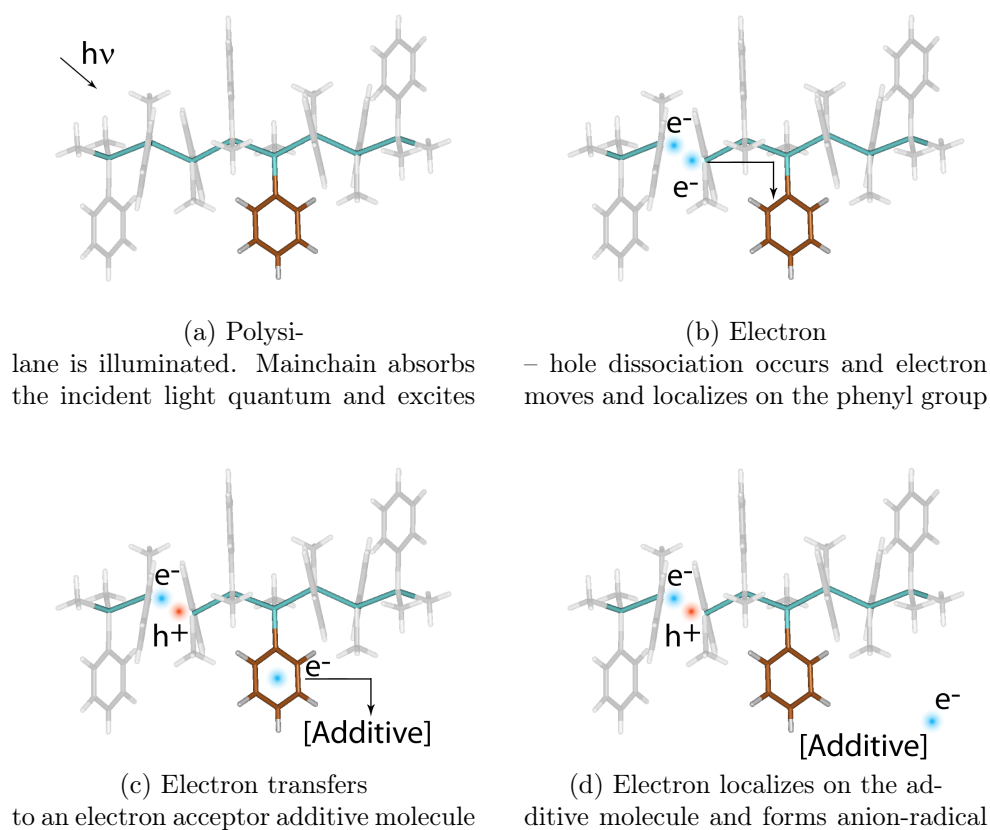


Figure 2.8: Photophysical processes in PMPSi (depicted molecule of PMPSi is schematic and only important parts are highlighted)

## 2.4 Phthalocyanines

Phthalocyanines (Pcs) are molecules of great interest and have many possible applications. Structural formula of basic Pc is shown in Scheme 2.9

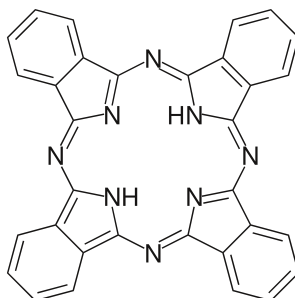
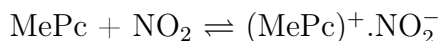


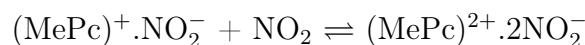
Figure 2.9: Structural formula of non-substituted Pc

The development of gas sensors still belongs among actual problems, as many human activities require qualitative and quantitative detection of gases. Detection of  $\text{NO}_2$  is important due to two main reasons: (1) it is a gas which is harmful for human health and pollutes the environment; (2)  $\text{NO}_2$  appears in many industrial processes as it is one of the products of combustion. Phthalocyanines are promising materials to be applied as sensing matrix for  $\text{NO}_2$  detection. They are thermally and chemically stable, environmentally friendly and cheap in production.

Pcs absorb light in UV and visible regions. Optical absorption is the result of the transitions of electrons in  $\pi$ -conjugated Pc skeleton; the orbitals of the central metal atoms are also included (Frag, 2007; Kumar *et al.*, 2000). The absorption of visible light and photovoltaic properties makes it possible to use Pcs for the construction of gas sensors with optical detection. The influence of  $\text{NO}_2$  leads to the decrease of the intensity of Q-band (550–700 nm) in the absorption spectrum and the appearance of new bands with maxima at about 500 and over 700 nm. Similar changes were observed in the spectrum during the formation of donor-acceptor complex between Pcs and electron acceptors (Bortchagovsky *et al.*, 2004).

Capobianchi *et al.* proposed two-step mechanism of  $\text{NO}_2$  interaction with Pc (Baldini *et al.*, 1998; Capobianchi *et al.*, 1998). First step consists of transferring one electron from Pc to  $\text{NO}_2$ . During the second step, another electron is transferred from Pc to the gas molecule, thus forming bication of Pc complexed with two  $\text{NO}_2$  molecules:





The equilibrium of the first step is strongly shifted to the direction of reaction products. The second step reaction is equilibrated closer to the initial reagents. The formation of charge transfer complex (CTC) usually changes the conductivity of the material (Lee & Chang, 2006; Maggioni *et al.*, 2008; Maggioni *et al.*, 2006). Literature sources confirm the decrease of electrical resistivity in the presence of nitrogen dioxide.

Non-substituted Pcs are not soluble, thus preparation of sensing layers requires expensive vacuum evaporation. The use of substituted Pcs solves the problem with solubility, and potentially can improve the recovery rate. Alkyl-substituted Pcs show similar sensoric properties as nonsubstituted derivatives (Fernandes & Richardson, 2006). However, an optimal material with suitable response rate and sensitivity was still not found.

## 2.5 Theoretical computing

Contemporary variety of numerical calculations, which can be used for molecular modeling, is very wide. In this section I will provide brief description of methods which were actually used in this thesis.

### 2.5.1 Quantum mechanics

Quantum mechanics calculations origin from solution of the Schrödinger equation (see Eq. 2.10). According to the level of approximation, methods can be separated into these three groups:

1. *Ab-initio* - "From first principles". These methods solve the Schrödinger equation as accurate as possible. The first widely used method was Hartree-Fock.
2. *Semi-empirical* - These methods are based on the Hartree-Fock formalism, but make many approximations and some of the parameters are fitted to experimental data. They are vital for treating large molecules, where full ab-initio approach cannot be used, as it is computationally too expensive.
3. *Empirical* - Methods solve the Schrödinger equation in very rough approximation. E.g. the solution is restricted to  $\pi$ -electrons only.

### Basis sets

When solving Schrödinger equation (Eq. 2.10) the wave function approximation must be given:

$$\Psi_j^{MO-LCAO} = \sum_{i=1}^n C_{ij} \Phi^{AO}, \quad (2.26)$$

where  $\Psi^{MO-LCAO}$  is MO constructed as linear combination of the atomic orbitals (AO)  $\Phi^{AO}$  and  $C_{ij}$  are coefficients of this expansion.

AOs can be taken as solution of the Hartree-Fock equations for single atom. However, such form of AO is computationally very expensive and thus different approximations with the aid of analytical functions are used. First suggested were so called Slater type orbitals (STO)

$$\Psi_i^{AO-STO}(\zeta, n, l, m, r, \theta, \phi) = N r^{N-1} e^{\zeta r} Y_{lm}(\theta, \phi), \quad (2.27)$$

where  $N$  is normalization factor,  $r, \theta, \phi$  are spherical coordinates,  $Y_{lm}$  is angular function,  $n, l, m$  are principal, azimuthal and magnetic quantum numbers.

STO AOs are usually further decomposed into Gaussian type orbitals (GTO), which are more suitable for fast calculations since product of two GTOs is GTO.

$$\Psi_i^{AO-GTO}(\alpha, l, m, n; x, y, z) = N e^{-\alpha f^2 r^2} x^l y^m z^n, \quad (2.28)$$

where  $N$  is normalization factor,  $x, y, z$  are cartesian coordinates,  $\alpha$  is exponential factor;  $l, m, n$  are exponents of cartesian coordinates,  $r^2 = x^2 + y^2 + z^2$  and  $f$  is factor, which is adjusted according to experimental results.

In actual calculation, so called split-valence basis sets are most often used. In these, inner and valence electrons are defined by different number of functions. E.g. basis set 3-21G denotes basis set, which uses single STO decomposed into 3 GTOs for the inner electrons and 2 STOs (first decomposed into 2 GTOs and second as a single GTO) for valence electrons.

Basis set, which is created from the occupied states solely, cannot properly describe all the effects in the molecule. Thus, polarization and diffusion functions can be added to it:

1. *Polarization functions* - These functions represent unoccupied orbitals and are necessary for description of excited and cation states.
2. *Diffusion functions* - Functions with small  $\alpha$  coefficient thus they extend further. They are necessary for anion simulations.

### Methods

First developed ab-initio methods was Hartree method in Born-Oppenheimer (adiabatic) approximation with Schrödinger equation for a molecule in the form (Skala, 1994):

$$\left( -\frac{1}{2} \sum_i \frac{\hbar^2}{2m_e} \Delta_i + \frac{1}{2} e^2 \sum_{i \neq j} \frac{1}{r_{ij}} - e^2 \sum_{i,A} \frac{Z_A}{r_{iA}} \right) \Psi_R = U(R) \Psi_R, \quad (2.29)$$

where first term on the left side is kinetic energy of the electrons, second term represents electron-electron interaction and third is electron-nuclei interaction (positions of the nuclei are only parameters in adiabatic approximation,  $R$ ). Schrödinger equation for the nuclei with  $U(R)$  potential is given

$$\left( -\frac{1}{2} \sum_j \frac{\hbar^2}{2M_j} \Delta_j + U(R) \right) \xi(R) = E \xi(R), \quad (2.30)$$

where  $\xi(R)$  is wave function of the nuclei and first term on the left side represents kinetic energy of the nuclei ( $M_j$  is the mass of the  $j^{\text{th}}$  nucleus).

In Hartree method the wave function is given by a simple product of the wave functions of the single electrons. This form does not fulfil Pauli's exclusion principle (static correlation of the electron movement) and method, as is, does not comply with dynamic electron correlation (movement of the electrons is correlated, since two electrons have the same charge sign, thus they repulse each other via Coulombic interaction).

Improvement over Hartree is Hartree-Fock method which constructs the wave function in the form of Slater determinant. This form ensures that Pauli exclusion principle is built-in<sup>2</sup>:

$$\Psi(r_1, \dots, r_N) = \frac{1}{\sqrt{N!}} \sum_P \epsilon_P P \{ \psi_1 \xi_1(\sigma_{z1}) \dots \psi_N \xi_N(\sigma_{zN}) \}, \quad (2.31)$$

where  $\epsilon_P$  is the sign of the permutation  $P\{\dots\}$ ,  $\xi$  is spin part of the wave function and  $\psi$  is spatial part of the wave function. This modification leads to accounting of the exchange potential to the resulting energy, but only for the electrons with the same spins (due to the utilization of a single Slater determinant).

---

<sup>2</sup>Slater determinant is zero if two columns or rows in matrix are same

Qualitatively different approach represent Density function theory (DFT). Instead of searching energy solution in the form of functional of the wave function, it searches solution as a functional of the electron density<sup>3</sup>:

$$\rho(\vec{r}) = \sum_{i=1}^N |\psi_i(\vec{r})|^2 \quad (2.32)$$

Energy is then given by expression:

$$E(\rho) = T[\rho(\vec{r})] + \int \nu(\vec{r})\rho(\vec{r})d\vec{r} + \frac{1}{2}e^2 \int \frac{\rho(\vec{r})\rho(\vec{r}')}{|\vec{r} - \vec{r}'|} + E_{xc}[\rho(\vec{r})], \quad (2.33)$$

where terms on the right side of the equation have the following meaning respectively: kinetic energy, external potential (also accounts for electromagnetic interaction of the nuclei), electron-electron interaction and the last term supplies for all the other effects (such as exchange and correlation potential).

Condition of minimum for Eq. 2.33 is:

$$\frac{\delta E[\rho(\vec{r})]}{\delta \rho(\vec{r})} = \frac{\delta T[\rho(\vec{r})]}{\delta \rho(\vec{r})} + \nu(\vec{r}) + \frac{1}{2}e^2 \int \frac{\rho(\vec{r}')}{|\vec{r} - \vec{r}'|} d\vec{r}' + \frac{\delta E_{xc}[\rho(\vec{r})]}{\delta \rho(\vec{r})}, \quad (2.34)$$

When  $E_{xc}[\rho(\vec{r})]$  can be written in following form:

$$E_{xc}[\rho(\vec{r})] = \int \nu_{xc}(\vec{r})\rho(\vec{r})d\vec{r}, \quad (2.35)$$

we can introduce effective potential  $\nu_{eff}$

$$\nu_{eff}(\vec{r}) = \nu(\vec{r}) + e^2 \int \frac{\rho(\vec{r}')}{|\vec{r} - \vec{r}'|} d\vec{r}' + \nu_{xc}, \quad (2.36)$$

thus extremal condition will yield form:

$$\left[ -\frac{\hbar^2}{2m}\Delta + \nu_{eff}(\vec{r}) \right] \psi(\vec{r}) = \epsilon_j \psi_j(\vec{r}), \quad (2.37)$$

where  $\epsilon_j$  are lagrange multipliers, which do not have direct physical meaning (they do not fulfil Koopmans theorem (Skala, 1994)).

If the form of the  $E_{xc}[\rho(\vec{r})]$  would be known to us, the equations of the DFT methods could be solved by iterative method as HF's are. However,

---

<sup>3</sup>Hohenberg-Kohn theorem ensures that for each wave function  $\psi$ , there is unique electron density  $\rho$ ; i.e. none two physically distinct states are described by the same electron density

this term is unknown and Eq. 2.33 is its definition equation. In the meantime several approximations were introduced:

1. *LDA - Local density approximation* - Solution with the usage of homogeneous non-interacting electron gas. Best results were achieved with method  $\chi_\alpha$

$$\nu_{xc} = \nu_{\chi_\alpha} = \frac{3}{2}\alpha \left[ \frac{3}{4} \left( \frac{3}{\pi} \right)^{1/3} \right] \rho^{1/3}, \quad (2.38)$$

where  $\alpha \in (2/3, 1)$  and depends on the correlation of electrons.

2. *GCA - Gradient corrected methods* - Anticipates non-homogeneous electron gas and thus  $E_{xc}[\rho(\vec{r})]$  depends also on the gradient of the electron density. Several approaches were derived:

- (a) Becke (B88, (Becke, 1988)) - exchange energy can be written in the following form:

$$E_x = E_x^{LDA} + \Delta E_x^{B88}, \quad (2.39)$$

where

$$\Delta E_x^{B88} = -\beta \rho^{1/3} \frac{\chi^2}{1 + 6\beta \chi \operatorname{asinh} \chi}, \quad (2.40)$$

where  $\beta$  is fitted to experimental results and  $\chi$  is non-dimensional quantity

$$\chi = \frac{|\nabla \rho|}{4 \rho^{2/3}} \quad (2.41)$$

- (b) Perdew-Wang (PW86, (Perdew, 1986))

- (c) Lee-Yang-Parr (LYP, (Lee *et al.*, 1988))

**B3LYP** (Becke, 1992a; Becke, 1992b; Becke, 1993a) method belongs to the family of hybrid functionals, which combine exchange-correlation energy functional in DFT and incorporate a portion of exact exchange from the Hartree-Fock theory. This approach was introduced by (Becke, 1993b). Hybridization with exact Hartree-Fock exchange provide simple scheme for improving many molecular properties, such as atomization energies, bond

lengths and vibration frequencies, which tend to be poorly described with simple "ab initio" functionals (Perdew *et al.*, 1996). A hybrid exchange-correlation functional is usually constructed as a linear combination of the Hartree-Fock exact exchange functional  $E_x^{HF}$  and any number of exchange and correlation explicit density functionals. The parameters determining the weight of each individual functional are typically specified by fitting the predictions to experimental or accurately calculated thermochemical data. Exchange-correlation functional of method B3LYP is given:

$$E_{xc}^{B3LYP} = E_{xc}^{LDA} + a_0(E_x^{HF} - E_x^{LDA}) + a_x(E_x^{GGA} - E_x^{LDA}) + a_c(E_c^{GGA} - E_c^{LDA}), \quad (2.42)$$

where  $a_0 = 0.20$ ,  $a_x = 0.72$  and  $a_c = 0.81$  are the three empirical parameters determined by fitting the predicted values to a set of atomization energies, ionization potentials, proton affinities and total atomic energies (in this sense, the method is semi-empirical, since it has been adjusted to fit experimental results);  $E_x^{GGA}$  and  $E_c^{GGA}$  are B88 exchange functionals (Becke, 1988) and correlation functionals of Lee, Yang and Parr (Lee *et al.*, 1988) and  $E_c^{LDA}$  is the local-density approximation to the correlation functional.

**CAM-B3LYP** (Yanai *et al.*, 2004) is improved hybridization method based on the B3LYP which is unsuccessful in a number of important applications: (1) the polarizability of long chains, (2) excitations using time dependent theory (TDDFT) for Rydberg states, and perhaps most important (3) charge transfer (CT) excitations. The reason for these failures is understood; at long-range the exchange potential behaves as  $-0.2r^{-1}$ , instead of the exact value  $-r^{-1}$ . The improvement of the CAM-B3LYP lies in the different mixing ratio between DFT exchange and HF (see Fig. 2.10) depending on distance. With increasing spacing between interacting particles, the ratio of the HF and DFT exchange potentials shifts in favor of the HF functional.

**Extended Hückel** The extended Hückel method is a semi-empirical quantum chemistry method, developed by Roald Hoffmann (Hoffmann, 1963). It is based on the Hückel method, but while the original only considers  $\pi$ -orbitals, the extended method also includes the  $\sigma$ -orbitals. It is not very successful in determining structural geometry, but can be employed for determining molecular orbitals. Since it is a semi-empirical method, it is much faster than ab-initio methods and can be used for larger systems.



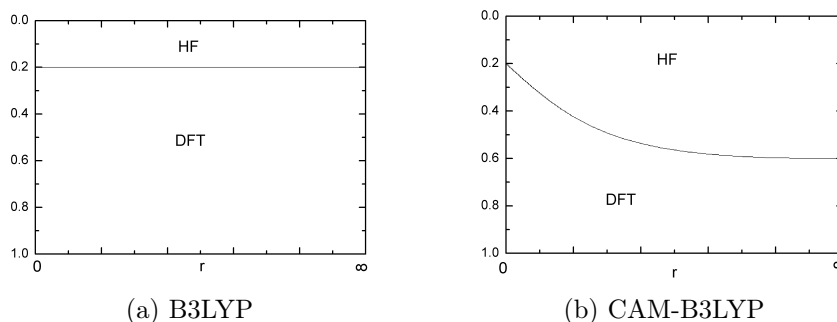


Figure 2.10: Schematic plots of the contribution to exchange from  $r^{-1}$  (interaction distance), apportioned into DFT and HF.

### Basis set superposition error (BSSE)

This error emerges as a consequence of basis set truncation, i.e. origins in finiteness of the basis set. Then subsystem, which is part of a larger system, is usually described in more complete sense: at least its interacting atoms have basis set effectively composed of a sum of all interacting subsystems. Therefore, the energy of the supersystem is calculated as lower, which comes from greater completeness of the basis set and not from the interaction energy.

The counterpoise correction (one of the available treatments) can be formally described as follows: The uncorrected interaction energy of the dimer  $AB$  is

$$E_{int}(G,AB) = E_{AB}(G,AB) - E_A(A) - E_B(B), \quad (2.43)$$

where  $E_{int}(Q,AB)$  is the interaction energy of the dimer  $AB$  in the full basis set of the dimer (sum of basis sets of the monomer  $A$  and  $B$ ),  $E_{AB}(G,AB)$  is the energy of the dimer  $AB$  at given geometry  $G$  in the full basis set of the dimer,  $E_A(A)$  is the energy of standalone monomer  $A$  solely in the monomer basis set  $A$  and  $E_B(B)$  is the energy of standalone monomer  $B$  solely in the monomer basis set  $B$ . The counterpoise corrected interaction energy is then

$$E_{int}^{cc}(G,AB) = E_{AB}(G,AB) - E_A(G,AB) - E_B(G,AB), \quad (2.44)$$

where  $E_A(G,AB)$  and  $E_B(G,AB)$  are total energies of the monomers  $A$  and  $B$ , respectively, computed with full dimer basis set at geometry of the dimer,  $G$ ; i.e. in the calculation of monomer  $A$  the basis set of the "other" monomer  $B$  is present at the same location as in dimer  $AB$ , but the nuclei of  $B$  are not. In this way, the basis set for each monomer is extended by the functions of the other monomer.

When estimating dissociation energies, one should take into consideration the *zero point energies* as well (ZPE - energy of the the ground state of the quantum harmonic oscillator and its null oscillations). Then corrected dissociation energy  $E_{diss}^{cc}$  is given as:

$$E_{diss}^{cc} = -E_{int}^{cc}(G, AB) - E_{AB}^{ZPE}(G, AB) + E_A^{ZPE}(A) + E_B^{ZPE}(B), \quad (2.45)$$

where  $E_{AB}^{ZPE}(G, AB)$  is the ZPE energy of the dimer in optimized geometry  $G$  and  $E_A^{ZPE}(A)$  and  $E_B^{ZPE}(B)$  are ZPE energies of the monomers  $A$  and  $B$ , respectively, in their equilibrium geometries (optimized solely as monomers) and their monomer basis sets.

### 2.5.2 Molecular mechanics and dynamics

Different approach to molecular modeling represents *Molecular mechanics* (MM) which solves classical Newton's equations in order to determine molecular properties. Exact estimation of the atom positions in the molecule requires solution of the Schrödinger equations for electrons (Eq. 2.46) and nuclei (Eq. 2.47)

$$H\psi(r; R) = U(R)\psi(r; R) \quad (2.46)$$

$$H\Phi(R) = E\Phi(R) \quad (2.47)$$

where  $r$  denotes coordinates of the electrons and  $R$  are coordinates of the nuclei. Eq. 2.47 is Schrödinger equation for the motion of the nuclei on the potential energy surface. This surface is given as a solution of Eq. 2.46. However, the effort required to solve Eq. 2.46 is computationally too costly for large systems, thus an empirical fit of the potential energy surface is commonly used, i.e. *Forcefield* (FF). Since the nuclei are relatively heavy objects, quantum mechanical effects are often insignificant, hence Eq. 2.47 is replaced by Newton's equation of motion:

$$-\frac{dV}{dR} = m \frac{d^2 R}{dt^2}, \quad (2.48)$$

where  $V$  is energy on potential surface (FF).

#### Forcefield

Forcefield contains necessary building blocks for the energy and force calculations:

1. *A list of atom types* - the same atom in different environment (e.g. double bonded or single bonded) reaches different type and FF assigns to it different properties.
2. *A list of atomic charges*
3. *Functional forms for the components of the energy expressions* - Potential energy surface is calculated from several expressions.

FFs commonly used for molecular modeling employ a combination of internal coordinates and terms to describe the bond part of the potential energy surface, non-bond terms to describe the van der Waals and electrostatic interactions between atoms. Functional forms range from simple quadratic polynomial through the Morse formula, Fourier expansions, Lennard-Jones potentials, etc.

Purpose of a FF is to describe a class of molecules with reasonable accuracy. Empirical data of a small set of molecules are used to parametrize FF and then they are extrapolated to fit larger range. Some FFs aim for high precision for smaller set of molecule types other can be of general purpose with mediocre accuracy but able to accommodate larger class of molecular types.

The main advantages of FF approach are:

1. Simulation of large systems - FF simulation are several orders faster than quantum mechanical calculations.
2. Analysis of the energy contributions at the level of individual classes of interactions - energy can be decomposed to bond energy, torsion energy, interaction energy, etc.
3. Relatively simple introduction of constraints to the calculations and addition of external functional terms.

On the other hand, one has to understand limitations of the FF model, which cannot be treated properly. Such are:

1. Electronic transitions (photon absorption).
2. Electron transport phenomena.
3. Proton transfer (acid/base reactions)

**The energy expression** is an equation that describes the potential energy surface of a particular molecule as a function of its atomic coordinates. It can be decomposed to sum of three energy expression classes

$$E_{total} = E_{valence} + E_{crossterm} + E_{nonbond}, \quad (2.49)$$

where  $E_{valence}$  is the energy of the valence terms which is generally accounted for by diagonal terms, i.e. bond stretching ( $E_{bond}$ ), valence angle bending ( $E_{angle}$ ), dihedral angle torsion ( $E_{torsion}$ ).  $E_{crossterm}$  - found in modern (second-generation) FFs; correction of valence terms caused by nearby atoms.  $E_{nonbond}$  - Accounts for non-bonding interactions, i.e. van der Waals, electrostatic and hydrogen bonds.

Many types of FFs exist to this day. At present, the most commonly used are second-generation force fields which are parametrized by data from quantum chemical calculations. Such parametrization has several advantages over parametrization from experimental data:

1. Sufficient data are available for accurately determining all the forcefield parameters.
2. Resulting FF can be used to broad variety of molecules, since data for even unusual transient species can be acquired from quantum calculations.
3. FF is *consistent*, since all parameters are fitted from the same data source.

**PCFF** (Polymer consistent forcefield, (Maple *et al.*, 1994; Hwang *et al.*, 1994; Sun *et al.*, 1994)) belongs to second-generation class FFs. It was parametrized for macromolecules and polymers along with about 20 inorganic metals.

**COMPASS** (Sun *et al.*, 1998; Rigby *et al.*, 1997; Sun & Rigby, 1997; Sun, 1998) is another second-generation force field. It was derived from PCFF and corrects its flaws (original PCFF was parametrized with results at zero temperature, what limited its use). Further, COMPASS utilizes different models for different systems (ionic model, model for transition metals) and is specifically parametrized for silanes.

### Molecular mechanics

Knowledge of the potential energy surface can be utilized for finding equilibrium positions of the nuclei and harmonic vibrations. Both of these *static*

solutions are usually lumped together as *molecular mechanics*, when time evolution of the system is not considered.

**Minimization process** - search for the geometry, in which the energy of the structure is minimal, is done in two steps. First, an equation describing the energy of the system as a function of its coordinates must be defined (i.e. Forcefield) and evaluated for a given conformation. Second, atom positions are adjusted to lower value of the target function. These two steps are repeated until a conformation with minimum energy is found.

Simplest algorithm for searching a conformation with lower energy is *line search*. Consider example in Fig. 2.11. Initial geometry is represented by the point  $a$ . Direction toward the new nuclei conformation with the lower energy is given by vector which is gradient of the potential energy surface at the initial point. Then in the 2-dimensional example, the movement along the gradient vector can be expressed as:

$$(x', y') = \left( x_0 + \alpha \left. \frac{\partial E}{\partial x} \right|_{x_0, y_0}, y_0 + \alpha \left. \frac{\partial E}{\partial y} \right|_{x_0, y_0} \right) \quad (2.50)$$

where  $(x', y')$  are coordinates along the line away from the current point  $(x_0, y_0)$  in the direction of the derivative at  $(x_0, y_0)$ . If the energy of the line search is plotted against coefficient  $\alpha$  it will yield graph depicted in Fig. 2.11(b). The minimum in point  $c$  coincides with the point at which the line is tangential to the energy contour. Thus, the gradient of the energy surface in the point  $c$  will be perpendicular to the previous line segment.

The fact that each new step in the process is perpendicular to the previous one is causing convergence problems in the area of actual minimum (especially if the minimum is rather flat), thus several improved algorithms, called *conjugate gradient*, were developed in order to suppress this behaviour. These methods calculate the direction of the new step with respect (weighted) to the previous gradients (one or more; information in more detail can be found in (Accelrys, 2010)).

**Vibrational calculations** are another application of the molecular mechanics. Even though the harmonic vibrational frequencies are dynamic property of the system, they can be calculated from the potential energy surface at the minimum conformation. At this point the potential can be expanded as a Taylor series and truncated after the second term. Thus, Newton's equations of motion will yield form of the harmonic oscillator.

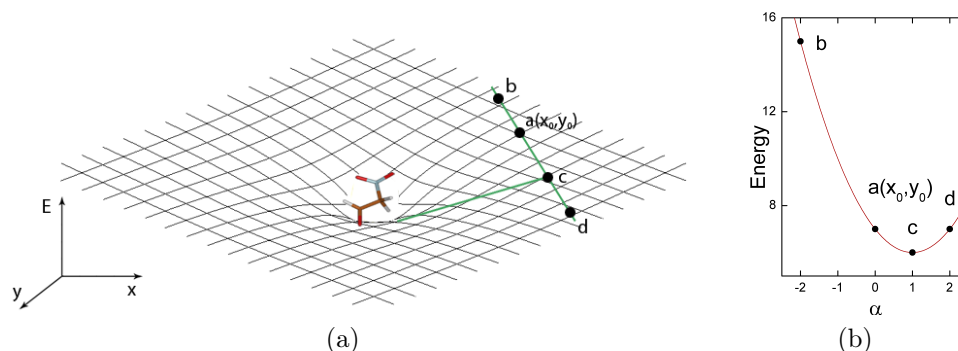


Figure 2.11: (a) Schematic illustration of the line search algorithm starting from point  $a(x_0, y_0)$ . Direction toward the new conformation with lower minimum is found as gradient of potential energy surface. Fig. (b) cross section of the energy surface in line search path

### Molecular dynamics

Molecular dynamics solves the classical equations of motion for a system of  $N$  atoms interacting according to a potential energy given by a FF. Some of the applications of the molecular dynamics are:

1. *Performing conformational search* - system can access different parts of the phase space during the dynamic process, thus new stable geometries can be found.
2. *Generating statistical ensemble* - statistical ensembles for thermodynamic quantities can be generated, as molecular dynamics offers several mechanisms of controlling the temperature and pressure.
3. *Studying motion of molecules* - time evolution of the system can be studied by means of the molecular dynamics.

At its simplest, molecular dynamics solves Newton's equation of motion:

$$\vec{F}_i(t) = m_i \vec{a}_i(t), \quad (2.51)$$

where  $m_i$  is the mass,  $\vec{a}_i$  is the acceleration and  $\vec{F}_i$  is the force acting on the atom  $i$ , and  $t$  represents time. This equation can be rewritten in the following form with the aid of potential energy (i.e. forcefield) and position of the  $i^{\text{th}}$  atom,  $r_i$ :

$$\frac{\partial V}{\partial \vec{r}_i} = m_i \frac{\partial^2 \vec{r}_i}{\partial t^2} \quad (2.52)$$

Note, that classical equations are deterministic as opposed to the quantum mechanical Schrödinger equation. However, trajectories are sensitive to initial conditions, thus calculations from different simulation engines do not have to produce identical outcomes.

**Integrators** are used to numerically integrate Eq. 2.52. Well designed integrator needs to fulfil several conditions:

1. *Speed* - integrator should be fast and ideally require only one energy evaluation per timestep.
2. *Memory* - minimal computer memory should be required.
3. *Long timesteps* - it should permit the use of relatively long timesteps.
4. *Energy conservation* - Should preserve energy of the system as far as possible.

Several integrators are available at present time and details can be found in (Accelrys, 2010). As an example, *Verlet leapfrog integrator* equations are shown bellow.

$$\vec{v}\left(t + \frac{1}{2}\Delta t\right) = \vec{v}\left(t - \frac{1}{2}\Delta t\right) + \Delta t\vec{a}(t) \quad (2.53)$$

$$\vec{r}(t + \Delta t) = \vec{r}(t) + \Delta t\vec{v}\left(t + \frac{1}{2}\Delta t\right) \quad (2.54)$$

$$\vec{a}(t + \Delta t) = \frac{\vec{f}(t + \Delta t)}{m} \quad (2.55)$$

**Timestep** (i.e.  $\Delta t$  in 2.53) must be estimated properly with respect to the selected integrator and fastest motion calculated. In general, timestep should be an order smaller than the fastest motion in the molecule (e.g., if fastest motion is C-H vibration with period  $10^{-14}$  seconds, then  $\Delta t$  should not be greater than 1 femtosecond). If this rule is not met, simulated system can be stuck in artificial vibration motion or even dissociate.

**Quench dynamics** Method used for finding new equilibrium geometries. In this case the structure is set into motion by random distribution of the velocities over the atoms. System is given time to evolve and at some point its geometry is taken and optimized to new energy minimum. Afterwards, time evolution of the system continues from the geometry from which the

optimization started. This method is used for finding new accessible conformations. Through the additional energy, which is introduced to the system via random velocity distribution, the system is able to overcome barriers and reach new parts of the phase space.



# Chapter 3

## Thesis aims

From the wide variety of problems, that need to be solved in the field of molecular electronics, we have chosen to concentrate on the following:

1. *Detailed study of the influence of geometry changes on the charge carrier localization* - Geometry of the molecule is strongly coupled with the problem of the charge carrier localization and transport phenomenon in silane polymers, as shown in sections 6.1, 6.2 and 6.3. Its importance comes forward when one realizes that the effect on resulting mobility of the charge carrier can be as high as several orders.
2. *Effect of the charge transfer on system stability and spectrum* - Stability of the molecule can be closely related to charge transfer and is vital for applications. Both destabilization (for instance in the photolithography) and stabilization (necessary in all electronic devices) can be employed with success in manufacturing process. Results for this area are presented in section 6.4.
3. *Influence of the additives on the charge carrier localization and on the intra-molecular transfer* - Transport of the charge carrier can be controlled by means of the closest surroundings, where additive molecules can be placed. This way, one can create barrier for the transport or enhance it by providing electron acceptors, which will result in higher charge carrier generation or act as a junction bridge. Results of studies, which concentrated on the manufacturing of a gas sensor are presented in the section 6.5.

All studied problems are closely related to the charge carrier transport in molecules, where very strong emphasis is given to the geometry of the system and its closest surroundings. The topics were studied by theoretical means, but several results were subsequently supported by experiments.



# Chapter 4

## Computational methods

In this chapter, computational methods, which were used to acquire results in this thesis, are presented.

Where appropriate, source codes or input files will be added in this typeface. If such text would be too extensive it will be added as one of the appendices.

### 4.1 Quantum mechanics

This section contains explanation of the methods which were utilized in the quantum chemistry computational packages, Gaussian 03 (Frisch *et al.*, 2003) and 09 (Frisch *et al.*, 2009).

#### 4.1.1 Potential energy surface scan

A *potential energy surface* (PES) scan is generally used within adiabatic or Born–Oppenheimer approximation in quantum mechanics to model chemical reactions and interactions in simple chemical and physical systems. For given molecule, its potential energy can be shown as a polynomial (hyper)surface dependent on the atom coordinates. When one of the coordinates is varied and *single-point energy* (SPE) of the molecule is calculated along this change, plot of the SPE of the molecule on the atomic position is found; i.e. profile of the PES along the varied coordinate. Bellow is an example of input file for Gaussian program, which calculates PES scan for H<sub>2</sub>O molecule, when O-H bond is stepwise prolonged.

```
#P B3LYP/6-31G*  
opt
```

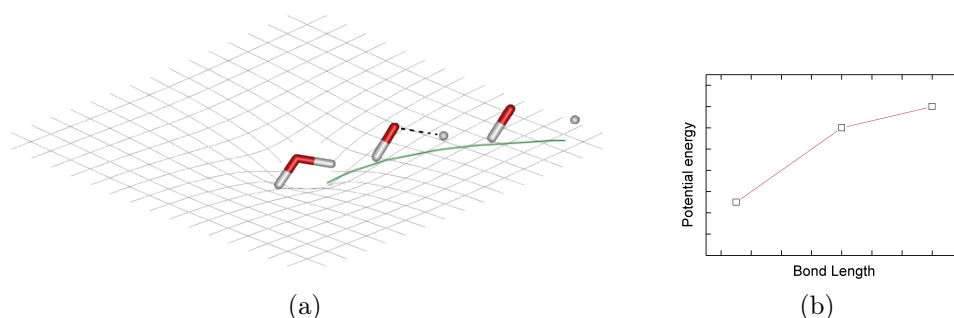


Figure 4.1: Illustration of the PES scan. In the given molecule (in here only schematic), one of the bonds is stepwise prolonged. For each different bond-length the energy of the molecule is estimated.

scan

Example of the Gaussian input file for PES scan of water molecule. Bond length of the second hydrogen will be 10 times stepwise incremented by 0.01 Angstroms. This version of PES scan starts from optimized geometry, but steps of the scan are performed over a non-optimized geometries.

```
0 1
O
H 1 ho2
H 1 ho3 2 hoh3

ho2 0.95
ho3 0.95 10 0.01
hoh3 109.471
```

Depending on the plot, one can make conclusions about the energetics of the modified molecular parameter. E.g. if a single molecular bond acts as a variable (see Fig. 4.1), then stability of this bond can be studied. Fig. 4.2 shows different outcomes of PES scan for stable (Fig. 4.2(a)), non-stable (Fig. 4.2(b)) and meta-stable (Fig. 4.2(c)) bonds.

Note, that I have used only *non-relaxed* PES scans in this thesis. That means, that initial structure was optimized to the ground state and from this point, all parameters, except the varied one, were kept constant. PES scan can be performed in *relaxed* form as well, when varied parameter is fixed to required value and the rest of the structure is optimized.

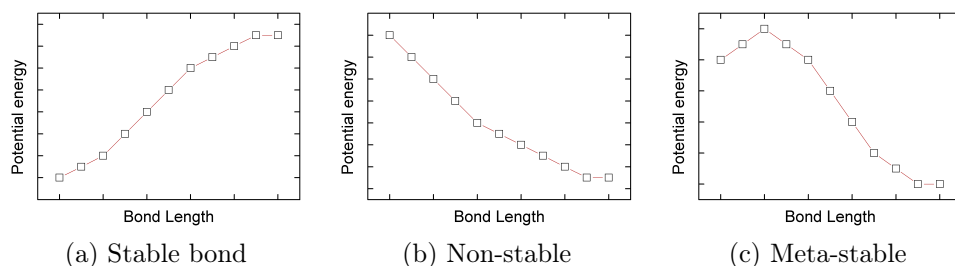


Figure 4.2: Examples of the PES scans for different types of bond stabilities.

### 4.1.2 Stabilization energies

*Stabilization energy* is the energy, which is needed to decompose a molecule (i.e. difference of SPE of original molecule and sum of the SPEs of the separated submolecules). In literature, it is also called *heat of formation* (given in  $kJ/mol$  or  $kcal/mol$ ). The difference in energy comes from electron delocalization in newly formed atomic bonds, when two reactants merge and form a molecule.

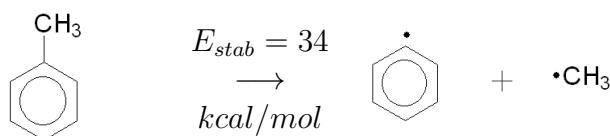
The stabilization energy can be calculated for any bond in a molecule, with the following procedure:

1. Molecule is optimized and its SP energy ( $E_{molecule}$ ) is calculated.
2. Selected bond is broken and molecule is separated in into two substructures.
3. Both substructures are optimized (by the same method and basis set as the original molecule) and their SP energies are calculated (one obtains  $E_{subpart1}$  and  $E_{subpart2}$ ).

The stabilization energy is then given by the Eq. 4.1. If  $E_{stab}$  is positive, then given bond is stable. If  $E_{stab} < 0$  then bond is non-stable and may undergo scission. However, it can still be meta-stable state. Detailed answer is given by the PES scan analysis.

$$E_{stab} = (E_{subpart1} + E_{subpart2}) - E_{molecule} \quad (4.1)$$

Stabilization energy for different bonds and formations is throughout this thesis depicted in the form of reactions (the example shown here is only illustrative; shown value of stabilization energy does not comply with reality):



Note, that if stabilization energy for non-covalent compounds is calculated, one must take BSSE correction into consideration.

### 4.1.3 Deformation energy

Deformation energy ( $E_{def}$ ) represents the amount of work which is needed to transform a molecule from neutral to charged state. It is calculated using the following procedure:

1. Geometry of neutral ground state of given molecule is found (optimization runs under conditions: charge = 0, multiplicity = 1). This state is called *neutral*.
2. Using the neutral geometry, electronic energy of *hot* state is calculated ( $E_{hot}$ , geometry of neutral molecule, charge = 1, multiplicity = 2), which represents molecule with excess positive charge, that is not yet relaxed to its ground state.
3. The neutral optimized geometry is taken as the initial geometry (to make sure that the closest potential minimum is found) and the geometry of charged molecule is optimized. This state is called *relaxed* (geometry of charged molecule, charge = 1, multiplicity = 2). Its electronic energy is denoted as  $E_{relaxed}$
4. Using the *relaxed* geometry, energy of *cold* state is calculated ( $E_{cold}$ , geometry of charged molecule, charge = 0, multiplicity = 1), which represents molecule that has just lost the excess charge carrier, but its geometry has not returned to the neutral configuration yet.

Deformation energy can be calculated as follows:

$$E_{def} = E_{hot} - E_{relaxed} \quad (4.2)$$

Several notes can be given on this term:

1. *Deformation energy is always positive* - Follows from the fact that *hot* state is not in the ground state for charged configuration (charge = 1, multiplicity = 2), while *relaxed* state is. Thus  $E_{hot}$  is always greater than  $E_{relaxed}$ .

2. *Deformation energy contains all polarization effects of electrons* - Since deformation energy is difference between two electronic energies, it includes all electron polarization effects as described in 2.1.
3. *Small polaron approximation* - Given procedure provides values of deformation energy in small polaron approximation, where all intermolecular interactions are omitted.

Example of Gaussian input file which calculates all values needed for the estimation of the  $E_{def}$  can be found in the Appendix 7.3.

#### 4.1.4 Electron-phonon term

Relaxation from *hot* state to *relaxed* has another energetic effect besides the deformation energy. It also alters frequencies of vibration modes. Hence, the energy correction for the zero point vibrations is (see also Fig. 2.7):

$$E_{e-ph} = \frac{1}{2} \sum_{k=1}^{3M-6} \hbar(\omega_p^{(k)} - \omega_0^{(k)}), \quad (4.3)$$

where  $\omega_0^{(k)}$  and  $\omega_p^{(k)}$  is the angular frequency of the  $k^{th}$  vibration mode of the neutral and charged molecule, respectively. The summation is performed over all vibration modes of the molecule ( $M$  is the number of atoms in the molecule). Note, that this term stands as zero-point vibration correction for the deformation energy, which would represent difference between tips of the inverse parabolas in Fig. 2.7. Then electron-phonon term shifts the difference to the level of  $0^{th}$ -vibration mode.

The vibration frequencies of the molecule can be calculated by the Gaussian program. Vibration analysis is always performed on optimized structure with the same method and basis set as the one which was utilized for the geometry optimization.

Since the differences of vibrations in this term are of first power, its value does not depend on the matching of the modes from neutral and charged molecule<sup>1</sup>. Below is illustrative input for Gaussian program, which will calculate IR and Raman active vibration modes.

```
#P B3LYP/6-31G*
freq
```

---

<sup>1</sup>In general, order of vibration modes in neutral and charged system can change as their frequencies shift independently.

Input file for calculating vibration frequencies  
of methane.

```

0 1
  C
  H  1.089
  H  1.089      109.0
  H  1.089      109.0      120.0
  H  1.089      109.0      120.0

```

### 4.1.5 Polaron binding energy

When charge carrier localizes on a site it deforms the molecule and alters its vibration frequencies. Hence, it creates potential well around itself, which causes its self-trapping. The depth of this well is known as *polaron binding energy* ( $E_p$ ) and its value can be calculated as:

$$E_p = E_{def} + E_{e-ph} \quad (4.4)$$

## 4.2 Molecular mechanics and dynamics

Molecular dynamics simulation were run in program MaterialsStudio (Accelrys, 2010). Method of quenched dynamics and forcefield Compass was used. Simulations were performed at 298K.

Polymer chains were 100 monomer units long. Their geometry was artificially set to ideal parameters resulting from quantum chemical calculation at the B3LYP/6-31G\* level of theory, actual values are shown in Tab. 4.1. Conformation of the side groups was slightly randomized (except for twist angle of bipheny in PBMSi, which was set to 37.7°).

Table 4.1: Ideal parameters used for initial geometries of the MD calculations.

| Polymer | Si-Si distance | Si-angle | Si-dihedral angle |
|---------|----------------|----------|-------------------|
| PMPSi   | 2.389Å         | 111.6°   | 173.7°            |
| PBMSi   | 2.395Å         | 111.3°   | 172.1°            |

After the MD calculations, the snapshots of geometrical conformations were selected and for these, the spin densities were calculated using the extended Hückel molecular orbital (EHMO) method. Fig. 4.3 shows compari-



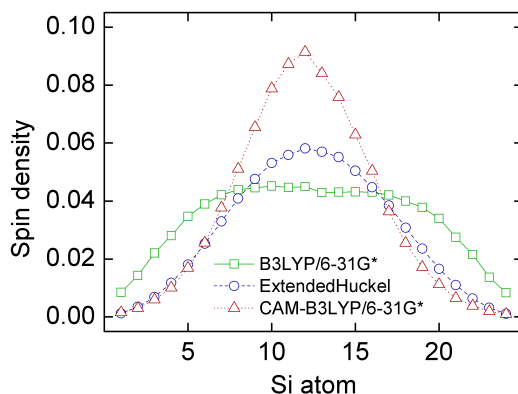


Figure 4.3: Comparison of calculated spin densities on MPSi-24-mer with ideal geometry on three different levels of theory.

son of spin density distribution over the silicon backbone calculated on the same ideal (parameters from Tab. 4.1) geometry of MPSi-24-mer. One can see that methods EHMO and CAM-B3LYP/6-31G\* give very similar results, while method B3LYP/6-31G\* overestimates the delocalization of the charge carrier.

## 4.3 Charge carrier mobility

Theoretical background of carrier transport in molecular materials was given in section 2.1.3. This section contains description of actual methodology used in this thesis with practical examples. Software used for these calculations was Gaussian (Frisch *et al.*, 2003) and NWChem (Straatsma *et al.*, 2009).

### 4.3.1 Electronic coupling

Electronic coupling can be calculated using program NWChem. When jump of an electron between two molecules occurs, it can be described by following reaction:



where  $A^e$  denotes that charge is localized on the monomer  $A$ ,  $B$  is target site for the charge carrier. After the jump  $A$  is in the *neutral* form and the charge carrier resides on the monomer  $B^e$ . For actual electron coupling estimation, one needs to find molecular orbitals (MO) for all four structures in the reaction ( $A^e$ ,  $A$ ,  $B$  and  $B^e$ ). Once these are found, their overlap can be calculated.

In further text, *dimer* will denote super-structure of *monomers A* and *B* in their interaction geometry.

**Monomer geometry** - To obtain geometries for the MO calculations, it is best to optimize dimer structure into ground state geometry. Then separate the monomers from each other and calculate the MO's for each monomer with the atom positions same as in the dimer structure.

**MO's calculations** - 4 different molecular orbital files need to be provided when electronic coupling is to be calculated:

1. MO's of the monomer *A*, when it is occupied by the charge carrier.
2. MO's of the monomer *B*, when it is charge carrier free.
3. MO's of the monomer *A*, when it is charge carrier free.
4. MO's of the monomer *B*, when it is occupied by the charge carrier.

The same input geometry is used for the calculation of the MOs for charged and neutral monomer. This comes from the fact that electron transfer is much faster than relaxation processes and thus the molecule does not have time to relax to the new ground state.

**Electronic coupling input file** - Once all 4 MO files have been calculated, the electronic coupling can be estimated. The job is done in three separate steps:

1. Molecular orbitals of the *reactants* are calculated (i.e. structure  $A^e + B$ )
2. Molecular orbitals of the *products* are calculated (i.e. structure  $A + B^e$ )
3. From the orbitals of the reactants and products, the electronic coupling is estimated

Atom coordinates of the monomers are kept same (in absolute values) as in dimer structure. Program can estimate the proper distance between jumping sites through this consistency. Example of full input file for NWChem, which calculates MOs of monomers and then the electronic coupling of dimer can be found in Appendix 7.2.

### 4.3.2 Dynamic electron-phonon term

Section 2.2 explains that charge carrier is clothed in a cloud of vibronic variances. When it moves, this perturbations move along with it. Energy required for the transfer of this cloud from one molecule ( $A$ ) to another ( $B$ ) can be calculated from following expression (for single vibration mode):

$$\begin{aligned} \Delta E_{e-ph}^{A \rightarrow B} = & \frac{1}{2} \left( n_p^{(A)} + \frac{1}{2} \right) \hbar \omega_p^{(A)} \left[ \frac{(\omega_p^{(A)})^2 - (\omega_0^{(A)})^2}{(\omega_0^{(A)})^2} \right] \\ & + \frac{1}{2} \left( n_0^{(B)} + \frac{1}{2} \right) \hbar \omega_0^{(B)} \left[ \frac{(\omega_0^{(B)})^2 - (\omega_p^{(B)})^2}{(\omega_p^{(B)})^2} \right], \end{aligned} \quad (4.6)$$

where  $n$  is the number of phonons in given vibration mode, indices  $0$  and  $p$  denote neutral and charged state, respectively, and  $\omega$  is the vibration frequency (in corresponding state).

Eq. 4.6 can be modified into following form (details of derivation can be found in Appendix 7.1) for jumps between molecules of same nature:

$$\Delta E_{e-ph} = \sum_{k=1}^{3M-6} \frac{e \frac{\hbar \omega_0^{(k)}}{k_B T}}{\left( \frac{\hbar \omega_0^{(k)}}{e k_B T} - 1 \right)^2} \frac{(\hbar \Delta \omega^{(k)})^2}{k_B T} + \left( \frac{1}{\frac{\hbar \omega_0^{(k)}}{e k_B T} - 1} + \frac{1}{2} \right) \hbar \frac{(\Delta \omega^{(k)})^2}{\omega_0^{(k)}}, \quad (4.7)$$

where  $\omega_0$  is the angular frequency of given vibration mode in neutral molecule,  $\Delta \omega$  is difference between frequencies of positive and neutral molecules and summation is performed over all vibration modes.

Since vibration frequencies  $\omega^{(k)}$  are of second power, the value of this term depends on the matching order of the vibration modes in neutral and charged molecule. However, this matching was not doable due to the complexity and number of the vibration modes. Therefore, when this term will be calculated, I will anticipate that order of the modes has not changed upon transition from neutral to charged molecule. This approach will in effect cause, that calculated value will represent minimum of this term<sup>2</sup>.

---

<sup>2</sup>If matching would be done, then some of the differences  $\Delta \omega$  would be greater and same number of them would be smaller. Since difference is of second power, then contribution of greater  $\Delta \omega$ 's would outperform decrease of smaller  $\Delta \omega$ 's. E.g.: lets have two vibration

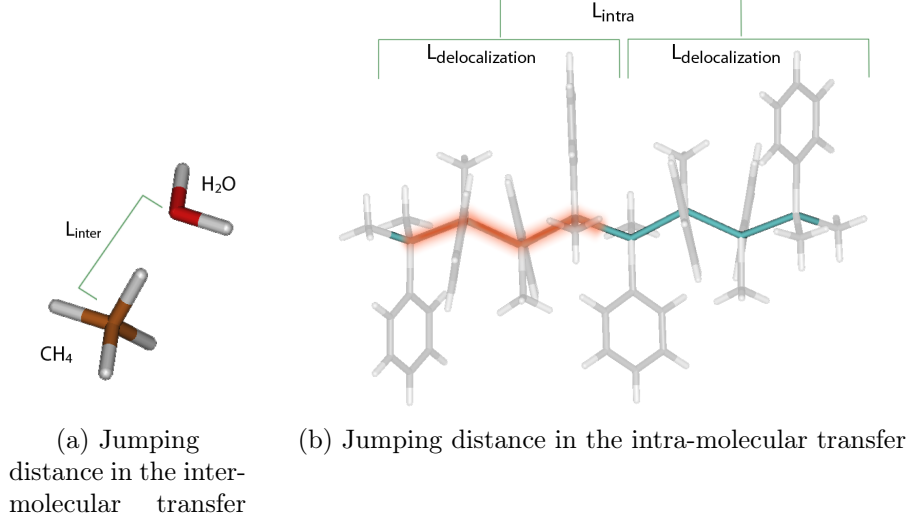


Figure 4.4: Effective jumping distances between non-bonded molecules (a) and intra-chain jumping distance (b)

### 4.3.3 Reorganization energy

When a charge carrier jumps from molecule  $A$  onto  $B$ , reorganization energy (see section 2.1.3 for formalism) can be calculated as follows:

$$\lambda = E_{redef}^{(A)} + E_{e-ph}^A + E_{def}^{(B)} - E_{e-ph}^B + \Delta E_{e-ph}^{A \rightarrow B}, \quad (4.8)$$

where  $E_{redef}^{(A)}$  is the reformation energy of the molecule  $A$  (i.e. energy needed to transfer from *relaxed* geometry back to *neutral*).  $E_{def}^{(B)}$  is the deformation energy of the molecule  $B$  (see section 4.1.3 for details).  $E_{e-ph}$  is the electron-phonon term.  $\Delta E_{e-ph}^{A \rightarrow B}$  is dynamic electron-phonon term for the jump between the two molecules  $A$  and  $B$ . Redeformation energy is calculated as follows:

$$E_{redef} = E_{cold} - E_{neutral} \quad (4.9)$$

#### 4.3.4 Effective distance between jumping sites

Effective jumping distance needs to be provided, when diffusion coefficient is calculated according to Eq. 2.17. In the case of jumps between two molecules, which are not covalently bonded, this distance can be taken as distance of those parts of the molecules, where the charge carrier resides in relaxed state (illustrative example of transfer between methane and water in Fig. 4.4 (a); distance is approximately equal to the distance between carbon and oxygen atoms,  $L_{inter}$ ). However, when mobility is to be calculated on intra-chain basis (such as mobility of hole in polysilylenes), the jumping distance will be estimated from delocalization length (see Fig. 4.4 (b); the jump occurs over distance of centers of the delocalized sections,  $L_{intra}$ ).

---

modes  $\omega_{01} = 10$ ,  $\omega_{02} = 10$  in neutral state and two  $\omega_{p1} = 15$  and  $\omega_{p2} = 24$  in charged state. If order of vibration modes does not change then  $((\omega_{p1} - \omega_{01})^2 + (\omega_{p2} - \omega_{02})^2) = 41$ . If vibrations change its order then  $((\omega_{p1} - \omega_{02})^2 + (\omega_{p2} - \omega_{01})^2) = 221$



# Chapter 5

## Investigated molecules

This chapter contains characteristics of all studied molecules. Some supplementary results are already presented in following sections, so that they can be used in argumentation in Chapter 6 and do not decrease readability of the main text. Theoretical results (all of them were achieved by simulations in vacuum) will be compared with experiment as far as possible.

### 5.1 Sigma conjugated polymers

Poly(organylsilanes) are of considerable research interest because of their unusual electrical, photoelectrical and non-linear optical properties. The effect of  $\sigma$ -electron delocalization is strong and the charge carrier transport proceeds predominantly along the Si backbone (Kepler *et al.*, 1987).

Two sigma conjugated polymers were investigated. The following sections put together their basic properties. These polymers were selected as models, since many experimental results from our and also other research groups are available for them. Thus the comparison of theoretical and experimental results allows us to distinguish between realistic results and computational artifacts.

#### 5.1.1 PMPSi

Poly[methyl(phenyl)silylene] for experimental purposes (PMPSi, see Fig. 5.1) was synthesized by Wurtz coupling of distilled dichloro(methyl)phenylsilane by sodium metal in dried toluene containing 15% of n-heptane in an inert atmosphere in dark (Zhang & West, 1984). The insoluble part of the polymer (mostly crosslinked PMPSi) was removed by centrifugation and polymer was precipitated with excess methanol, filtered off and dried in vacuum. Low-

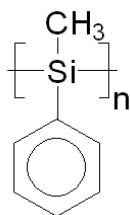


Figure 5.1: Chemical structure of poly[methyl(phenyl)silylene] (PMPSi)

molecular-mass cyclic oligomers were removed by boiling the precipitate in diethylether. PMPSi was filtered off and dried in vacuum at 40 °C for 24 h. PMPSi was characterized by a Perkin Elmer Lambda 20 spectrophotometer (characteristic absorption maximum of the Si-Si bond was located at 336 nm) and GPC ( $M_w = 20\,500$ ,  $M_n = 7200$ ).

### Structure

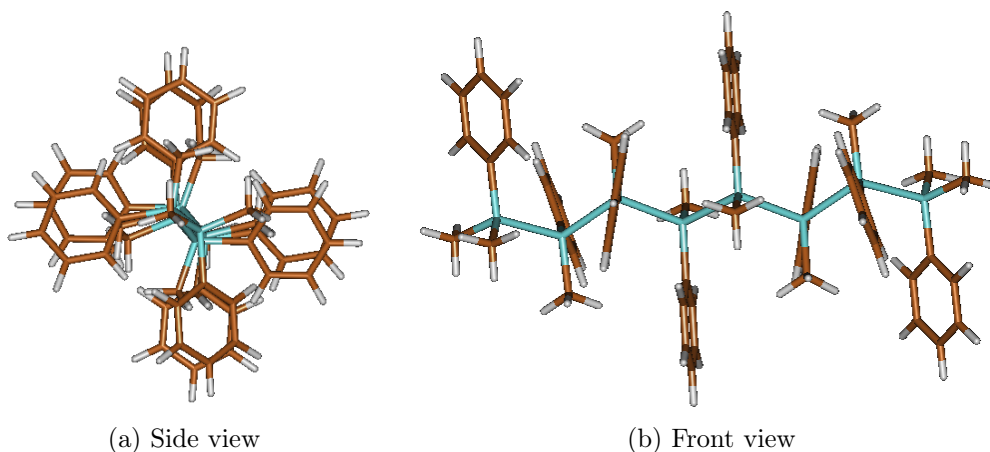


Figure 5.2: Example of MPSi-8-mer molecule

Geometries of PMPSi (see Fig. 5.1 and 5.2, mass of the monomer unit is 120.23 a.u.) molecules and its charged forms were optimized from all-trans conformation, since it is the ground state geometry (Teramae & Takeda, 1989), with no symmetry assumptions. Calculations were performed for isolated molecules in vacuum with no influence of solution or any other surroundings. Neighbor side groups were located on the opposite sides of the chain and next couple was shifted by 90° phase angle (see Fig. 5.3). Ends of the chain were capped with methyl groups.



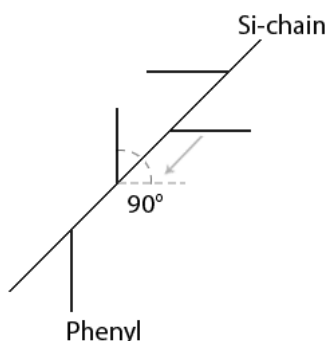


Figure 5.3: Layout of the side groups in the PMPSi molecule

Optimized parameters of the PMPSi for utilized methods and basis sets are summarized in the Table 5.1. One can see, that B3LYP/STO-3G\* underestimates the inter-silicon distance. Angle and dihedral angles are similar for all method-basis set combination.

Table 5.1: Optimized parameters of *neutral* PMPSi. Values were obtained from optimized geometries of MPSi-16-mer, from its central part.

| Method/Basis set  | Si-Si dist. | Si-angle | Si-dihedral |
|-------------------|-------------|----------|-------------|
| B3LYP/6-31G*      | 2.389Å      | 111.6°   | 173.7°      |
| B3LYP/STO-3G*     | 2.277Å      | 112.5°   | 176.2°      |
| CAM-B3LYP/6-31G*  | 2.369Å      | 111.3°   | 177.4°      |
| CAM-B3LYP/STO-3G* | 2.260Å      | 111.8°   | 175.3°      |

Table 5.2: Optimized parameters of *relaxed* PMPSi. Values were obtained from optimized geometries of MPSi-16-mer, from its central part.

| Method/Basis set  | Si-Si dist. | Si-angle | Si-dihedral |
|-------------------|-------------|----------|-------------|
| B3LYP/6-31G*      | 2.412Å      | 107.2°   | 174.7°      |
| B3LYP/STO-3G*     | 2.286Å      | 108.8°   | 179.9°      |
| CAM-B3LYP/6-31G*  | 2.409Å      | 102.6°   | 180.0°      |
| CAM-B3LYP/STO-3G* | 2.278Å      | 105.4°   | 178.4°      |

Table 5.2 contains optimized geometry parameters of positively charged PMPSi. One can see that Si-Si bond generally tends to grow (by about 1-2%)

upon removal of single electron from the molecule as a consequence of weakened bond. However, angle between silicon atoms shrinks (by about 5%). Overall, volume of the molecule decreases as a result of the lacking electron, thus delocalization volume of the electrons is smaller. Dihedral angle grows and molecule becomes less twisted. Detail study using B3LYP method and 6-31G\* basis set, concerning the conformation changes was published elsewhere (Toman, 2000; Toman *et al.*, 2002).

### Infrared spectra

Infrared spectra were calculated for different chain lengths of PMPSi. Theoretical results are in good agreement with experimental data (see Table 5.1.1; theoretical spectra shown in Fig. 5.4 were fitted with Gaussian curves with half-width of  $7\text{cm}^{-1}$ ). Note, that band intensities do not play any role for the calculation of polaron binding energy terms (see Eq. 4.3 and 4.7). Both spectra, neutral and positive, were scaled with the same scaling factor (in full range) calculated based on the data in Tab. 5.1.1.

Table 5.3: Data of experimental spectrum of PMPSi and theoretical spectra of MPSi-8-mer for basis sets 6-31G\* and STO-3G\* (method B3LYP). For both basis sets the *raw* calculated values are shown, from which the average scaling factor is calculated, which is then used to calculate values in column *scaled*.

| Exp. | Theory                |        |         |        | Vibration type                   |
|------|-----------------------|--------|---------|--------|----------------------------------|
|      | 6-31G*                |        | STO-3G* |        |                                  |
|      | $\nu(\text{cm}^{-1})$ |        |         |        |                                  |
|      | raw                   | scaled | raw     | scaled |                                  |
| 618  | 642                   | 615    | 727     | 634    | Valence Si-CH <sub>3</sub>       |
| 668  | 689                   | 660    | 749     | 654    | –                                |
| 696  | 714                   | 684    | 774     | 675    | Out of plane ring deformation    |
| 727  | 810                   | 776    | 897     | 783    | C-H deformation on methyl        |
| 783  | 826                   | 791    | 919     | 802    | C-H deformation on methyl        |
| –    | 856                   | 820    | 949     | 828    | C-H deformation on methyl        |
| 998  | 1014                  | 971    | 1104    | 963    | Planar C-H deformation on phenyl |
| 1025 | 1119                  | 1072   | 1158    | 1010   | Planar C-H deformation on phenyl |
| 1098 | 1125                  | 1078   | 1230    | 1073   | Valence Si-phenyl                |
| 1247 | –                     | –      | 1425    | 1243   | –                                |

|           |       |      |       |      |                                      |
|-----------|-------|------|-------|------|--------------------------------------|
| 1300      | 1325  | 1269 | 1505  | 1313 | Symmetric def. of C-H on methyl      |
| 1334      | 1373  | 1315 | 1548  | 1351 | Planar C-H deformation on phenyl     |
| 1427      | 1473  | 1411 | 1620  | 1414 | Planar C-H deformation on phenyl     |
| 1484      | 1535  | 1471 | 1708  | 1490 | Planar C-H deformation on phenyl     |
| 2896      | 3043  | 2915 | 3291  | 2872 | Symmetric valence def. C-H on methyl |
| 2957      | 3116  | 2985 | 3456  | 3016 | Non-symmetric of C-H on methyl       |
| 3050      | 3189  | 3055 | 3462  | 3021 | Valence of C-H on phenyl             |
| 3068      | 3205  | 3071 | 3273  | 3030 | Valence of C-H on phenyl             |
| Sc. fact. | 0.958 | –    | 0.873 | –    |                                      |

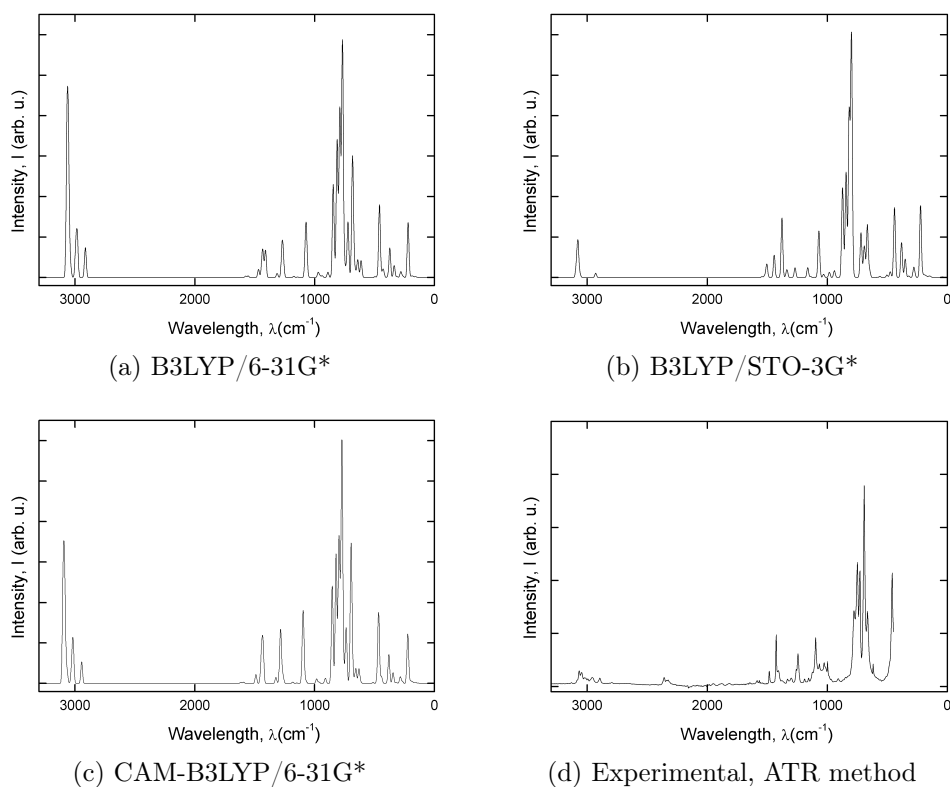
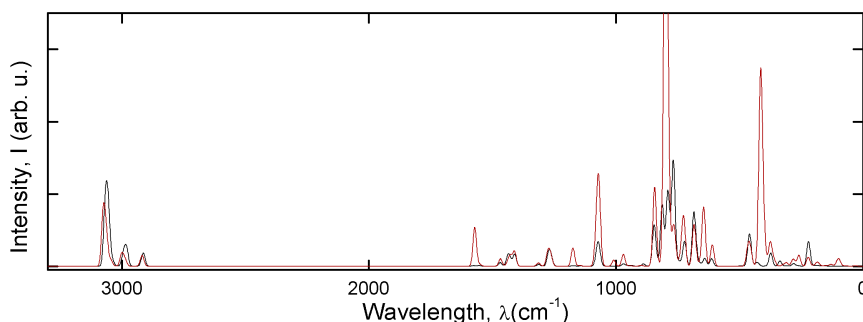


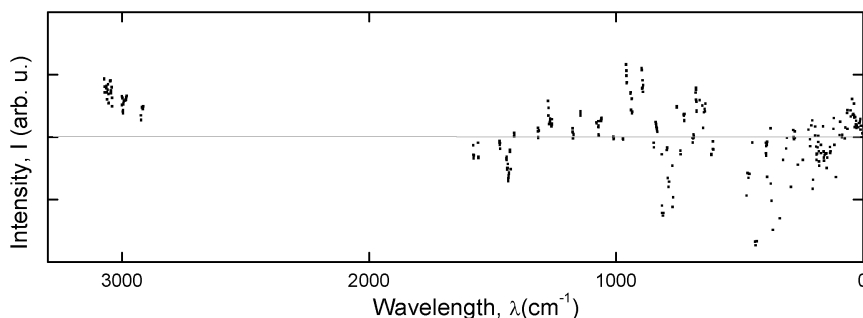
Figure 5.4: Comparison of theoretical and experimental IR spectra of the PMPSi. Theoretical plots were obtained for MPSi-8-mer. Experimental data were acquired by the ATR method.

Comparison of the IR spectra of the *neutral* and *positive* PMPSi can be seen in Fig. 5.5(a). Systematic change in the wavelengths can be only seen

in the area of hydrogen vibrations in range of  $3000\text{ cm}^{-1}$ . Fig. 5.5(b) shows differences between frequencies of vibration modes of the neutral and positive IR spectra (difference is calculated from vibration modes of the molecules in the same order as they appear in the spectrum). Similar distribution applies to all used methods and basis sets. One can see, that shift of the vibration frequencies is not consistent in the whole range. Vibration modes in different areas of spectrum react differently upon electron removal.



(a) Theoretical IR spectra fitted with gaussian curve with half-width of  $7\text{ cm}^{-1}$ . *Neutral* spectrum (-), *relaxed* spectrum (-)



(b) Difference between vibration frequencies of the *relaxed* and *neutral* theoretical IR spectra

Figure 5.5: Comparison of the IR spectrum of the *neutral* and *relaxed* PMPSi. Example given for 8-mer; B3LYP/6-31G\* level of theory.

### UV-VIS spectra

The position of the maximum of long – wavelength absorption band is about 338 nm for solid films (Navratil *et al.*, 1999; Harrah & Zeigler, 1987) and 336 nm in solution. It has been shown that this absorption band reflects mainly delocalized ( $\sigma\text{-}\sigma^*$ ) transitions of silicon backbone (Miller & Michl, 1989). The energy of these transitions is conformation-dependent and is

strongly affected by the effective conjugation length of the macromolecule; the contribution of ( $\pi-\pi^*$ ) transitions is weak. These aryl-like excitations are responsible for the shorter wavelength absorption (maximum at  $\approx 276$  nm).

Experimental spectrum of the PMPSi in solution (tetrahydrofuran, THF) is shown in Fig. 5.6. The solution (concentration  $10 \text{ gl}^{-1}$ ) was prepared under intensive shaking for at least 30 min. Absorption spectra were measured by UV-VIS spectrophotometer Perkin Elmer LAMBDA 950.

Theoretical UV-VIS spectra significantly differ in absolute values depending on utilized method and basis set. This can be seen from the differences of values of HOMO-LUMO gap shown in next section. However, absolute values will not be taken into consideration in this thesis. When any properties of the UV-VIS spectra will be utilized, always only relative values will be of interest.

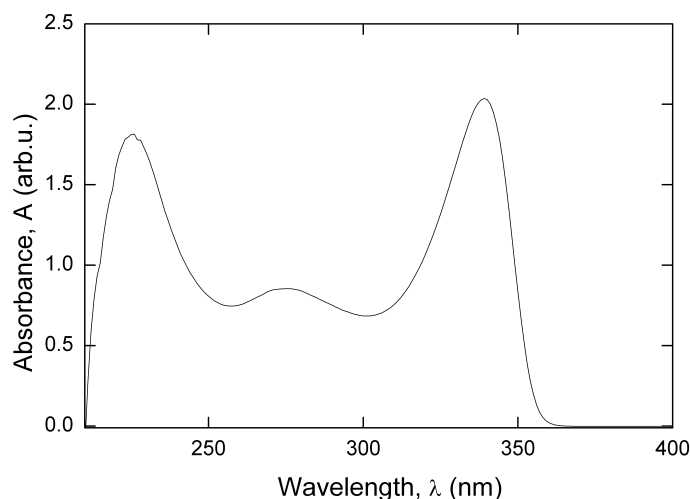


Figure 5.6: UV-VIS spectrum of neat PMPSi in tetra-hydrofuran (THF) solution.

### HOMO-LUMO Gaps

Well known dependence of decreasing HOMO-LUMO gap with increasing polymer chain length (and thus the increasing delocalization length), was confirmed for all utilized methods and basis sets. Obtained dependencies are shown in Fig. 5.7. Absolute values of the calculated gaps differ significantly for different methods and basis sets, but the overall dependence is common to all of them.

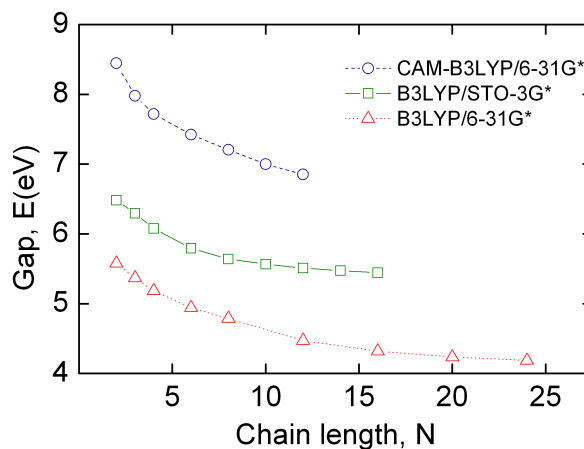


Figure 5.7: Dependence of the HOMO-LUMO gap in neutral molecules on the length of the PMPSi chain for utilized methods and basis sets.

### Distribution of states and orbitals

Distribution of states (DOS) for PMPSi for neutral and positive molecules is shown in Fig. 5.8. One can see, that prolongation of the polymer leads to the increase in the density of states in the vicinity of transport orbital. First blue bar from the left side on the Figs. 5.8(b) and 5.8(d) is vacant orbital, which emerged after electron removal. As the chain length increases, the density of states near the vacant orbital increases as well. Thus, a band for the hole transport is being formed.

Fig. 5.9 shows location of HOMO and LUMO orbitals in the PMPSi optimized molecules. The HOMO orbital in the neutral structure is localized on the main chain in Si-Si bond space. LUMO is mostly localized on the separated silicon atoms. Once, an electron is removed from the system and polaron is formed, HOMO orbital from the neutral molecule becomes LUMO orbital of the positive molecule. This orbital stays localized on the main chain as well (see Fig. 5.9(c)), as a further supporting evidence for the  $\sigma$ -delocalization. On the other hand, LUMO+1 orbital is localized on the phenyl rings. Thus, if the hole is induced by excitation, then excited electron will be probably localized on one of the pendant phenyls.

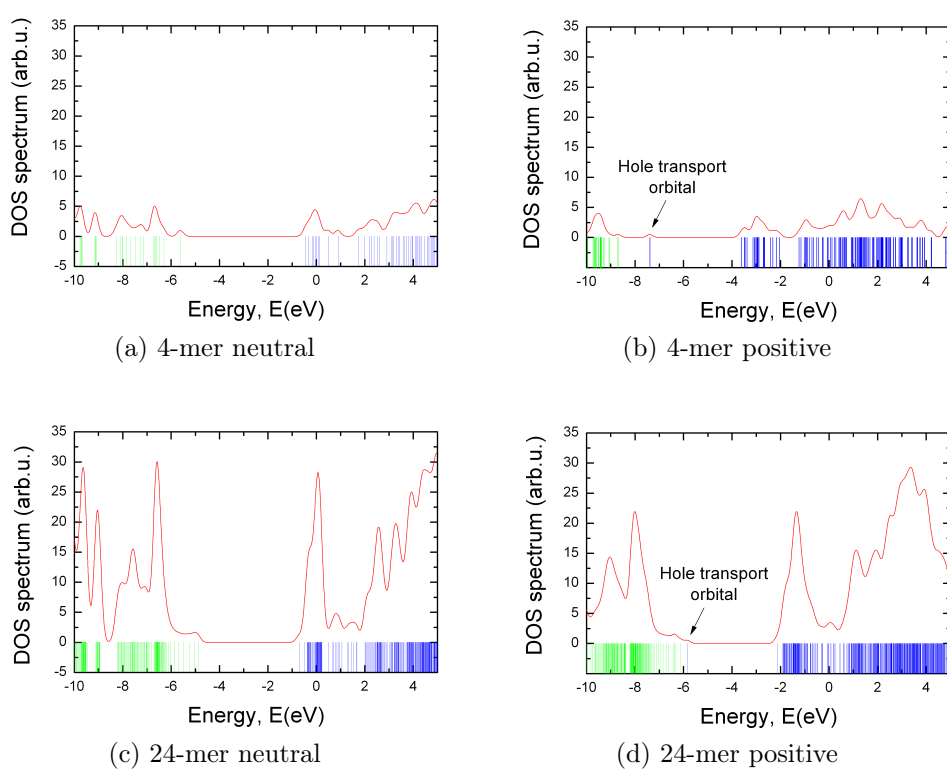


Figure 5.8: Density of states for PMPSi (B3LYP/6-31G\*). Green bars represent occupied orbitals, blue bars are virtual orbitals.

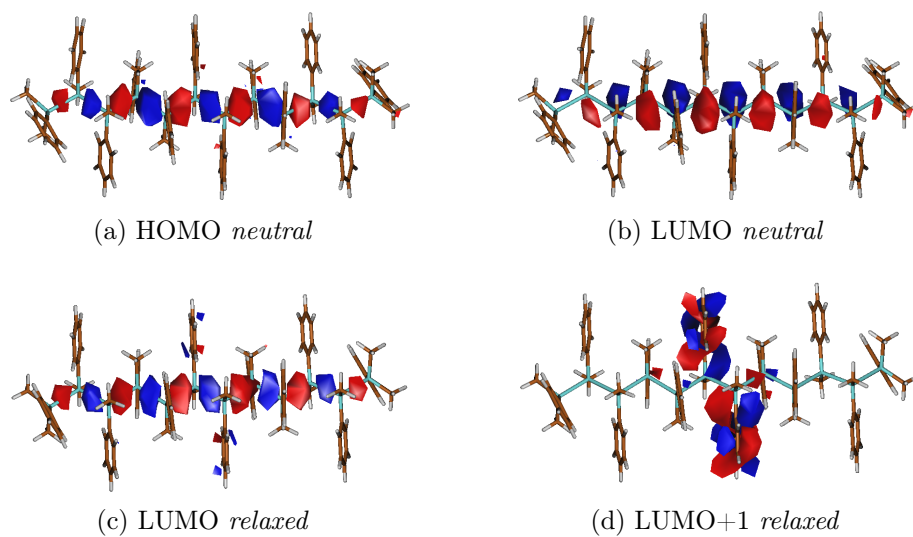


Figure 5.9: Comparison of important orbitals on the optimized neutral and positive geometries of MPSi-12-mer. Method B3LYP/6-31G\*.



### 5.1.2 PBMSi

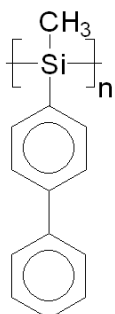


Figure 5.10: Chemical structure of poly[biphenyl(methyl)silylene] (PBMSi)

Structure of the poly[biphenyl(methyl)silylene] (PBMSi) molecule is very similar to PMPSi. Thus, this section will point out mostly differences between the two. When same observations and conclusions will be at hand, reader will be referred to the proper section in PMPSi part.

#### Structure

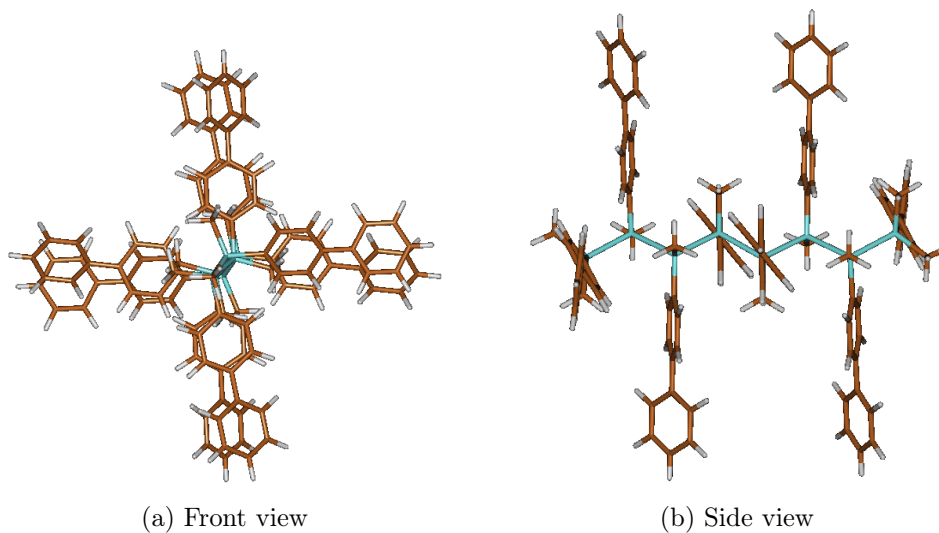


Figure 5.11: BMSi-8-mer molecule

PBMSi geometries follow the same rules as the geometries for PMPSi (see part 5.1.1). Scheme is given in Fig. 5.10 (weight of the monomer unit is 196.32 a.u.)

Table 5.4: Optimized parameters of neutral PBMSi. Values were obtained from optimized geometries of BMSi-10-mer, of its central part.

| Method/Basis set  | Si-Si dist. | Si-angle | Si-dihedral | Biphenyl angle |
|-------------------|-------------|----------|-------------|----------------|
| B3LYP/6-31G*      | 2.395Å      | 111.3°   | 172.1°      | 37.7°          |
| B3LYP/STO-3G*     | 2.275Å      | 112.5°   | 177.5°      | 31.8°          |
| CAM-B3LYP/6-31G*  | 2.369Å      | 111.1°   | 170.2°      | 39.9°          |
| CAM-B3LYP/STO-3G* | 2.259Å      | 111.3°   | 180.0°      | 32.8°          |

Table 5.5: Optimized parameters of positive PBMSi. Values were obtained from optimized geometries of BMSi-10-mer, of its central part.

| Method/Basis set  | Si-Si dist. | Si-angle | Si-dihedral | Biphenyl angle |
|-------------------|-------------|----------|-------------|----------------|
| B3LYP/6-31G*      | 2.426Å      | 105.4°   | 174.5°      | 36.2°          |
| B3LYP/STO-3G*     | 2.289Å      | 107.9°   | 180.0°      | 30.5°          |
| CAM-B3LYP/6-31G*  | 2.424Å      | 102.6°   | 177.8°      | 40.8°          |
| CAM-B3LYP/STO-3G* | 2.279Å      | 105.4°   | 180.0°      | 32.3°          |

Fig. 5.12 summarizes dependence of the biphenyl twist angle on the chain length. Level of conjugation of the biphenyl is strongly dependent on the value of this angle (follows the cosine-squared rule (Woitellier *et al.*, 1989)). Thus, it affects electronic properties and positions of the molecular orbitals. One can see that for short chains, the biphenyl twist angle is decreasing upon polaron formation. As the chain length increases, this effect vanishes.

### Infrared spectra

Infrared spectra of PBMSi were scaled using the same scale factors calculated for PMPSi in part 5.1.1. Comparison of IR spectra calculated on different level of theory and experimental spectrum obtained by the ATR method are shown in Fig. 5.13. Compared to the PMPSi, PBMSi IR spectrum is more complicated what follows from greater number of atoms in monomer unit. In general, the distribution of the differences between neutral and positive spectrum, however, follows the same rules as the PMPSi spectrum does (see Fig. 5.5), thus it is not shown here.

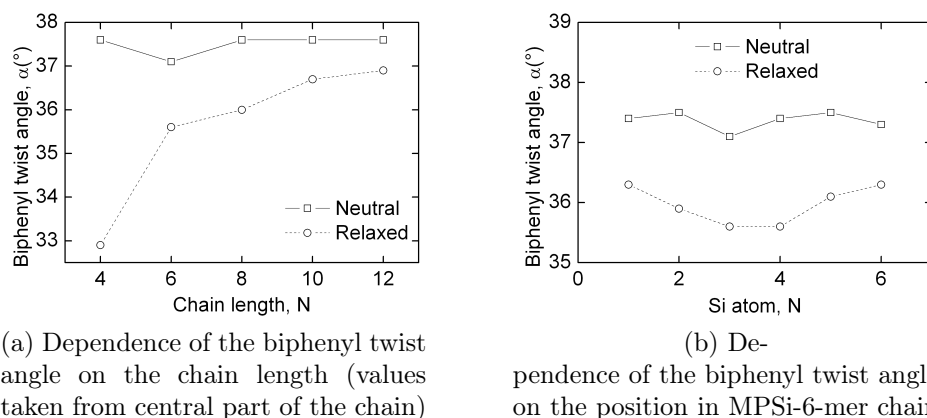


Figure 5.12: Changes of the biphenyl twist angle upon polaron formation. Calculated on the level B3LYP/6-31G\* (similar dependencies apply to other methods and basis sets utilized in this thesis.)

### Distribution of states and orbitals

Rules, which apply to the DOS of the PBMSi, are same as those valid for the PMPSi. Hence, I refer reader to the section 5.1.1. Important orbitals are shown in Fig. 5.14. The difference compared to the PMPSi is that LUMO orbital in neutral system is already localized on the phenyl rings. This concludes from the fact, that biphenyl, even if twisted (Venkataraman *et al.*, 2006), is partly conjugated and thus its orbital is lower in energy than that of single phenyl.

### 5.1.3 Summary and Discussion

Both polymers poses similar geometries. DOS and orbital analysis suggest that they should be good candidates for the hole transporting material. The reason, why two such similar molecules are investigated side by side is the difference between their side groups, i.e. phenyl versus biphenyl. Aim is to estimate the effect of size of the pendant groups and of the increased conjugation in these groups on the polaron binding energy.

One expected result is that the electron-phonon term (see part 4.1.4) will be greater in the PBMSi, since more vibration modes are present in this polymer.

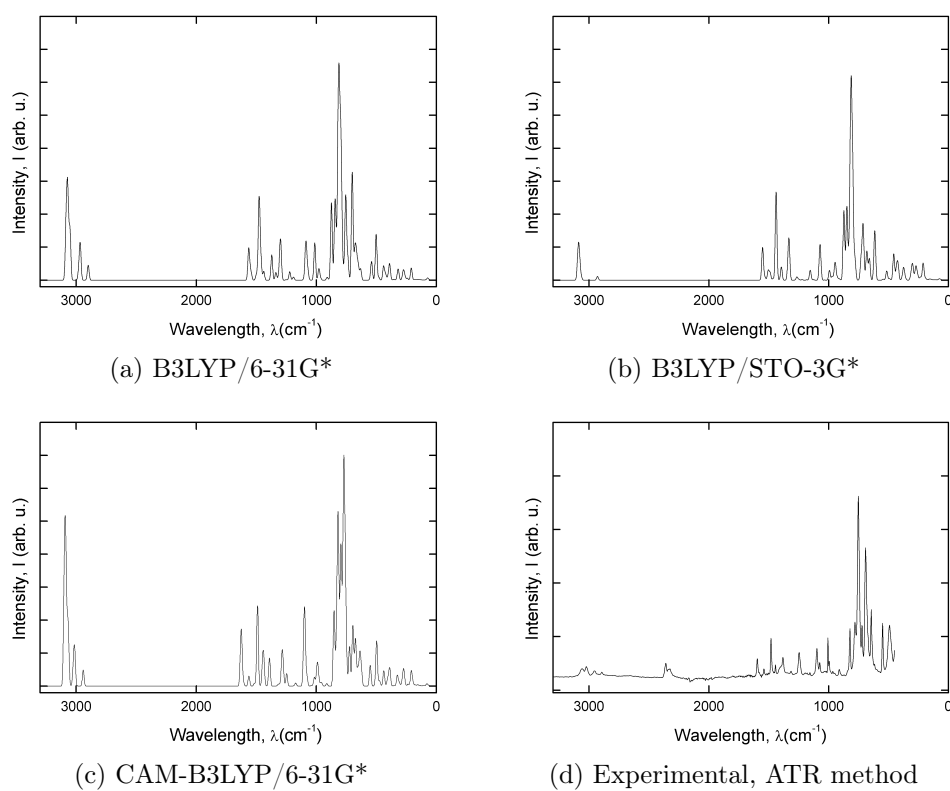


Figure 5.13: Comparison of IR spectra of the PBMSi. Theoretical plots are obtained from MPSi-6-mer. Experimental data were obtained by the ATR method.

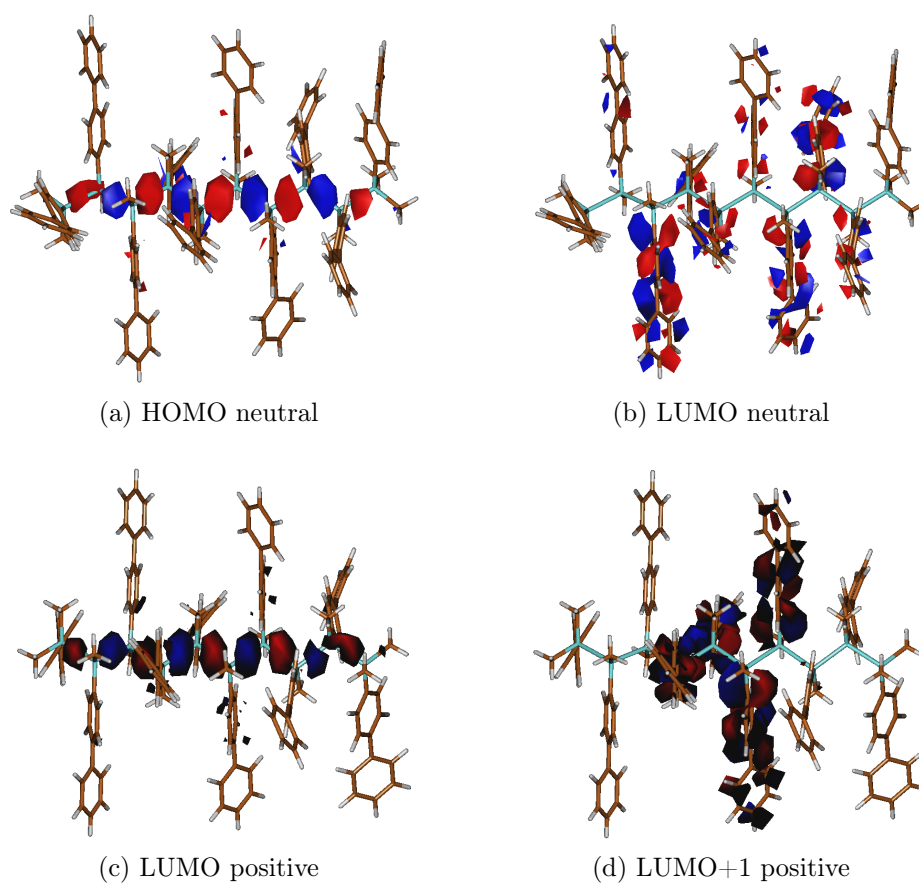


Figure 5.14: Comparison of significant orbitals on the optimized neutral and relaxed geometries of BMSi-12-mer. Method B3LYP/6-31G\*.

## 5.2 Phthalocyanines

Phthalocyanines (Pcs) are potential materials for gas sensing applications. Great number of derivatives of base core has been already synthesized, as properties of the molecules and bulk samples depends on central atom and side groups. In this thesis, I was concerned with Pcs substituted with sulphonamide alkyl groups.

### 5.2.1 Structures

There were two 3-diethylamino-1-propylsulphonamide substituted phthalocyanines studied in this work: one with zinc atom (ZnPcSu) and the other with two hydrogen atoms ( $H_2$ PcSu) in the center of the Pc skeleton (see Fig. 5.15(a), where central atom M stands for zinc atom for ZnPcSu phthalocyanine and represents two hydrogen atoms in case of for  $H_2$ PcSu).

The Pc structure was simplified for the purposes of theoretical modeling (see Fig. 5.15(b)). Side chains were shortened and their position was symmetrized in order to speed up the calculations. However general structure was kept undisturbed, thus we believe that simplification did not have any significant effect on results.

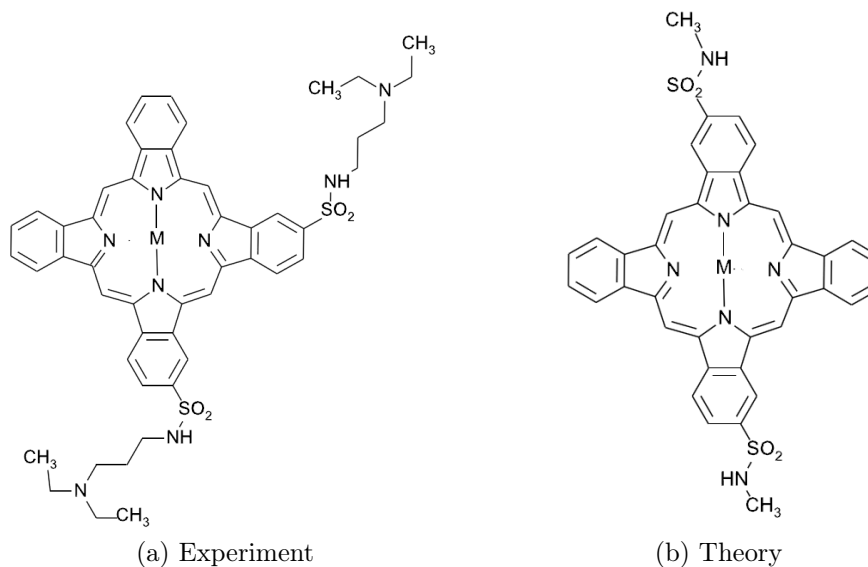


Figure 5.15: Structural formulas of PCs under study

Pcs have planar geometry and they tend to create self-organized layers of stacks. This  $\pi - \pi$  stacking then results in creation of 1-dimensional wire,

which can transport charge carriers. This feature can be with advantage employed in spectroscopic and electric measurements.

## 5.3 Degradation additives

Polysilanes are unstable materials under UV-illumination. The fact can be used with great advantage in technology of lithography (as explained in section 2.3). However, from industrial point of view, this degradation process is not fast enough. Thus, there is a need to study processes and methods which would lead to increased pace of decomposition.

Several electron acceptor molecules were modeled in order to find the mechanism of induced breakage of the polymer chain and point out the best candidates for the practical applications. These additives are supposed to act as catalysts of chain scission.

### 5.3.1 Structures

Altogether 8 electron acceptor (EA; with respect to PMPSi) molecules were modeled in my study of the polysilane degradation. For demonstration purposes, I have selected only two of them, which chemical structures are shown in Fig. 5.16 (other EAs gave similar or worse results than the ones presented here): 1,4-dicyanobenzene ( $C_6H_4(CN)_2$ , Sigma-Aldrich, CAS: 623-26-7; see Fig. 5.16(a)) and dibenzoyl peroxide ( $C_{14}H_{10}O_2$ , Sigma-Aldrich, CAS: 94-36-0, purified by crystallization; see Fig. 5.16(b)).

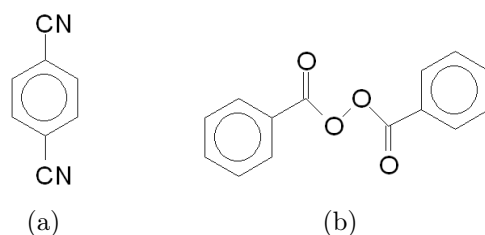


Figure 5.16: Model electron acceptors for polysilane degradation





# Chapter 6

## Results and Discussion

This chapter compiles results acquired on the systems presented in Ch. 5 with aid of methods described in Ch. 4. It is divided into several sections, where in each of them is discussed different topic, connects to the outcome of the previous and ends with a short conclusion.

First section (6.1) investigates the energetics of the polaron quasi-particle in silane polymers introduced in section 5.1. Both molecules are compared to each other on the basis of different side group and conformation changes upon polaron formation. Results here were achieved by purely quantum chemical calculations with Gaussian program package (Frisch *et al.*, 2003; Frisch *et al.*, 2009).

In the second section (6.2) the focus is shifted to delocalization length of the polaron, as this problem emerged from conclusions of the previous part. The dependence of the spin density on conformational disorder over the silicon chain is studied here. Molecular dynamics simulations allowed us to uncover time frame of polaron formation and its movement in environment with quasi-random effects.

In hopping model, polaron width represents jumping distance, which needs to be overcome in the process of electron transfer. Thus, once the delocalization length from the second section is known, the third section (6.3) can utilize it in quantification of the charge carrier mobility on the silicon chain.

Problems of stability of the polysilane chain in the presence of excess positive charge were inspected in the fourth section (6.4). Mechanism of polymer decomposition is proposed here and supported by the theoretical and experimental results with aid of the additives introduced in part 5.3. Based on it, methods how to stabilize or destabilize polysilane materials are suggested.

Last section (6.5) summarizes results acquired on phthalocyanines, which

are another model material for 1-D semiconductors. Transfer pipeline is formed by self-organized stacks, which hold together through weak interactions. This unique structure is investigated for possibility of manufacturing gas sensor based on variances in its conductivity.

## 6.1 Polarons in polysilylenes

Theoretical background and terms for this section were given in section 2.2.2 and computational methods were described in detail in sections 4.1.3 (deformation energy,  $E_{def}$ ) and 4.1.4 (electron-phonon term,  $E_{e-ph}$ ).

This section summarizes results of energetics of polaron formation in PMPSi and PBMSi polymers. Results were acquired at four different levels of theory: (1) B3LYP/6-31G\* level is well known and there are many references on its use for polysilane modeling (Toman *et al.*, 2002). (2) B3LYP/STO-3G\* utilizes rather small basis set, but it allowed us to calculate IR spectra for longer oligomers, and thus confirm the dependence of the polaron binding energy on chain length. Values obtained from simulations with this basis set were always taken into account with respect to the results of calculations with 6-31G\* basis set. (3) CAM-B3LYP/6-31G\* is relatively recent method (Yanai *et al.*, 2004). It improves long range interactions of the B3LYP method, which were expected to play significant role in polaron delocalization. (4) CAM-B3LYP/STO-3G\* was used for the same reason as the level (2). Results in the following text and tables will refer to these levels of theory according to their numbers for short.

### 6.1.1 PMPSi

**Charge distribution** Silicon backbone is positively charged even in the *neutral* state, while side phenyls have partial negative charge. The addition of an excess positive charge results in charge redistribution during the relaxation process which has only a minor effect on Mulliken charges on the Si atoms. The most of the excess charge is localized on the side groups, what follows from Columbic repulsions. Plots in the Fig. 6.1(a) represent charge distribution along the silicon backbone, and methyl and phenyl side groups. They were obtained by the following procedure: Si backbone was approximated by an axis, which connected the first and the last silicon atom in the chain. Then, perpendicular distances of the atoms in the side groups from this virtual axis were determined and atomic charges were summed up (e.g., if p-hydrogens on two different phenyls have the same distance of 6Å from the Si-axis and one of them has charge 0.2e and the other one 0.3e, then

the charge in the graph at distance  $6\text{\AA}$  is plotted as  $0.5e$ ). One has to take into account, when interpreting the curves in Fig. 6.1(a), that the values represent the charges obtained by the integration in angle of  $360^\circ$  around the Si-axis at the certain distance; different types of atoms, directions from the Si-axis and side groups are not distinguished (e.g., if hydrogen on methyl and carbon on phenyl have the same distance from the Si-axis, their charges were summed up). Also note, that scheme of the molecule in Fig. 6.1 is only schematic and does not comply with all-trans conformation of the modeled PMPSi molecule.

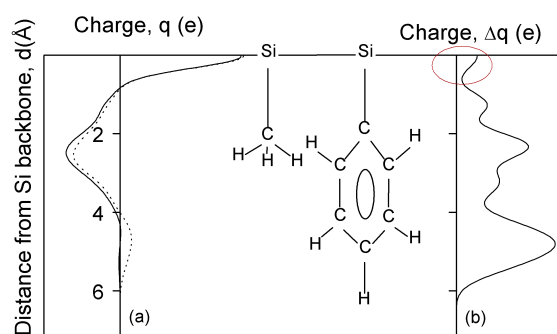


Figure 6.1: (a) Charge distribution on side phenyls and methyl groups of *neutral* (full line) and *relaxed* (dashed line) state of MPSi-8-mer (calculated on B3LYP/6-31G\* level; similar qualitative results were obtained at the other levels of theory). (b) Difference between the charge distributions on the side groups in *neutral* and *relaxed* state (difference of the curves in (a); see details in the text)

As follows from Fig. 6.1(b), which plots the difference between *relaxed* and *neutral* state, the most of the excess charge is localized on the side groups. Fig. 6.2(a) shows the partial charges on the Si atoms in *relaxed* form for all combinations of method/basis set. One can see, that the use of STO-3G\* basis set leads to greater concentration of the charge in the central region of the chain, compared with the results of 6-31G\* basis set (regardless of the method). Fig. 6.2(b) plots the difference of the charge distribution over the silicon atoms in the backbone between *neutral* and *relaxed* state. 6-31G\* basis set results significantly differ from the results obtained with STO-3G\* basis set, since it concentrates most of the additional charge to the central region of the chain again. Due to the Coulombic repulsion, one would expect that the excess charge would be localized mostly at the ends of the chain, just like results with 6-31G\* basis set suggest.

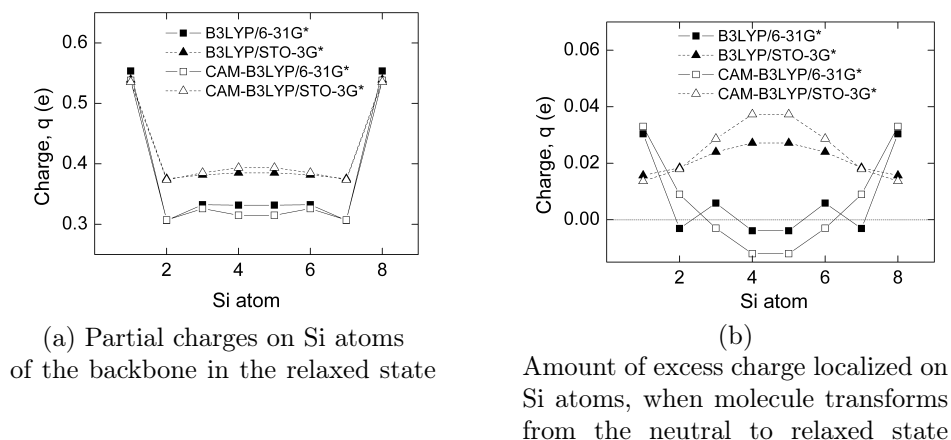


Figure 6.2: Partial charges on the silicon atoms of optimized MPSi-8-mers. Results obtained at B3LYP/6-31G\* (■), B3LYP/STO-3G\* (▲), CAM-B3LYP/6-31G\* (□) and CAM-B3LYP/STO-3G\* (△)

**Spin distribution** Level of the delocalization of the excess charge was studied through the spin distribution over the silicon backbone. Compared to the charge distribution, all levels of theory gave similar qualitative and quantitative results for it. Fig. 6.3(a) shows distribution of the spin densities on the side phenyl and methyl groups for *hot* and *relaxed* molecule of MPSi-8-mer (details of the creating these plots were described in the section 6.1.1). Fig. 6.3(b) shows the difference between spin distribution of *hot* and the *relaxed* state of MPSi-8-mer. In contrast with the charge distribution, the most of the excess spin density is localized on Si atoms (area marked with the ellipsis). Fig. 6.4(a) depicts the distribution of the spin density over the silicon backbone (detail study of this distribution can be found in (Toman *et al.*, 2002)), where one can see that the highest spin density is in the middle of the chain, as opposed to charge distribution (compare with Fig. 6.2(a)). Fig. 6.4(b) shows the dependences of the total spin densities on the chain length. The amount of the spin density on the silicon atoms increases with the length of polymer chain suggesting increasing conjugation. All levels of theory gave same qualitative results and only slightly differ in absolute values.

**Polaron binding energy** Tables 6.1.2 and 6.1.2 contains calculated values of deformation energy and electron-phonon term, respectively, for all utilized levels of theory and various oligomer lengths. According to the Eq. 4.4, the polaron binding energy is given as sum of both terms. One can see, that

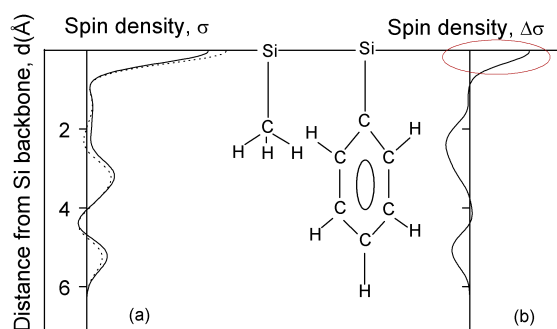


Figure 6.3: (a) Spin density distribution on side phenyls and methyl groups of *hot* (full line) and *relaxed* (dashed line) state of MPSi-8-mer (calculated on B3LYP/6-31G\* level; similar results were obtained at all the other levels of theory). (b) Difference between the spin density distributions on the side groups in hot and the relaxed state (difference of the curves in (a))

contribution of the deformation energy ( $E_{def}$ ) to the polaron binding energy ( $E_p$ ) is about 10 fold greater than contribution of the electron-phonon term ( $E_{e-ph}$ ). This is in contradiction with the results presented for molecular crystals (Silinsh & Capek, 1994). The difference arises from the fact that polymer chains are usually softer and are deformed more, than crystal lattice under the influence of the excess charge.

Table 6.1: Calculated values of the deformation energy,  $E_{def}$ , of PMPSi oligomers of different lengths and for all employed levels of theory. Values marked as n/a were not calculated due to excessive computer requirements. Numbers have following meaning: (1) B3LYP/6-31G\*, (2) B3LYP/STO-3G\*, (3) CAM-B3LYP/6-31G\* and (4) CAM-B3LYP/STO-3G\*

| Length | (1)   | (2)   | (3)   | (4)   |
|--------|-------|-------|-------|-------|
| 2      | 0.377 | 0.710 | 0.596 | 0.511 |
| 3      | 0.290 | 0.511 | 0.416 | 0.374 |
| 4      | 0.258 | 0.242 | 0.388 | 0.375 |
| 6      | 0.244 | 0.221 | 0.357 | 0.355 |
| 8      | 0.215 | 0.212 | 0.328 | 0.312 |
| 10     | n/a   | 0.191 | 0.298 | 0.290 |
| 12     | 0.183 | 0.174 | 0.286 | 0.270 |
| 14     | n/a   | 0.155 | n/a   | 0.255 |
| 16     | 0.137 | 0.143 | 0.261 | 0.221 |

|    |       |     |       |       |
|----|-------|-----|-------|-------|
| 20 | 0.106 | n/a | 0.249 | 0.220 |
| 24 | 0.103 | n/a | n/a   | n/a   |

Absolute values of the deformation energy for method B3LYP are in very good agreement for both basis sets for chains longer than 3 monomer units. Values obtained by CAM-B3LYP method are significantly greater. On the other hand, electron-phonon term calculated with the STO-3G\* basis set is about three times greater than value obtained for both methods with 6-31G\* basis set, which even yields negative values for longer oligomers. Since the  $E_{e-ph}$  term is given by difference of vibration frequencies, negative outcome would suggest increase of vibration frequencies, which could be interpreted as bond strengthening. In fact, some of the bonds in the polymer molecule are shortened upon electron removal. However, since infrared spectrum with this basis could be calculated for few different lengths only, we cannot conclude if this is just a fluctuation, error in calculations or consistent behavior. In general, both terms tend to decrease with increasing chain length.

Table 6.2: Calculated values of the electron-phonon term,  $E_{e-ph}$ , of PMPSi oligomers of different lengths and for all employed levels of theory. Values marked as n/a were not calculated. (1) B3LYP/6-31G\*, (2) B3LYP/STO-3G\*, (3) CAM-B3LYP/6-31G\* and (4) CAM-B3LYP/STO-3G\*

| Length | (1)    | (2)   | (3)    | (4)   |
|--------|--------|-------|--------|-------|
| 2      | 0.000  | 0.062 | 0.001  | 0.060 |
| 3      | 0.018  | 0.064 | 0.002  | 0.060 |
| 4      | 0.014  | 0.062 | -0.012 | 0.052 |
| 6      | -0.010 | 0.044 | -0.022 | 0.045 |
| 8      | -0.011 | 0.037 | -0.028 | 0.036 |
| 10     | n/a    | 0.041 | n/a    | 0.035 |
| 12     | n/a    | 0.039 | n/a    | 0.042 |
| 14     | n/a    | 0.038 | n/a    | 0.037 |
| 16     | n/a    | 0.042 | n/a    | n/a   |

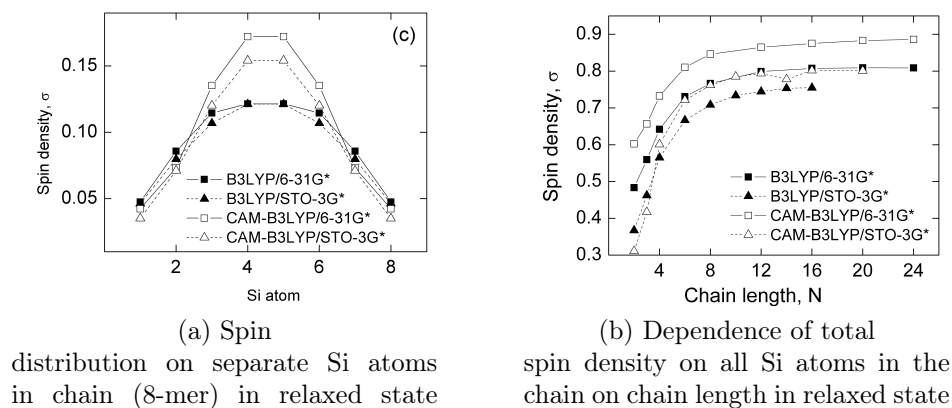


Figure 6.4: Spin distribution in PMPSi molecule. Results obtained at B3LYP/6-31G\* (■), B3LYP/STO-3G\* (▲), CAM-B3LYP/6-31G\* (□) and CAM-B3LYP/STO-3G\* (△) level of theory

Dependence of the deformation energy and polaron binding energy on the chain length is shown in Fig. 6.5. Values for all utilized levels of theory exhibit steadily decreasing dependency for the chain lengths greater than 3 monomer units. The first two points were not taken into account, since they are obviously out of range due to extreme deformations that take place on them. Anyhow, such short chains are not important for the charge carrier transport phenomenon in polymers. From the qualitative point of view, all combinations of methods and basis sets provide similar results. Slight saturation is visible for the longest modeled chains, as one would expect.

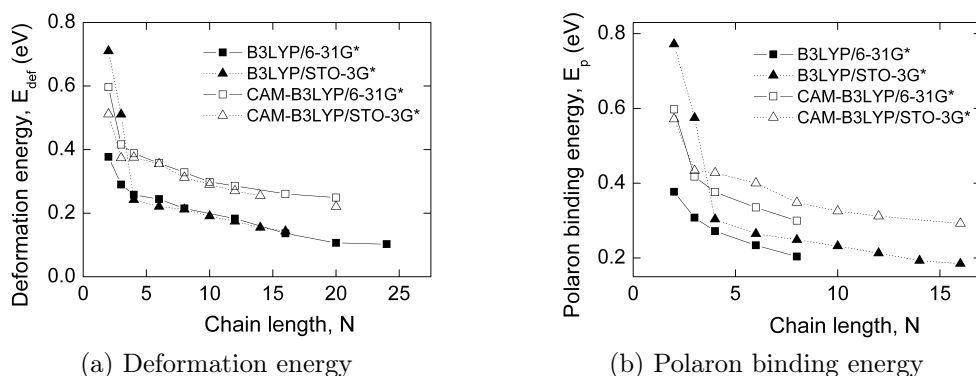


Figure 6.5: Dependences of the deformation energy (a) and the polaron binding energy (b) on chain length (in number of monomer units) for PMPSi. Results obtained at B3LYP/6-31G\* (■), B3LYP/STO-3G\* (▲), CAM-B3LYP/6-31G\* (□) and CAM-B3LYP/STO-3G\* (△)

## 6.1.2 PBMSi

Results for the charge and spin distribution of PBMSi are very similar to the plots presented for the PMPSi polymer. Thus, all conclusions are virtually the same and reader is referred to the previous section 6.1.1. This section provides only final values of the polaron binding energy and its components.

**Polaron binding energy** The plot of the deformation energy and the polaron binding energy does not obey the same dependence as results for the PMPSi. As one can see from Fig. 6.6, the dependence is very flat for chains shorter than 8-12 monomer units and then it starts to descent in the same manner as the PMPSi results (see Fig. 6.5).

Since only difference between PBMSi and PMPSi is in their side groups, we looked for the reason for this extraordinary behaviour there. Biphenyl group consists of two phenyls, which are connected to each other by a single bond. Generally, this molecule is not planar, the rings are skewed towards each other. It is well known phenomenon, that extent of the conjugation is dependent on this angle. Thus, it affects charge carrier transport within the molecule. Figure 6.7 shows the dependence of the difference between average twist angle in the biphenyl group in *neutral* and *relaxed* molecules of the same length (biphenyls on the very edge of the oligomer chain were omitted from the mean value calculation, since their value was approximately same for all investigated lengths). The actual plot in the figure is obtained from the geometries optimized on the CAM-B3LYP/STO-3G\* level of theory,



but qualitatively similar results hold for all four employed combinations of the method and basis set.

Straightening of the twist angle of the biphenyl results in increased delocalization of the electrons in the molecule. Thus, deficit of one electron in the *relaxed* state can be more effectively compensated, what results in flat dependence of the polaron binding energy on the chain length (see Fig. 6.5(b)). Once, this effect vanishes at the length of about 6-8 monomer units, the dependence starts to descend. We suggest, that this is caused by the following: when biphenyl twist angle stops lowering upon polaron formation, electrons are not anymore effectively transferred to the silicon backbone, and thus cannot compensate the missing electron. When this happens, plot starts to point down as it normally should.

Table 6.3: Calculated values of the deformation energy,  $E_{def}$ , of PBMSi oligomers of different lengths and for all employed levels of theory. Values marked as n/a were not calculated due to excessive computer requirements. Numbers have following meaning: (1) B3LYP/6-31G\*, (2) B3LYP/STO-3G\*, (3) CAM-B3LYP/6-31G\* and (4) CAM-B3LYP/STO-3G\*

| Length | (1)   | (2)   | (3)   | (4)   |
|--------|-------|-------|-------|-------|
| 2      | 0.155 | 0.154 | 0.372 | 0.279 |
| 3      | 0.134 | 0.108 | 0.304 | 0.236 |
| 4      | 0.137 | 0.106 | 0.325 | 0.265 |
| 6      | 0.184 | 0.133 | 0.324 | 0.294 |
| 8      | 0.146 | 0.135 | 0.304 | 0.273 |
| 10     | 0.162 | 0.130 | 0.315 | 0.261 |
| 12     | 0.146 | 0.120 | 0.312 | 0.244 |
| 14     | n/a   | n/a   | n/a   | 0.257 |
| 16     | n/a   | n/a   | n/a   | 0.223 |
| 20     | n/a   | n/a   | n/a   | 0.204 |

Table 6.4: Calculated values of the electron-phonon term,  $E_{e-ph}$ , of PBMSi oligomers of different lengths and for all employed levels of theory. Values marked as n/a were not calculated due to extensive computer requirements. Numbers have following meaning: (1) B3LYP/6-31G\*, (2) B3LYP/STO-3G\*, (3) CAM-B3LYP/6-31G\* and (4) CAM-B3LYP/STO-3G\*

| Length | (1)    | (2)   | (3)    | (4)   |
|--------|--------|-------|--------|-------|
| 2      | 0.000  | 0.055 | 0.006  | 0.071 |
| 3      | -0.008 | 0.065 | 0.005  | 0.066 |
| 4      | -0.001 | 0.064 | -0.015 | 0.054 |
| 6      | -0.020 | 0.048 | -0.010 | 0.047 |
| 8      | n/a    | 0.051 | n/a    | 0.049 |
| 10     | n/a    | 0.045 | n/a    | 0.042 |
| 12     | n/a    | 0.049 | n/a    | 0.042 |

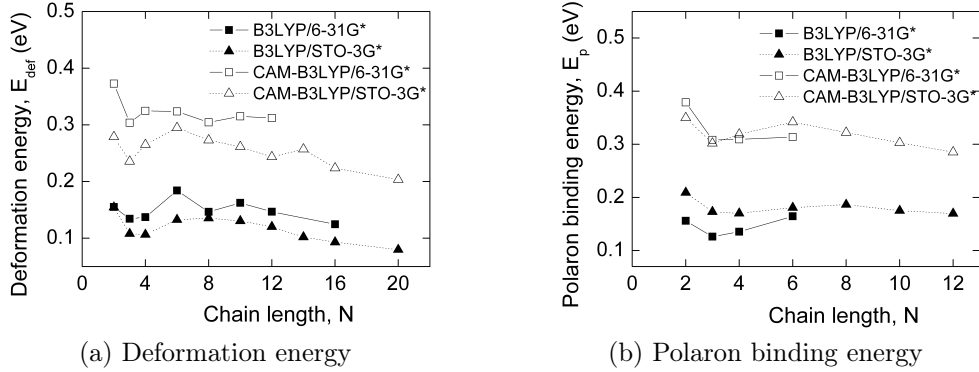


Figure 6.6: Dependences of the deformation energy (a) and the polaron binding energy (b) on chain length (in number of monomer units) for PBMSi. Results obtained at B3LYP/6-31G\* (■), B3LYP/STO-3G\* (▲), CAM-B3LYP/6-31G\* (□) and CAM-B3LYP/STO-3G\* (△)

### 6.1.3 Summary and Discussion

As presented above, values of the polaron binding energy for PMPSi and PBMSi, differ in some aspects. Comparison of dependencies of polaron binding energy for both molecules at the CAM-B3LYP/STO-3G\* level of theory can be found in Fig. 6.8. Similar plots are valid for all the other combinations of methods and basis sets. In general, for short chains, the deformation

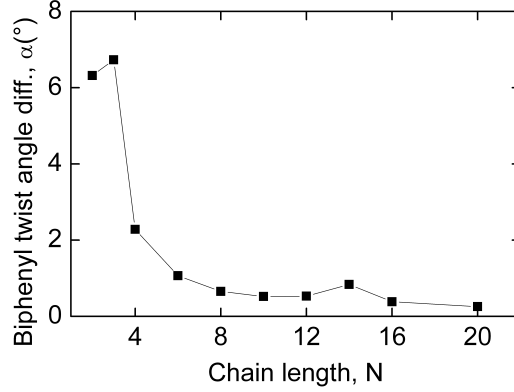


Figure 6.7: Difference of dihedral angle of biphenyl in PBMSi in *neutral* and *relaxed* form. Values obtained at the level of CAM-B3LYP/STO-3G\*.

energy  $E_{def}$  (as well as the polaron binding energy  $E_p$ ) are smaller for the PBMSi. As explained in the previous sections, this is the result of biphenyl group in the PBMSi molecule, which is capable of narrowing its twist angle under the influence of the polaron. Thus, allowing for better redistribution of the electrons in the molecule. As the chain length increases, differences in the values diminishes and energetic properties of polaron in PMPSi and PBMSi converge to very similar value.

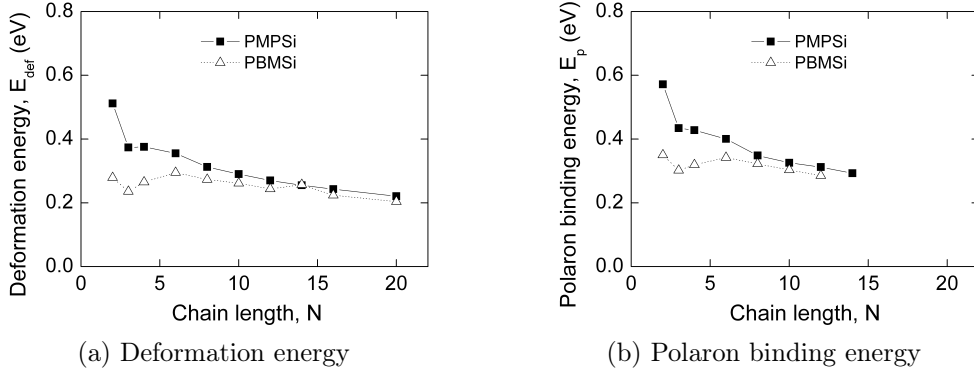


Figure 6.8: Comparison of dependence of the polaron energy properties for PMPSi (■) and PBMSi (△) at the CAM-B3LYP/STO-3G\* level of theory.

Since, deformation energy is calculated as difference between electronic energies, it must be strongly dependent on charge distribution in the molecule. Fig. 6.9 plots the following equation

$$\Delta q = \Delta q_{PMPSi} - \Delta q_{PBMSi}, \quad (6.1)$$

where  $\Delta q_{PMPSi}$  and  $\Delta q_{PBMSi}$  is difference of total charge on all Si atoms in the chain in *relaxed* and *neutral* state for PMPSi and PBMSi, respectively. This difference represents amount of additional charge localized in the central part of the molecule, which contributes most to the deformation (due to greater coulombic interaction, localized charge will cause more significant deformation of the skeleton, than the one evenly distributed over the volume or surface of the molecule). Then difference of these values is relative representative of the differences between deformation energies in both polymers. One can see, that for short chains the difference is greater and in favor of the PMPSi polymer, corresponding with the higher value of the deformation energy in this region. As the chain grows longer, the difference decreases, what complies with the results, that for chains longer than about 8 monomer units, the deformation energies are similar for both polymers.

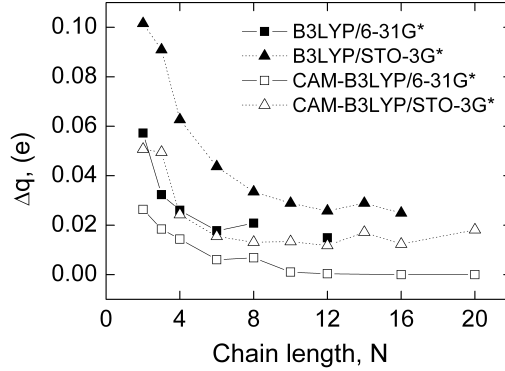


Figure 6.9: Comparison of difference of charge localized on the main chain in *relaxed* and *neutral* state of PMPSi and PBMSi (see Eq. 6.1) for different levels of theory: B3LYP/6-31G\* (■), B3LYP/STO-3G\* (▲), CAM-B3LYP/6-31G\* (□) and CAM-B3LYP/STO-3G\* (△)

As shown here, even though PBMSi polymer is significantly larger, deformation energy of the polaron (and also electron-phonon term; and thus, polaron binding energy) is similar in absolute value to the PMPSi polymer. Thus, the number of atoms per monomer unit is not as important to the energetic polaron properties as is the ability to redistribute the charge over the molecule's volume.

## 6.2 Polaron delocalization length

As found in previous section, delocalization length of the polaron is determining factor of the polaron binding energy. I believe that quantum chemical

calculation performed over single molecule cannot provide reliable estimation of the true extent of the polaron length in real materials. The reasoning is based on the fact, that unless simulations operate on the basis of statistical methods, they cannot capture all possible conformations accessible to the polymer chain.

In further text, I will present results, which were acquired by means of the *Molecular dynamics* (MD) methods. Randomness is introduced into the molecule, thus, many conformations can be explored. Computational details and methods utilized can be found in section 4.2.

### 6.2.1 Influence of conformational deformations on Si-backbone

Following results demonstrate importance of geometry conformation to the delocalization length of hole on the silicon backbone in PMPSi and PBMSi. Even a minor change in ideal parameters can lead to significant polaron localization. Tab. 6.5 shows initial geometry parameters for the calculations (parameters from 12-mer optimized geometry of neutral molecule; B3LYP/6-31G\* level of theory).

Table 6.5: Ideal parameters used for demonstration of the impact of geometry nuances on the polaron delocalization length in PMPSi and PBMSi

| Parameter         | PMPSi   | PBMSi   |
|-------------------|---------|---------|
| Si-Si bond        | 2.389 Å | 2.395 Å |
| Si-angle          | 111.6°  | 111.3°  |
| Si-dihedral angle | 173.7°  | 172.1°  |

Based on these parameters an ideal chain of length 100 monomer units was built, where all neighboring Si atoms obeyed values from Tab. 6.5. Other structural parameters were left with some randomness. Distribution of the spin densities on the silicon atoms in such an ideal chain is shown in Fig. 6.10 (plot is not smooth due to the slight randomness of parameters in the side groups which was kept on purpose).

In further calculations, ideal chain was intentionally disturbed, in order to uncover the impact of main chain geometry parameters on the delocalization length of the polaron. Starting from the 50<sup>th</sup> silicon atom either bond length, angle between silicon atoms or silicon dihedral angle was increased or

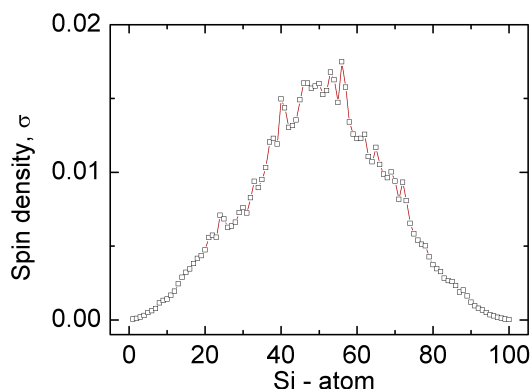


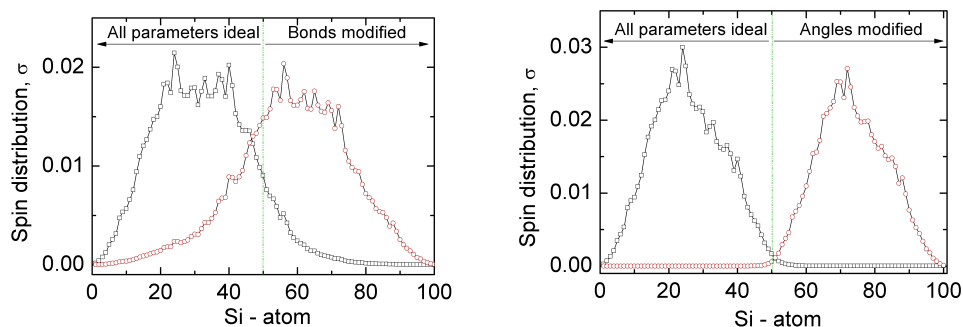
Figure 6.10: Spin distribution on the silicon atoms of an ideal chain (obeying parameters from Tab. 6.5); HückelExtended method.

decreased. Thus, only first 50 monomer units were maintained at the artificial ideal geometry conformation. Resulting spin distribution over the chain are shown in Fig. 6.11.

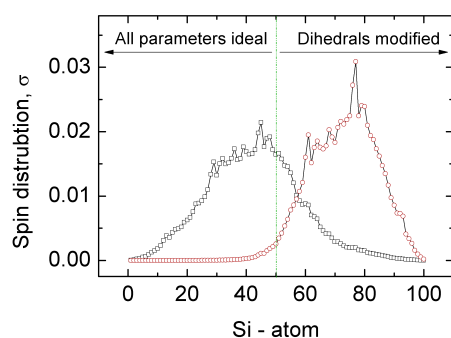
Results for different distortions in chain show that distribution in the PMPSi molecule is strongly affected by steric modifications. Silicon bonds in Fig. 6.11(a) are altered only by 0.5% and it leads to complete distinction on which half of the chain the polaron is localized. On the other hand, angles had to be modified by about 5% to achieve comparable localization. Hence, it seems, the spin density tends to localize in areas, where silicon atoms are closer to each other.

In order to confirm this theory, several ideal chains with single defect were created. In these, only one Si-Si bond, angle or dihedral angle in the central section of the chain was altered. Spin densities for chains that has one parameter increased are shown in Fig. 6.12. One can see that increased parameter acts as barrier since it brings silicon atoms apart. Polaron localizes on one side of it. Which it is, is given by actual randomness in side groups and length of chain available on each side of the barrier.

On the other hand, when a single bond, angle or dihedral angle is decreased it brings silicon atoms closer to each other. Hence, polaron should localize itself in the vicinity of such defect. In fact, this is true as shown in plots of spin distribution in Fig. 6.13. Parameter decreased by as little as 5% acts as potential well, where the charge carrier is localized. Spin distribution has very strong response to decrease in all parameters.



(a) Bonds prolonged to  $2.4 \text{ \AA}$  ( $\circ$ ) or shortened to  $2.38 \text{ \AA}$  ( $\circ$ )      (b) Angles increased to  $115^\circ$  ( $\circ$ ) or decreased to  $105^\circ$  ( $\circ$ )



(c) Dihedral angles increased to  $180^\circ$  ( $\circ$ ) or decreased to  $165^\circ$  ( $\circ$ )

Figure 6.11: Distribution of the spin density over the silicon atoms in chain. In each plot one of the parameters is disturbed starting from the  $50^{\text{th}}$  silicon atom.

## 6.2.2 Localization-time evolution

Time evolution of the localization of the polaron in model polysilylenes was studied using *Molecular dynamics* (MD) method described in section 4.2. Initial geometry was again the 100 monomers long ideal polymer chain. This artificial structure was used because none ab-initio method could optimize such large structure in reasonable time and amount of memory required.

### Short-term

Short-term results were obtained from MD trajectory, which was calculated with the following settings:

- ▷ Step = 0.1 fs

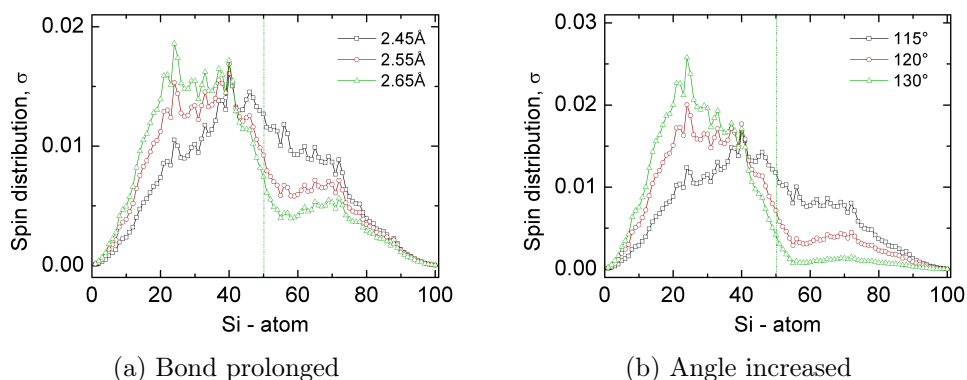


Figure 6.12: Distribution of the spin over the silicon atoms in chain. In each plot one of the parameters is increased in the central part of the chain (exact position is marked with vertical green dash-dot line).

- ▷ Quenching = 1 quenching cycle after each 1fs of the trajectory (at this point, geometry snapshot was created)
- ▷ Total time = 100 fs
- ▷ ForceField = Compass
- ▷ Statistical Ensemble = NVT
- ▷ Temperature = 298 K

After thermal activation, ideal chain of the PMPSi deforms rapidly. Several snapshots of the geometries were taken from molecular dynamics trajectory. These were then examined for basic structural parameters of silicon backbone, and spin distribution over the silicon main chain was calculated for them. Such structural snapshots for central part of the chain are shown in Fig. 6.14.

Short-term evolution of the spin distribution over the silicon backbone is shown in Fig. 6.15. One can see, that at initial point at the time 0 fs, the polaron is distributed over the most of the chain length. As time progresses, delocalization length decreases and polaron localizes itself. At the time of 50 fs it reaches its minimum width of about 20 monomer units for PMPSi. For PBMSi polymer chain, the localization time seems to be slightly shorter, about 30 fs, and short term evolution suggests, that localization length is smaller as well (about 10-15 monomer units). However, the snapshots of geometries in Fig. 6.15 are taken from the trajectory, which has not used quenching. Thus, structures are not optimized to its minimum energy, not even in the sense of molecular dynamics. Therefore, only conclusion, which can be derived from these results is the approximate estimation of the localization



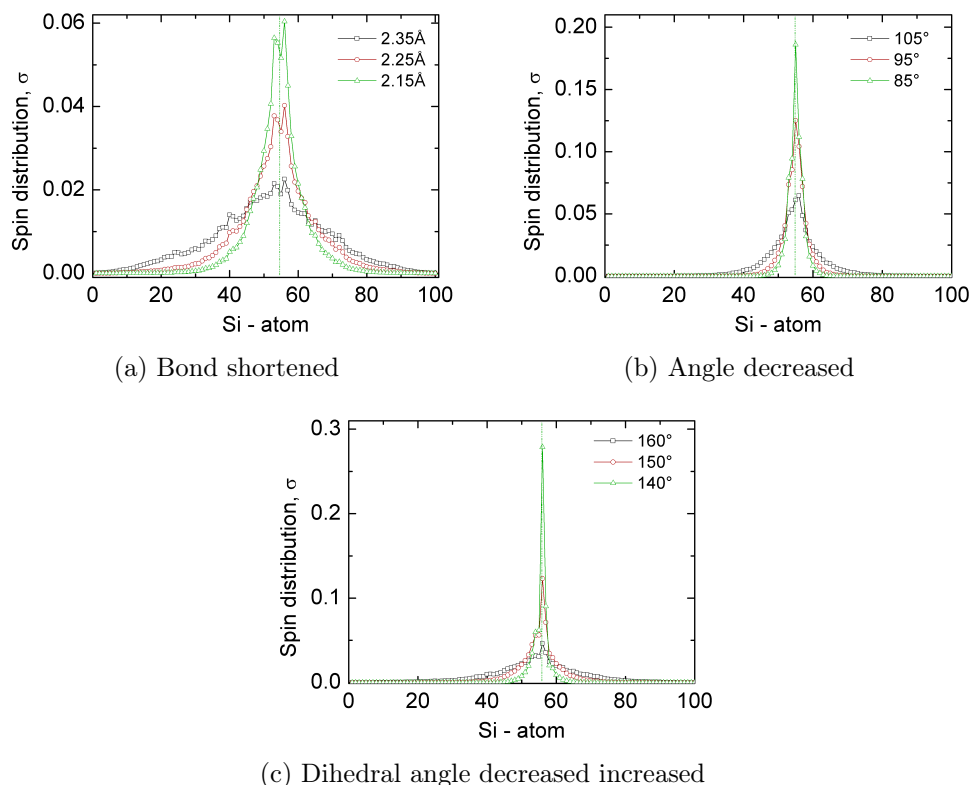


Figure 6.13: Distribution of the spin over the silicon atoms in chain. In each plot one of the parameters is decreased in the central part of the chain (exact position is marked with vertical green dash-dot line).

time.

In previous part 6.2.1, I have shown and discussed influence of the conformation changes on the polaron width. These seem to be driving force of the polaron localization as seen in Fig. 6.15. Fig. 6.16 shows the distribution of the spin, Si-Si bond lengths, Si-angles and dihedral angles of single snapshot geometry from MD trajectory. One can see, that all structural parameters fall into wide range of values. Even though, the distribution seems to be random, in case of Si-Si bond plot, we can find coincidence between position of the polaron (as calculated by the spin distribution) and area of decreased bond lengths. This pattern can be found on all snapshots taken at different times. The plot itself contains more than one of these regions, where silicon bonds are below the average value (e.g. chain part 0 - 10 monomer units in Fig. 6.16(b)), but none of them is wide enough to accommodate the polaron. As shown in section 6.1, polaron binding energy strongly depends on

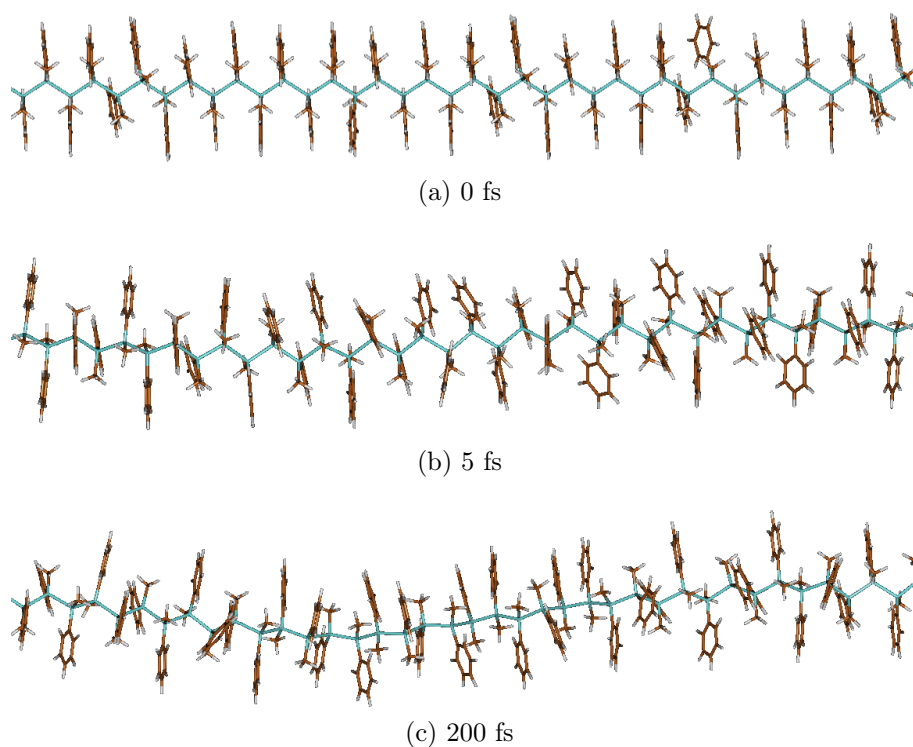


Figure 6.14: Snapshot geometries of cation radical PMPSi from molecular dynamics trajectory at 298K. Simulation started from ideal 100-mer chain. Shown are only 40 monomer units from central part of the chain.

its width. Thus, if it would be localized in the area of 10 monomer units, its energy would grow against general principle: all systems seek the ground state with minimal energy.

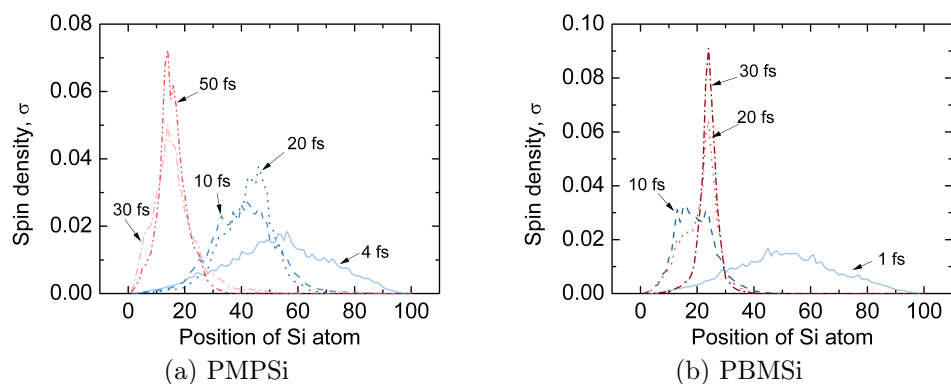


Figure 6.15: Short-term evolution of the spin distribution over the polymer chain. Geometry snapshots taken from molecular dynamics trajectory without optimization.

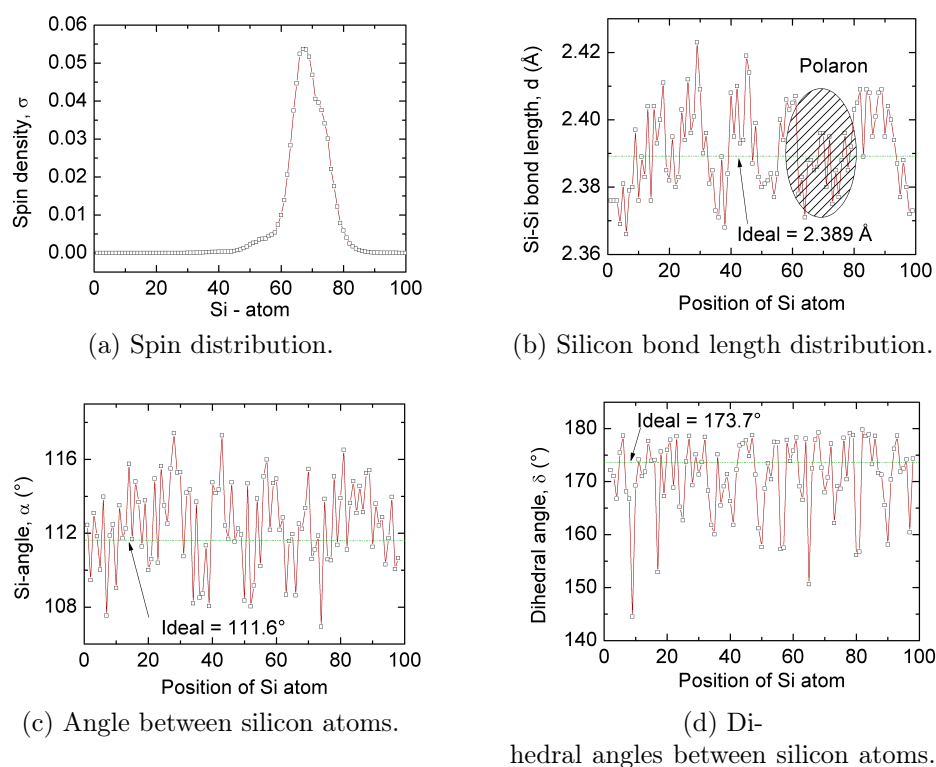


Figure 6.16: Comparison of the spin distribution over the backbone of PMPSi 100-mer with distribution of structural parameters. Snapshot geometry taken from MD calculations at 200 fs.

### Long-term

Long-term results were obtained from MD trajectory, which was calculated with following settings:

- ▷ Step = 0.1fs
- ▷ Quenching = Quenching to the minimum after each 1fs of the trajectory (at this point, geometry snapshot was created)
- ▷ Total time = 100 fs
- ▷ ForceField = Compass
- ▷ Statistical Ensemble = NVT
- ▷ Temperature = 298K

Once the polaron is localized, its width does not change anymore (at least not significantly). However, it moves on the chain, while dragging the deformation along. This movement can be clearly observed in the geometries gathered from long-term molecular dynamics calculations. Several of those are shown in Fig. 6.17. One can see, that the final optimized polaron width is similar in both polymers. By width of the polaron we understand the span of the spin density, which accounts for 90% of total spin density on all silicon atoms in the chain. Its value is approximately 19 monomer units for PMPSi and about 22 monomer units PBMSi.

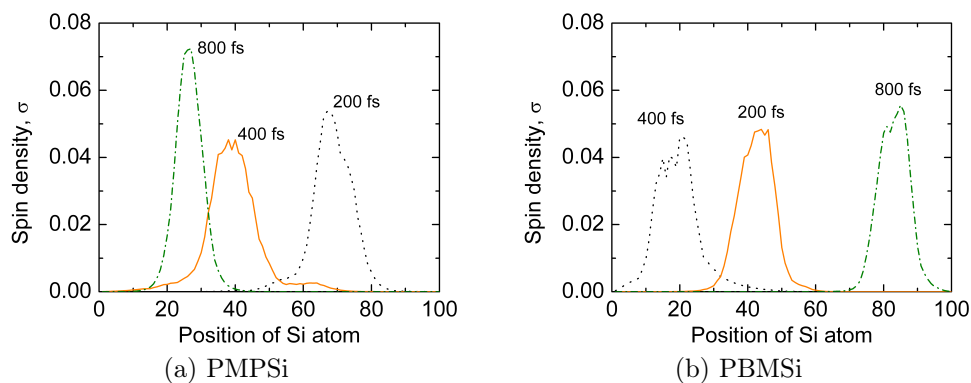


Figure 6.17: Long-term evolution of the spin distribution over the polymer chain. Geometry snapshots taken from molecular dynamics trajectory without optimization.

### 6.2.3 Summary and Discussion

The delocalization length of the charge carrier corresponds to the polaron width which is essential in determining the polaron binding energy. It has

been shown that structural defects leads to rapid localization of the polaron and thus they increase its energy. In general, the closer the silicon atoms in chain are, the greater the delocalization length can be achieved. However, if such defect is very limited in its extent over the silicon chain, then it will, on contrary, cause a decrease in delocalization length; it will create potential well, where polaron is localized (see Fig. 6.13). At this point, I doubt that significant bond length decrease is possible in real chain. However, angle and dihedral angle defects are certainly very common (e.g. they occur on the edges of lamellar crystallinities) thus they limit the polaron width significantly.

Actual localization of the polaron is fast process and according to recorded results it takes about 50 fs in PMPSi, and 30 fs in PBMSi to relax. This pace is comparable with the fastest vibration in studied polymers (C-H stretching has vibration period of 10 fs). Thus, it is possible to say that in polysilylene the complete relaxation of the charge carrier occurs at each hopping site.

Many approximations were introduced into the model presented here. The most questionable is the accuracy of bond lengths after MD calculations. Since in section 6.2.1 we have shown that this parameter has great influence on the polaron width, one can argue that MD geometries are not as reliable as geometries acquired from Quantum chemical methods. This is certainly true, however, the localization is not as much governed by the absolute length of bonds (or other structural parameters), but by the difference between actual residual site and neighborhood. Therefore, if geometry contains region where silicon atoms are closer to each other compared to the surroundings, then polaron will be most probably localized at that section of the chain.

EHMO method was used, because none ab-initio method could calculate such large system at reasonable time and computer resources. But as shown in Fig. 4.3 it offers very similar spin distribution as CAM-B3LYP/6-31G\* level of theory. Thus, we believe that its usage is reasonable and results are reliable at least at qualitative level.

Recorded delocalization length of 19/22 monomer units is in good agreement with experimental value obtained by (Irie & Irie, 1997), who measured absorption spectra of poly(methyl-n-propylsilylene) of different lengths and acquired value of 16 monomer units. Also Tachikawa (Tachikawa, 2007) performed similar simulation as we presented in this section, with different method for poly(dimethylsilylene) and came to similar results.

When all the results are put together (poly(dimethylsilylene), PMPSi and PBMSi), it seems that the delocalization length increases with the size of the side groups. This conclusion follows directly from the fact, that steric effects of larger groups more effectively hinder angle and dihedral angle variations. We suppose, that bond length variation is not significantly influenced by the

side groups. Tab. 6.2.3 shows actual values of FWHM of these properties in PMPSi and PBMSi. One can see, that FWHM of bond length distribution is same for both polymers, while the angles and dihedral angles is broader for the PMPSi chains than for PBMSi. Therefore, the polaron delocalization length is slightly smaller in PMPSi.

Table 6.6: FWHM of the distributions of silicon backbone properties. Values were obtained as average from 10 optimized geometries from MD trajectory.

| Property        | PMPSi | PBMSi |
|-----------------|-------|-------|
| Bonds           | 0.02Å | 0.02Å |
| Angles          | 4.07° | 3.60° |
| Dihedral angles | 9.73° | 7.33° |

### 6.3 Charge carrier mobility in polysilylenes chain

In polymer material, two mobilities needs to be taken into consideration: (1) intra-chain mobility, i.e. motion of the carrier along conjugated skeleton of the molecule; and (2) inter-chain mobility, which is provided by jumps of the charge carrier between two adjacent sites and is solely described by the hopping model.

In this thesis, we were only concerned with the intra-chain mobility. This is partly described by band conduction model, when the charge carrier moves along the conjugated regions of the molecule, and hopping model, when conjugation is distorted by chemical or steric effect.

Model equation for the mobility was presented in the theoretical part of this thesis. For convenience I will reproduce it here:

$$k_{et} = \frac{4\pi^2}{\hbar} \frac{1}{\sqrt{4\pi\lambda k_B T}} t^2 \exp\left(-\frac{(\lambda + \Delta G^0)^2}{4k_B T}\right), \quad (6.2)$$

where  $\lambda$  is reorganization energy,  $k_{et}$  is self-exchange rate and  $t$  is electronic coupling. Since, transfer between equivalent sites only will be calculated, the free energy difference  $\Delta G^0$  is zero. Reorganization energy in our model is given as

$$\lambda = E_{def} + E_{redef} + \Delta E_{e-ph}, \quad (6.3)$$

where  $E_{def}$  is the deformation energy,  $E_{redef}$  is the redeformation energy,  $\Delta E_{e-ph}$  is the dynamic electron-phonon term <sup>1</sup>.

<sup>1</sup>Note, that we are still working with model of small polaron, where all inter-molecular

Note, that electron-phonon term is absent from this equation, since we are calculating reorganization energy between equal sites. Thus, the terms for both sites are same in absolute value, but opposite in signs and annul each other<sup>2</sup>.

Eq. 2.12 contains also the electronic coupling term  $t$ . This can be calculated by *Corresponding Orbital Transformation Method* (King *et al.*, 1967). However, since modeled molecules are too large, we had to use approximative method:

$$t \approx (E_{HOMO} - E_{HOMO-1})/2, \quad (6.4)$$

where  $E_{HOMO}$  and  $E_{HOMO-1}$  are energies of HOMO and HOMO-1 orbital, respectively. These two highest occupied orbitals are levels on which the charge carrier transport occurs. Their energies were taken from the *neutral* structures.

### 6.3.1 Hole mobility

Our model of the intra-molecular charge carrier transfer anticipates, that movement occurs in the form of jumps between two conjugated subchains of the same polymer chain. Thus, length of the these subparts is essential variable for the calculation of the overall mobility. Using the different modeled lengths of the PMPSi and PBMSi, we were able to acquire the dependence of the HOMO/HOMO-1 split energy,  $\lambda$  and jumping distance  $L$  on the length of the conjugated subchain. When all these variables are known, they can be used for estimation of the hole mobility on the chain according to following equations (in detail described in section 2.1.3)

$$D = \frac{L^2 k_{et}}{2} \quad (6.5)$$

$$\mu = \frac{eD}{k_B T} \quad (6.6)$$

For the purposes of the transport over the single chain, it was calculated as geometrical distance of the first and last Si atom in the conjugated subchain, plus half of the average Si-Si bond length. Dependence of the hole mobility

---

effects are neglected. In general, they will also play role and can affect reorganization energy significantly. Solution of this problem is still great challenge, but (Lemaire *et al.*, 2005) estimated value of the external reorganization energy  $\lambda_e$  in range of 0.2-0.6 eV

<sup>2</sup>This is because, the term is governed by difference between the vibration frequencies of reactants and products. Since, both sites are identical, roles of the reactants and products are exchanged for source site and target site of the charge carrier.

on the conjugation length, according to the Eq. 6.6, is shown in the Fig. 6.18. Data in the plots are calculated with approximate value of electron coupling (see Eq. 6.4), thus resulting values are in arbitrary units and in absolute value strongly depend on the chosen method. However, they are almost independent of the utilized basis set (compare Fig. 6.18(a) and 6.18(b); or 6.18(c) and 6.18(d)).

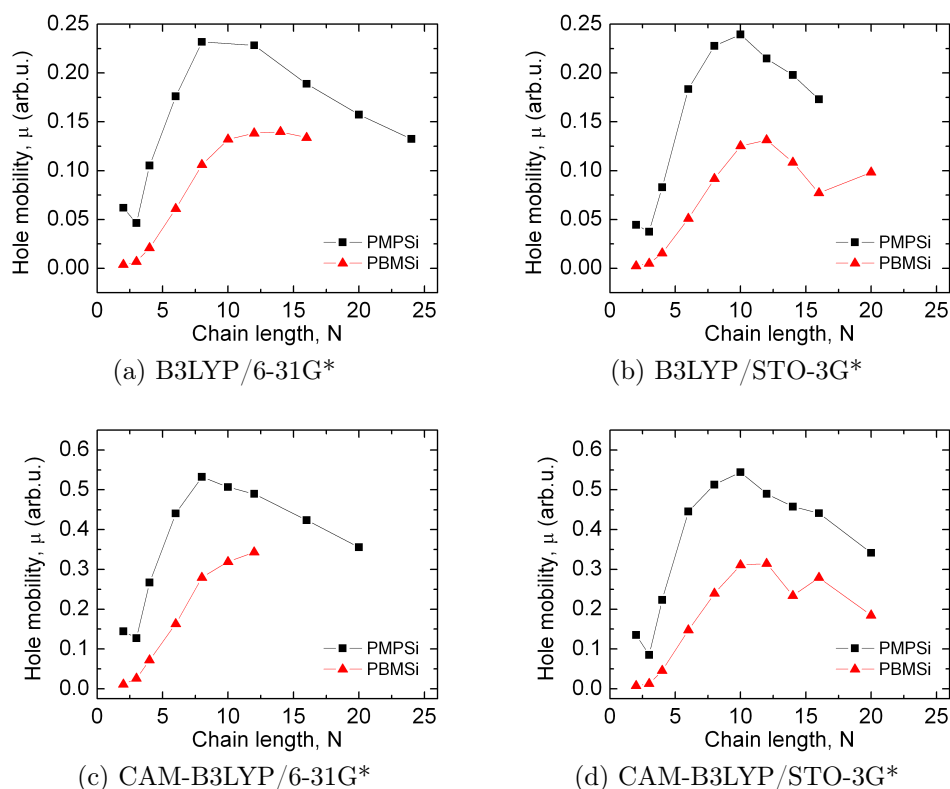


Figure 6.18: Dependence of the hole mobility on the conjugation length (i.e. polaron length) for different levels of theory. Results for PMPSi (■) and PBMSi (△)

One can see that on all levels of theory and any calculated chain length, mobility of the hole over the polymer chain is greater in the PMPSi than in the PBMSi. In general, ratio between mobility at the PBMSi and PMPSi chain is very low for short chains. As the chain length grows, the ratio increases to about 60-70% and then it drops again. The break point of the plot is at about 12-16 monomer units in the chain. Actual plot is shown in the Fig. 6.19 and comparison of the values for all levels of theory is given in the Tab. 6.7.



Table 6.7: Comparison of the hole mobility in the PMPSi and PBMSi. Values are given as average ratio (over the chain lengths equal or greater the 8 monomer units). Level of theory numbers have following meaning: (1) B3LYP/6-31G\*, (2) B3LYP/STO-3G\*, (3) CAM-B3LYP/6-31G\* and (4) CAM-B3LYP/STO-3G\*

| Average                   | (1) | (2) | (3) | (4) |
|---------------------------|-----|-----|-----|-----|
| $\mu_{PBMSi}/\mu_{PMPSi}$ | 53% | 47% | 57% | 53% |

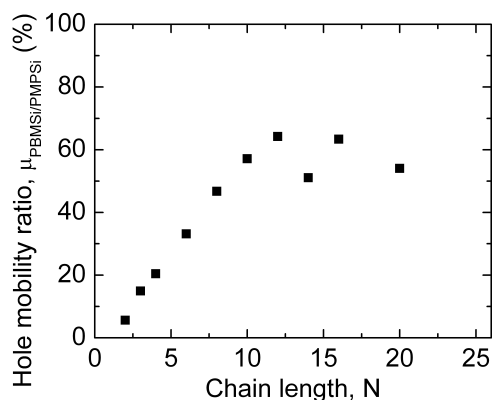


Figure 6.19: Dependence of the ratio between hole mobility in the PBMSi and PMPSi chain on the chain length. Calculated at the CAM-B3LYP/STO-3G\* level of theory (similar plots are valid for all the other methods and basis set combinations).

### 6.3.2 Summary and discussion

As shown in this section, absolute value of the intra-chain hole mobility and ratio between PBMSi and PMPSi is strongly dependent on the jump distance. According to the previous section 6.2, the polaron length, and thus the jumping distance, is about 19 monomer units for the PMPSi chain and 22 monomer units for the PBMSi chain. Values in the Tab. 6.7 indicate that at these lengths, the hole mobility in the PBMSi is approximately half of the PMPSi value. In fact, experimental results confirms this result. (Nespurek *et al.*, 2000) measured hole mobility in PMPSi with time-resolved microwave conductivity method and recorded values of  $2 \times 10^{-2} \text{ cm}^2/Vs$  (for PBMSi such value is not available).

Since the approximate value of the electron coupling was used in the calculations, the results cannot be used for direct estimation of the theoretical

absolute value of the intra-chain hole mobility. However, (Němec *et al.*, 2010) calculated the electron coupling for PMPSi 20 mer by *Corresponding Orbital Transformation Method* and estimated  $\mu$  as  $3 \times 10^{-3} \text{ cm}^2/Vs$ . When interpreting this value, one has to keep in mind, that polaron delocalization length is value, which is not estimated with high precision and the hole mobility is strongly dependent on it. When the value is altered to 16-monomer units, the resulting mobility is  $3.7 \times 10^{-2} \text{ cm}^2/Vs$ , which is in good agreement with experimental results.

The difference between intra-chain mobilities must originate in HOMO/HOMO-1 split value and reorganization energy, since jumping distance is essentially the same for both molecules. Indeed, in both cases, the values for PBMSi are lower than for PMPSi as can be seen in Fig. 6.20. The reorganization energy of both molecules converge to each other (see Fig. 6.20(b)), similarly as the polaron energy (see section 6.1). On the other hand, HOMO/HOMO-1 split dependence is more complicated (see Fig. 6.20(a)) with maximum at chain length of about 6-8 monomer units. Then, with increasing chain length, the value drops but difference between both molecules is approximately constant. At length of 14-16 monomer units is the relative difference smallest and thus ratio of hole mobility  $\mu_{PBMSi}/\mu_{PMPSi}$  greatest.

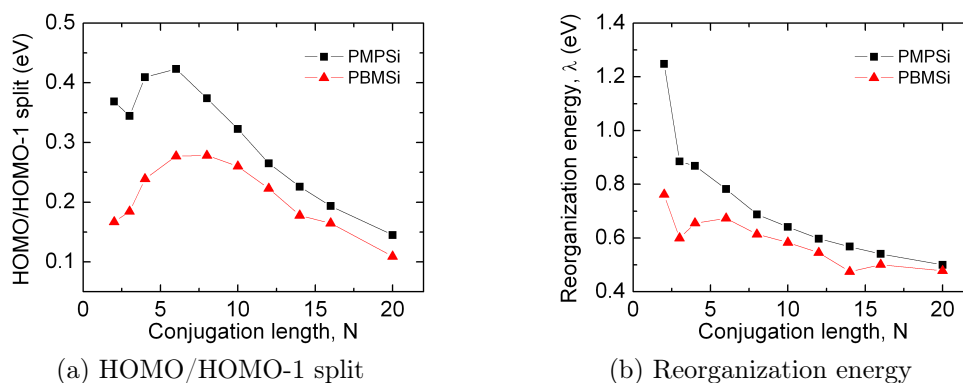


Figure 6.20: Comparison of terms which influence the final value of the intra-chain hole mobility. Results for PMPSi (■) and PBMSi (△) were obtained at the CAM-B3LYP/STO-3G\* level of theory (similar plots are valid for the other levels of theory).

## 6.4 Polysilanes degradation

Experimentally, the charge carriers in material are often generated by light. In this case electron-hole pairs are produced. The pairs can be dissociated by electric field and free charges are formed. In P-type material, the electrons are usually localized and only holes move through the material. In the case of PMPSi, electrons are localized on phenyl groups and “quasi-stable” electron-hole pair is formed; experimentally determined life-time is about 40  $\mu\text{s}$ . During this time the hole (cation-radical) on the main chain is movable. The electron can act in two ways: (1) transfer back to the main chain (in this case the electron deficit is compensated which leads to the chain stability) or (2) electron can be transferred to electron acceptor additive, which leads to the chain scission.

This section contains outcomes of our research in the field of polysilylenes degradation. The results will be presented mostly from the theoretical point of view, however, where possible, comparison with experimental measurements will be provided.

Experimental degradation was induced by UV-illumination of liquid samples. PMPSi was dissolved either in tetrahydrofuran (THF) or in toluene for the experiments with additive 1,4-dicyanobenzene (denoted as DKP in further text, Fig. 5.16(a)) and dibenzoyl peroxide (denoted as DBP in further text, Fig. 5.16(b)), respectively. The solutions (concentration of 10  $\text{g l}^{-1}$ ) were prepared under intensive shaking for at least 30 min. Then the solution of the additive was added (the concentrations of 3 mol% for the additive DKP and 8 mol% for DBP per MPSi monomer unit).

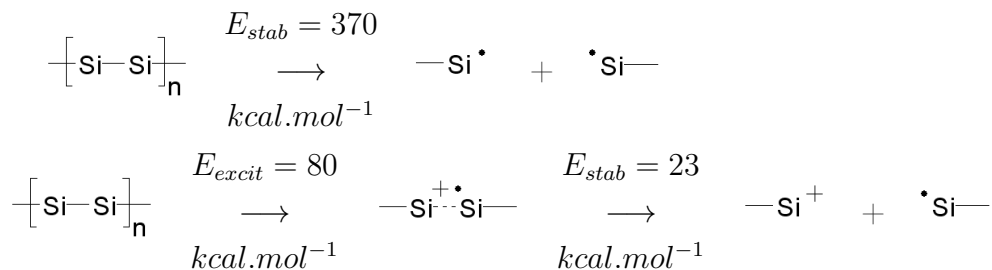
Absorption spectra were measured by UV-VIS spectrophotometer Perkin Elmer LAMBDA 950. Photodegradation was performed by 200W Hg-Xe arc discharge lamp (Hamamatsu LC6) with interference filter 365 nm (Melles Griot EDC 03 FIM 028). The samples were illuminated at room temperature on air; light power on the sample was 80  $\text{mW cm}^{-2}$ . Absorption spectra were measured immediately after the UV illumination.

Theoretical introduction to the degradation process was given in the section 2.3, where basic model for electron transfer from the polymer to the additive electron acceptor molecule was presented. Scheme 2.8 shows photo-physical processes which take place from the moment of the photon absorption up to the point when electron is transferred to an additive. Once the electron is localized on the additive molecule, two pathways are possible. Both are shown in Fig. 6.21. Each of the branches represents one of the models which were taken into account in this thesis.

**Model 1** Anticipates that the electron localizes itself on the additive molecule for sufficient time. Silicon chain is weakened by missing electron during this period and can more easily undergo scission. After some time electron thermalizes back to the polymer chain; i.e. *back-electron transfer* occurs.

**Model 2** The anion-radical of the additive molecule is not stable. It breaks down into an anion and radical particle and fast *back-electron transfer* is impossible; thus there is more time for Si-Si bond scission. At this point a nucleophilic attack may be important from the point of view of energy balance (Kani *et al.*, 1998).

Neat PMPSi decomposes under the UV-illumination. However, this decomposition is probably not spontaneous. Two evidence were recorded for this theory. First, the decomposition of the PMPSi molecule from the ground state is energetically unfavorable. When molecule is brought to the excited state, its stability is substantially lower but still fair amount of energy is needed in order to break down the silicon bond. Energetics of decomposition can be seen from the following reactions (values of stabilization energies were obtained from calculations at the B3LYP/6-31G\* level of theory, for MPSi-4-mer).



Homolitical scission of the Si-Si bond requires as much as 370 kcal mol<sup>-1</sup> of energy. However, breaking down a silicon bond in a polymer chain which is already one electron short (i.e. is in the cation-radical state, which can be accomplished by optical excitation of the main chain; 80 kcal mol<sup>-1</sup>) requires only 23 kcal mol<sup>-1</sup>. Hence, decomposition of the chain is more probable if the electron is transferred from silicon main chain to phenyl side group or even to an electron acceptor additive molecule. Anyway, one can see, that breakage of weakened bond of cation-radical still requires additional energy.

Second, energy balance results lead us to believe, that degradation of the silicon bond is more complex process, then just simple homo- or heterolytic scission. Therefore, we ran degradation experiment on the neat PMPSi so-

lution, which was additionally bubbled with nitrogen, in order to decrease number of contamination molecules from air. The results were compared to the degradation pace of non-bubbled neat PMPSi: as expected, the rate of degradation was lower in absence of the air additives (details of experimental results can be found in (Kochalska *et al.*, 2010)).

For given reasons, it is anticipated, that by addition of a strong electron additive to the polymer, one can increase the degradation rate.



### 6.4.1 Model 1

The DKP additive, which behaves as electron acceptor in respect to PMPSi chain, was selected for the demonstration of the model 1. Calculations suggest that an electron from the anti-bonding state can be transferred to the additive since LUMO orbital of the system in the ground state, and HOMO orbital of the system in the excited state are localized on the additive molecule (see Fig. 6.22).

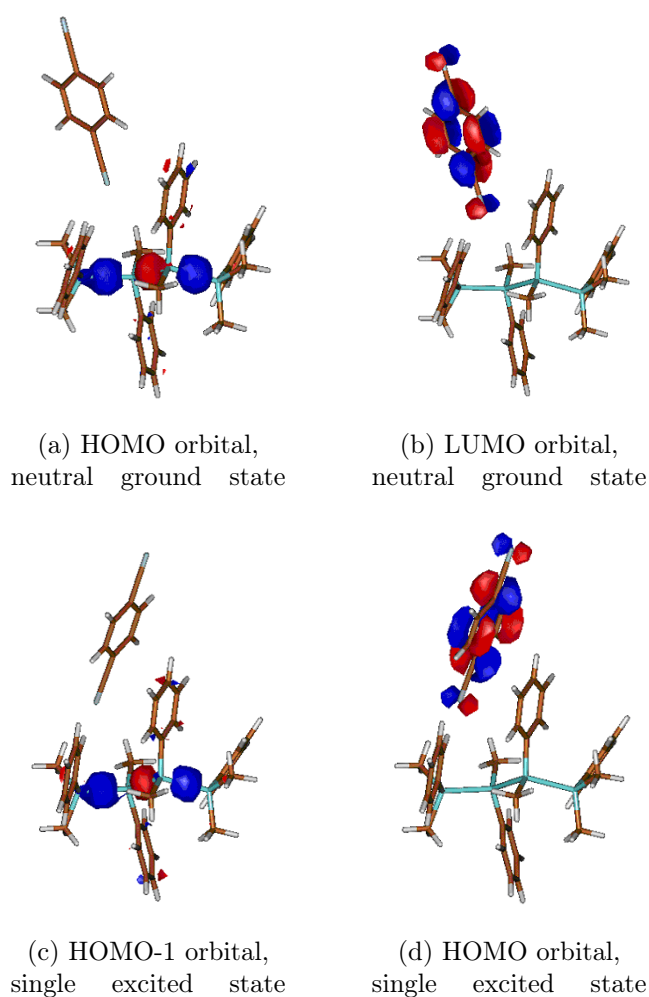
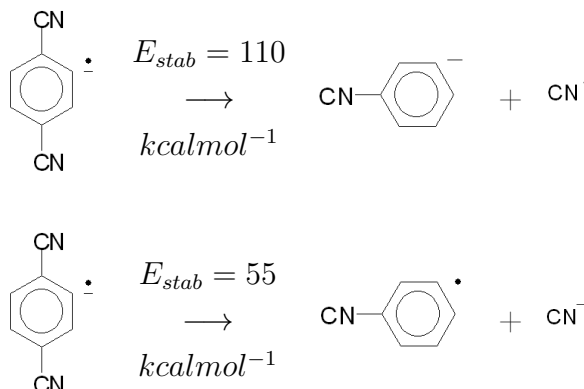


Figure 6.22: Important orbitals of optimized structure MPSi-4-mer and DKP (B3LYP/6-31G\*).

From following reactions, one can see, that the dissociation of the additive molecule is an endo-energetic process. Thus, it is not probable it would undergo the bond scission spontaneously. Therefore, only the *Model 1* can

be applied to it. Fig. 6.23 shows actual non-relaxed PES scans of separation of the CN group. The system is stable both in the neutral and anion-radical state.



Experimental results show that this additive has no effect on the rate of the decomposition (Kochalska *et al.*, 2010). It is expected to be due to the fast back-electron transfer from the additive to the PMPSi chain.

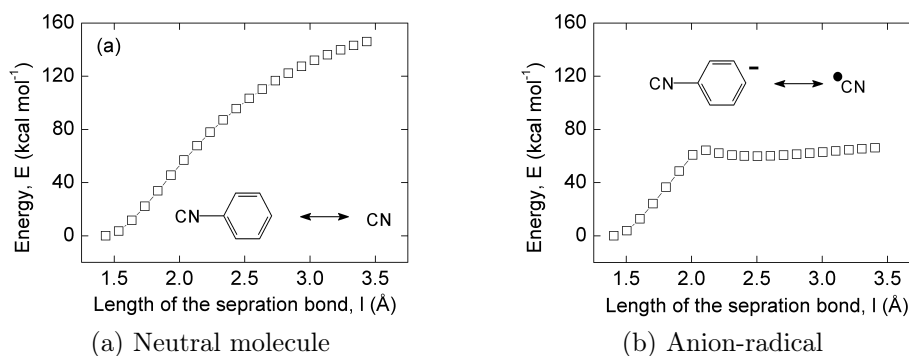


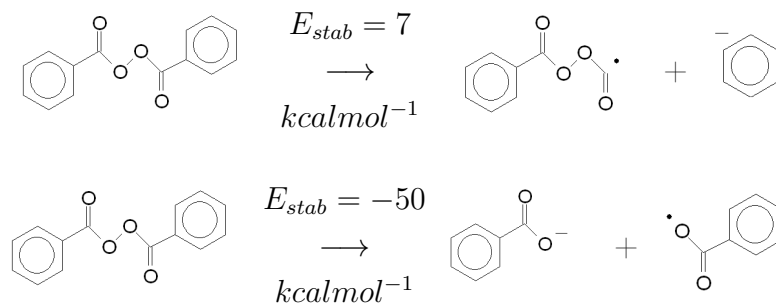
Figure 6.23: Non-relaxed PES scans of separation of the CN group from the phenyl for dikyanophenyl. First point in both graphs represents optimized bond length.

## 6.4.2 Model 2

The DBP additive was selected, for the demonstration of the *Model 2*. This molecule contains peroxide bond, which was expected to be unstable in the anion radical state. Decomposition of the peroxide (O–O) bond (see following reaction schemes) is exo-energetic process in the anion-radical state.



Note, that the scission of the (C–CO) bond does not lead to a system with lower energy. From these results we assume, that breakage of this additive is probable.



Non-relaxed PES scans of the scission of peroxide bond in the DBP additive are shown in Fig. 6.24. The peroxide bond is stable in the neutral system (see Fig. 6.24(a)), while in the presence of excess electron, the dissociation leads to energetically lower state. However, PES scan indicates that there is still some low potential barrier before bond breaks down (see Fig. 6.24(b)). In this case the results suggest that the additive molecule can form stable state in non-bonding distance of approximately 2.1 Å.

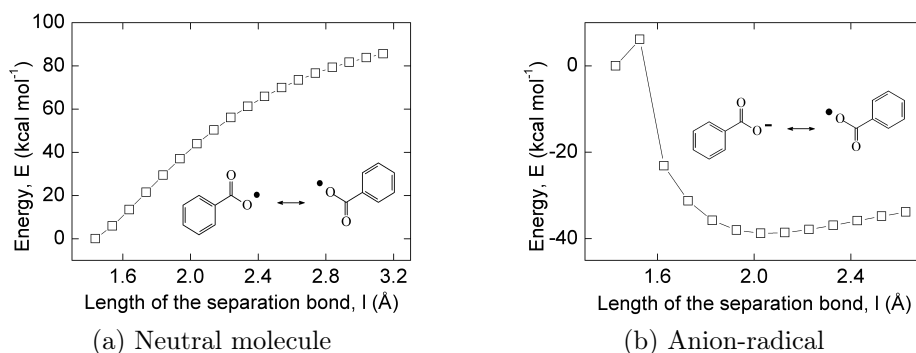
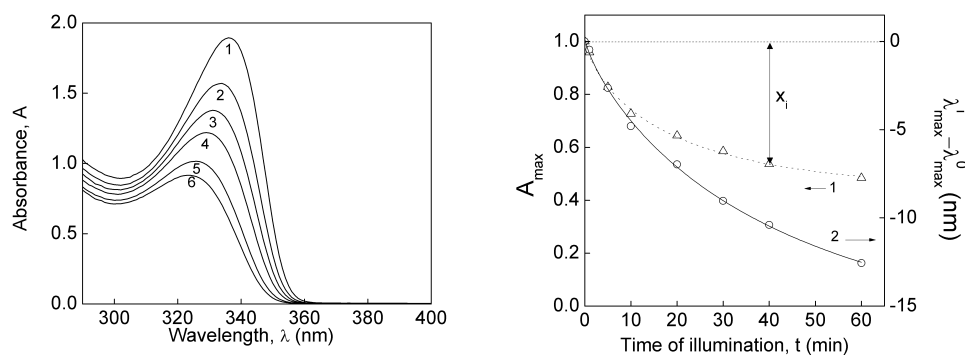


Figure 6.24: Non-relaxed PES scans of separation of the peroxide bond. First point in both graphs represents optimized bond length.

### 6.4.3 Experimental results

This subsection briefly presents experimental results acquired by our group. Detailed report can be found in published article (Kochalska *et al.*, 2010). Details about origins of the peaks in PMPSi UV-VIS spectra can be found in section 5.1.1.

The absorption maximum of the ( $\sigma$ - $\sigma^*$ ) band decreases and is shifted to higher energies during UV irradiation, i.e., bond scission of polysilane chain takes place. The example of absorption changes after UV illumination of neat PMPSi is shown in Fig. 6.25.



(a) Curve 1 – before the polymer degradation, curves 2, 3, 4, 5 and 6 – after 5, 10, 20, 40 and 60 min of UV illumination, respectively.

(b) PMPSi photodegradation detected by the blue shift (o) and decrease of the maximum of absorbance ( $\Delta$ ) during UV illumination.

Figure 6.25: Changes of UV-VIS spectra of PMPSi upon UV illumination.

Experimental results for both studied additives are summarized in Tab. 6.8 along with neat PMPSi. One can see, that DKP additive has no effect on the rate of photodegradation, since values of blue-shift and of the absorbance change are almost the same as for the neat PMPSi sample. However, when sample with admixture of DBP is exposed to the same dose of UV-radiation spectrum degrades significantly faster.

Table 6.8: Blue-shift of the absorption maximum  $\Delta\lambda$  and absorbance change  $x_i$  of the absorption maximum of PMPSi with different additives (in solution) after 40 min of UV illumination (reference to the degradation of neat PMPSi)

|                                | $\Delta\lambda$ | $x_i$ |
|--------------------------------|-----------------|-------|
| neat PMPSi                     | -10.4 nm        | -0.46 |
| PMPSi + $C_4H_4(CN)_2$ (DKP)   | -10.5 nm        | -0.45 |
| PMPSi + Benzoyl Peroxide (DBP) | -16.7 nm        | -0.60 |

### 6.4.4 Chain length after degradation

Degradation of the polymer was indicated by the decrease of the absorbance of the ( $\sigma$ - $\sigma^*$ ) band and by the wavelength shift (see Fig. 6.25). Both quantities were calculated by means of quantum chemistry in order to estimate approximate length of the polymer chain after the degradation process. To find the dependencies of these parameters on the length of the polymer a set of PMPSi molecules of different sizes were optimized and their UV-VIS spectra were calculated. Initial chain length of the experimental PMPSi samples was about 100 monomer units according to  $M_n$  from GPC measurements.

#### Absorbance change

Dependence of the oscillator strength of the ( $\sigma$ - $\sigma^*$ ) absorption band on the number of monomer units in chain is shown in Fig. 6.26. As expected, this dependence is linear, thus, it was fitted with equation:

$$I_n = I_0 + kn, \quad (6.7)$$

where  $I_n$  is the intensity of the transition of the chain composed of  $n$  monomer units,  $I_0$  is the intensity of the ( $\sigma$ - $\sigma^*$ ) transition of chain of theoretical zero length ( $I_0 = -0.375^3$ ),  $k$  is the slope ( $k = 0.175$ ) and  $n$  is the number of monomer units in the chain.

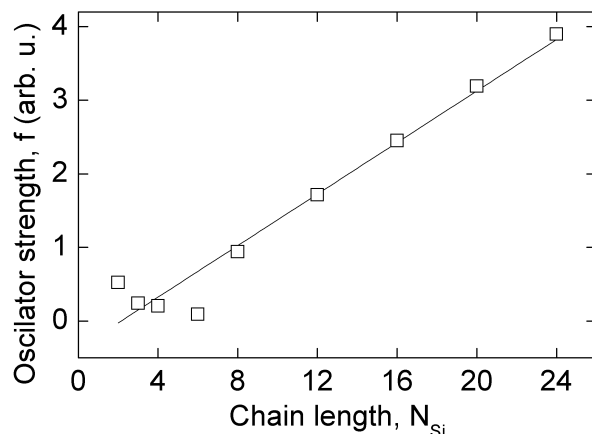


Figure 6.26: Theoretical dependence of the oscillator strength of ( $\sigma$ - $\sigma^*$ ) absorption band on the number of monomer units in PMPSi chain. B3LYP/6-31G\* level of theory.

<sup>3</sup>Fitted value should be zero if models were absolutely accurate. However, this result is sufficiently close.

Since the dependence is linear (and  $I_0$  is close to zero as it should be) we can easily estimate the length of the neat PMPSi chain after the decomposition. After 40 min of UV illumination the band intensity of neat PMPSi has dropped by about 46% in solution (see  $x_i$  value in Tab. 6.8). From the linearity we can assume that the polymer length decreased to 54 monomer units approximately after the illumination. By the same reasoning, for the mixture PMPSi–benzoyl peroxide (DBP) the average length of polymer chain decreases from 100 to 40 monomer units at the end of the experiment.

Note, that the reading of the  $\sigma\text{-}\sigma^*$  absorbance from the experimental spectrum (see Fig. 6.25 (a)) is not very accurate due to the overlapping of ( $\sigma\text{-}\sigma^*$ ) and ( $\pi\text{-}\pi^*$ ) bands. If this effect was eliminated, the drop would be larger<sup>4</sup>. Thus, the resulting chain would be shorter according to the calculations.

### Blue-shift

Calculated dependence of the wavelength shift of maximum of the ( $\sigma\text{-}\sigma^*$ ) band on the chain length is shown in the Fig. 6.27

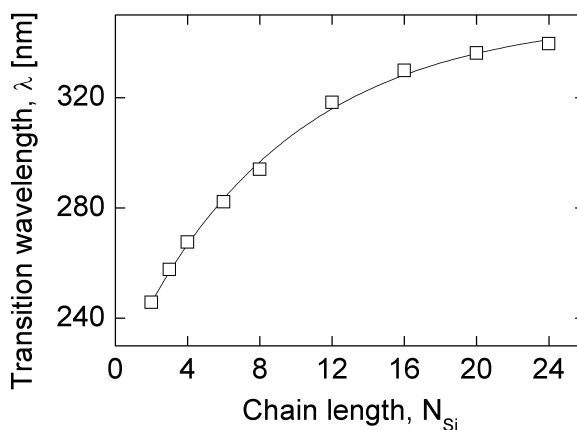


Figure 6.27: Theoretical dependence of the wavelength shift of maximum of the ( $\sigma\text{-}\sigma^*$ ) band on the number of monomer units in PMPSi chain. B3LYP/6-31G\* level of theory.

As the wavelength dependence possesses an asymptotic behavior it was fitted

---

<sup>4</sup> $\pi\text{-}\pi^*$  band absorption does not decrease with chain scission, since it originates in absorption of phenyl rings, which is not chain length dependent. It also affects reading of position of the absorption maxima, but not so significantly.

by the following function

$$\lambda_n = \lambda_\infty + kc^n, \quad (6.8)$$

where  $\lambda_n$  is the wavelength of the maximum of  $\sigma$ - $\sigma^*$  band of polymer consisting of length of  $n$  monomer units,  $\lambda_\infty$  is the wavelength of an ideal polymer of infinite length ( $\lambda_\infty = 349.8$  nm, experimental value yields 336 nm),  $n$  is the number of monomer units in the polymer chain and  $k$  and  $c$  are fitting parameters ( $k = -130.2$ ,  $c = 0.894$ ).

Since the fitted parameters were taken from the theoretical modeling, we cannot simply insert the experimental values into Eq. 6.8. This is due to the limitations of the basis and method of calculations and also due to the fact that the theoretical modeling is performed on ideal polymer chain (without deformations and free of interaction with the additive). However, we assume that determined theoretical dependence (Eq. 6.8) actually correctly describes the real behavior, except the value  $\lambda_\infty$  (vertical offset). Therefore, we eliminate this element by subtracting equation representing the final state (after illumination) from equation representing the initial state (note, that I assume the initial length of the polymer to be 100 monomer units).

$$\lambda_{100} - \lambda_n = kc^{100} - kc^n, \quad (6.9)$$

where  $\lambda_{100} = 336nm$  (see Fig. 6.25). After 40 min of UV illumination  $\lambda_n = 325nm$ . For neat PMPSi we obtained  $n = 22$  monomer units after the photodecomposition. For the mixture PMPSi – benzoyl peroxide (DBP) the length of polymer chain decreases from 100 to 18 monomer units at the end of the experiment.

### 6.4.5 Summary and Discussion

During the ( $\sigma$ - $\sigma^*$ ) excitations in PMPSi (the excitation of Si-Si bonding electrons), the electron is promoted from the bonding to an antibonding orbital. Thus, an electron-hole pair is formed. The electron transfer from the backbone to phenyl is quite probable because the ground state for optical transitions is predominantly  $\sigma_{Si-Si}$ , i.e. ionization potential  $I_p$  (Si-Si) <  $I_p$  (benzene). Then, electron can be transferred back to the main Si chain and recombine with positive polaron, or, if an acceptor additive is present, it can be transferred to the additive molecule, which will form anion-radical. If the anion-radical is not stable and decomposes, emerging nucleophilic anion can attack positively charged silicon chain and can cause bond scission – photodegradation of Si chain.

On the other hand, if additive is stable in the state of anion-radical and it allows fast back-electron transfer it could be used as stabilizer for polysilane electronic technology.

Results also support idea, that the decomposition of the polysilylenes is governed by accidental admixtures even in so-called neat samples. As polymers are never pure in inorganic sense, they will always contain chains of different lengths, leftovers of catalyzes or absorbed gases from the atmosphere. Some of these, probably, act as electron acceptors and can provide nucleophilic particles which can attack chain. As our experiment proved, PMPSi sample purified by bubbling with nitrogen has exhibited decreased degradation rate.

By calculating theoretical dependences of absorption intensity and position of the absorption maximum on the chain length, we were able to estimate approximate length of the polymer after the degradation. Dependence of absorbance suggests that final length was about 40 monomer units, while results from the blue-shift dependence gave 18 monomer units. Differences in absolute values from both dependencies origin in inability to read clearly the values from experimental spectrum. This is due to the fact, that readings of absorption changes are more affected by  $(\sigma-\sigma^*)$  and  $(\pi-\pi^*)$  band overlap than readings of the position of the absorption maximum.

Generally, electron transfer processes are also important in other physical processes. Transfer of an electron from donor to acceptor is utilized, e.g., in the processes of the preparation of oriented matrices for liquid crystal alignment and light emitting diodes. In the next chapter we will discuss the use of the electron transfer in acceptor gas ( $\text{NO}_2$ ) sensors. As model materials sulfonamide substituted phthalocyanines were chosen.

## 6.5 $\text{NO}_2$ sensors

Phthalocyanines are of great interest in many potential applications. As written in section 5.2, Pcs form a 1-dimensional quantum wire formed by self-organized stacking. Thus, they are candidates for the charge carrier transport on the molecular level as well as polysilylenes. However, in this thesis, we were not interested with this property of theirs directly, but rather in possibility to utilize it in manufacturing of gas sensors, specifically  $\text{NO}_2$  sensors.

Some of the results are supported by experimental measurements, which are in detail explained in phd thesis of Sergey Pochekailov (?). Theoretical results were achieved using method M05 (Zhao *et al.*, 2005) with basis set 6-31G\*.

### 6.5.1 Interaction with NO<sub>2</sub>

Two types of interactions between Pc and NO<sub>2</sub> are available. First, the interaction of the gas molecules with central atom of the Pc ring. Second, the interaction of gas molecules with substituents. We have found that the interaction directly with  $\pi$ -conjugated ring is very unprobable.

Complex of Pc and NO<sub>2</sub>, in which interaction runs through the sulfonamide group, does not show significant energetic minimum. Thus we assume that NO<sub>2</sub> tends to interact with Zn atom in case of ZnPcSu. There are two ways how NO<sub>2</sub> molecule can orient itself toward the central metal atom (Fig. 6.28):

1. Oxygen atom from NO<sub>2</sub> is the closest to zinc atom, thus forming coordinate bond Zn  $\cdots$  O=N=O (denoted as “Zn-O” complex in further text). The distance  $a$  between Zn and O is 1.97 Å.
2. Nitrogen atom from NO<sub>2</sub> is the closest to zinc atom, so the coordinate bond Zn  $\cdots$  NO<sub>2</sub> is formed (denoted as “Zn-N” complex in further text). The distance  $a$  between Zn and N is 2.03 Å.

In both cases, additive molecule disturbs planarity of the Pc skeleton and thus can disturb the stacking of the Pcs.

Quantum chemical calculations show, that both complexes are of similar nature and have similar properties. Electron density of HOMO level is shifted to NO<sub>2</sub> molecule, confirming the charge transfer complex (CTC) formation. Electrons in LUMO are delocalized on Pc and NO<sub>2</sub> molecules, forming common  $\pi$ -conjugated system (see Tab. 6.10 for orbital visualization). In practice, more than one molecule in the Pc stack can participate in the complex formation, thus, the electrical conductivity of the layer is expected to increase.

In order to answer the question, which complex is more probable to be formed, we have calculated the stabilization energies (see part 4.1.2 for computational details) for both systems (Tab. 6.9). After the correction with basis set superposition error (BSSE), one can see, that complex “Zn-N” has negative stabilization energy, thus, it is unlikely that it is formed. On the other hand, complex “Zn-O” seems to be stable with stabilization energy of 5.2 kcal/mol.

Obtained theoretical results are in good agreement with experimental observations. Theoretical absorption lines of the complex “Zn-O” were found in the same spectral region, where new experimental band appears, when Pc

---

<sup>5</sup>Full optimization with counterpoise option gave very similar results.

Table 6.9: Calculated stabilization energies for “Zn-O” and “Zn-N” complexes. M05/6-31G\* level of theory. Here  $E_{stab}$  is the stabilization energy of the complex;  $E_{stab}[BSSE]$  is the value of stabilization energy after BSSE correction<sup>5</sup>.

| Complex type | $E_{stab}$ (kcal/mol) | $E_{stab}[BSSE]$ (kcal/mol) |
|--------------|-----------------------|-----------------------------|
| Zn-O         | 12.6                  | 5.2                         |
| Zn-N         | 6.8                   | -0.6                        |

sample is exposed to NO<sub>2</sub> (Fig. 6.29(a)). At the same time, the oscillator strengths of the Pc absorption lines decreased.

Electrical properties follows the observations. Nitrogen dioxide causes the increase of the conductivity of ZnPcSu thin films by as much as two orders of magnitude (Fig. 6.30). This confirms the hypothesis about CTC formation. Apart from literature data, the response and recovery speed of this compound are much faster. Amplitude of the current rises promptly after the NO<sub>2</sub> exposure. Then, as soon as the supply of NO<sub>2</sub> is ceased, measured current drop follows immediately. This can be probably assigned to the fact that stabilization energy of “Zn-O” complex is close to energy of thermal vibrations (see Tab. 6.9). Thus, the complex diminishes as soon as NO<sub>2</sub> is not present in the air and released molecules are drafted away.

To further confirm the formation of the CTC, we have analysed charge distribution over the atoms in “Zn-O” complex. If it is formed, then electrons should be drawn to the NO<sub>2</sub> molecule from central part of ZnPcSu. Analysis shows that this is the fact as electron concentration increases on the NO<sub>2</sub> molecule and at the same time it decreases in the central part of the Pc as shown in Fig. 6.31. Values in the figure represent the change (in percents) of the partial charge upon complex formation. Positive value means that electrons were drawn to particular atom (thus partial charge on the atom decreased). As can be seen from the figure, whole central part of Pc loses electrons in favor of attached NO<sub>2</sub> molecule<sup>6</sup>.

Therefore, we suggest that NO<sub>2</sub> molecule, when present in the air, interpose itself in-between the Pc molecules in stack. There it forms a bridge for electron transfer between Pc molecules in the stack and increases the charge carriers concentration along it.

Simulation of H<sub>2</sub>PcSu interaction with NO<sub>2</sub> shows completely different mechanism. It appears, that no charge transfer complex is formed, but weak

<sup>6</sup>Sum of displayed numbers does not result in zero, since other atoms, which are not labeled, contribute to the transfer as well



van der Waals (NO<sub>2</sub> with the center) and hydrogen (NO<sub>2</sub> in the side-group) bonds take place (see Fig. 6.28). In the first case, the distance between Pc and NO<sub>2</sub> is 2.95 Å. In the second case, very probably the classical hydrogen bond is formed. The intermolecular distance between NO<sub>2</sub> and the substituent is 2.33 Å. The stabilization energies in both cases appear to be positive but very low (Tab. 6.11)

Delocalization of electrons is observed neither in the interaction with the center nor the side groups. Also, the planar geometry is not disturbed by NO<sub>2</sub> molecule attached to the core part of the Pc. Calculated absorption lines do not differ from the ones for pure phthalocyanine, which is in agreement with the data of optical gas sensing measurements (Fig. 6.29(b)). The electrical conductivity of such material should not significantly change, as it was found in experiments.

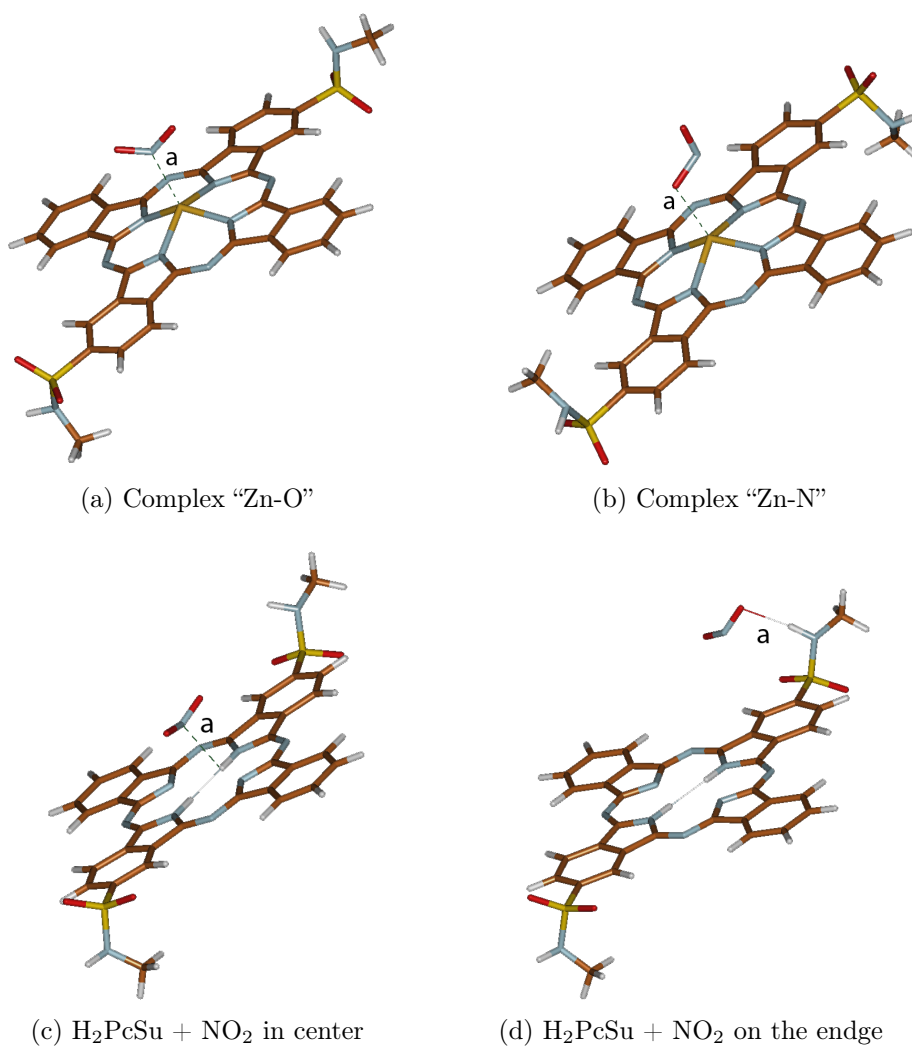
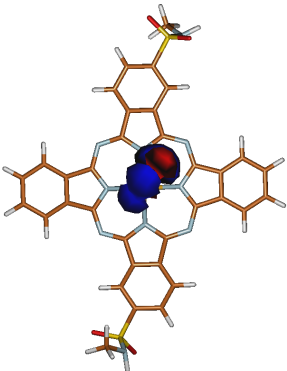
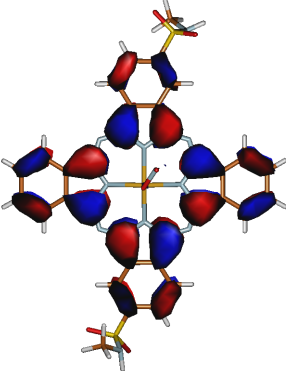
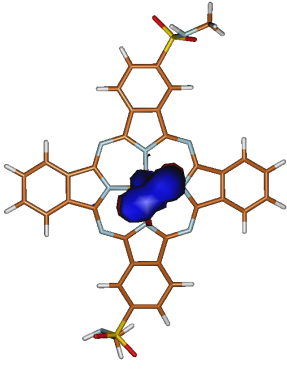
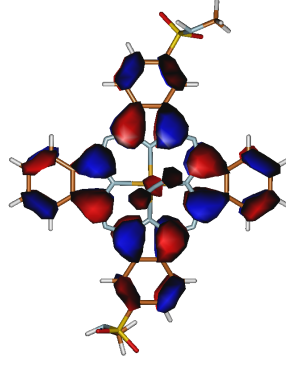
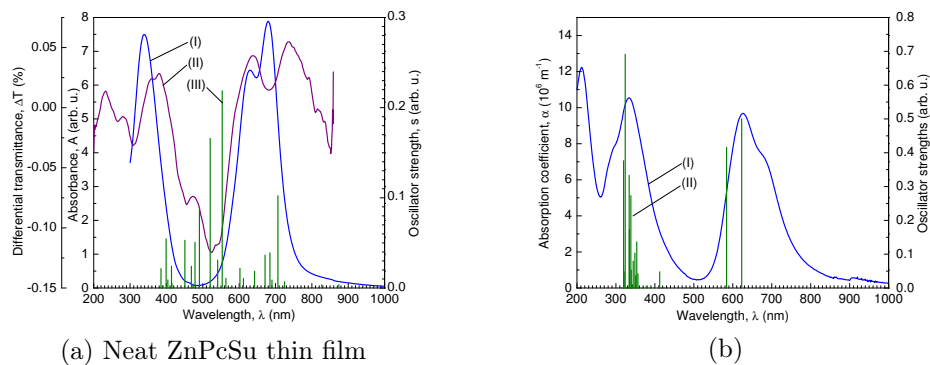


Figure 6.28: Complexes of Pc and  $\text{NO}_2$  molecule according to quantum chemical calculations. M05/6-31G\* level of theory.

Table 6.10: HOMO and LUMO orbitals of the ZnPcSu···NO<sub>2</sub> complex.

| Complex type | HOMO  | LUMO   |
|--------------|---|--|
| Zn-O         |    |    |
| Zn-N         |  |  |



(a) Neat ZnPcSu thin film  
 (I); differential transmittance spectrum measured in the presence of 2.5 ppm of  $\text{NO}_2$  (II); calculated absorption lines of “Zn-O” complex (III)

(b)  
 $\text{H}_2\text{PcSu}$  thin film (I) and calculated absorption for  $\text{H}_2\text{PcSu} \cdots \text{NO}_2$  structure adsorbed on the side-group (II).

Figure 6.29: Comparison of experimental and theoretical UVVIS spectra of Pc and  $\text{NO}_2$

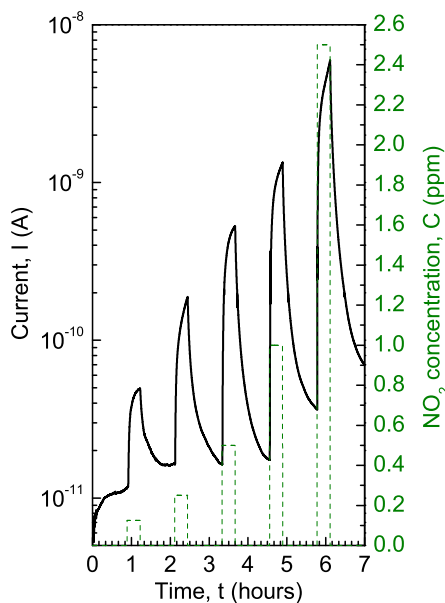


Figure 6.30: Influence of the certain concentration of nitrogen dioxide (green dashed line) on electrical conductivity of ZnPcSu (black solid line).

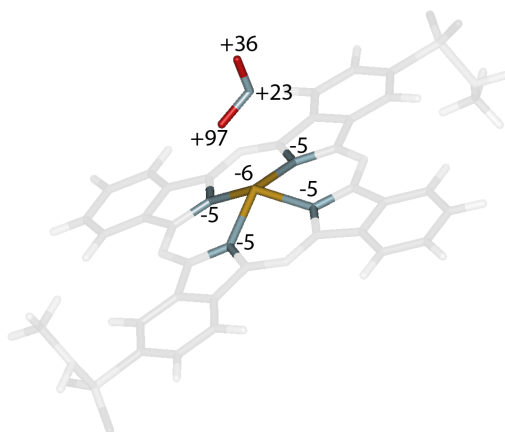


Figure 6.31: Central part of Pc and NO<sub>2</sub>. Numbers next to the atoms are charge differences (in percents) between charge on the atom when CTC is formed and when molecules are separated.

Table 6.11: Calculated stabilization energy of the systems H<sub>2</sub>PcSu···NO<sub>2</sub>. M05/6-31G\* level of theory. Here  $E_{stab}$  is the stabilization energy of the complex;  $E_{stab}$ [BSSE] is the value of energy after BSSE correction.

| Complex type | $E_{stab}$ (kcal/mol) | $E_{stab}$ [BSSE](kcal/mol) |
|--------------|-----------------------|-----------------------------|
| Center       | 3.6                   | 1.1                         |
| Edge         | 4.8                   | 2.7                         |

### 6.5.2 Summary and Discussion

Sulfonamide-substituted Zn phthalocyanine is optically and electrically sensitive to  $\text{NO}_2$ . Acquired results suggest that ZnPcSu forms charge transfer complex with  $\text{NO}_2$  with oxygen atom from gas molecule oriented to the zinc atom of the Pc. High electrical response to  $\text{NO}_2$  also confirms the conclusion on charge transfer complex formation as well as the theoretical modeling.

Metal-free sulfonamide-substituted phthalocyanines forms weak hydrogen bonds and van der Waals interactions between Pc and  $\text{NO}_2$ . Its sensing response is very small compared ZnPcSu.

# Summary and Outlook

In this thesis, I have used quantum chemical calculations to explore charge carrier transport in polymer molecules and utilization of charge carrier transport in the polysilane chain photodegradation and acceptor gas detection. As model systems polysilylenes PMPSi (poly[methyl(phenyl)silylene]) and PBMSi (poly[biphenyl(methyl)silylene]) and two phthalocyanines were selected. Both polymers are representatives of sigma conjugated chains and hole transport materials.

Results have shown, that charge carrier is indeed delocalized over the silicon main chain and creates self-consistent state - *polaron* quasiparticle. Aim of the first section of the results (section 6.1) was to evaluate depth of potential well created around the localized charge carrier. Calculations revealed that the polaron binding energy is for longer chains the same for both studied polymers (even though the PBMSi is much larger than PMPSi) and decreases with increasing chain length. However, for short chains the PMPSi polaron binding energy is greater. This result can be ascribed to the fact that during the polaron formation, biphenyl groups are deformed, which allows better redistribution of charge over the molecule and thus compensate for electron loss.

This observation can be used for designing molecules suitable for facile charge transport in electronic devices. The key is either in (1) ability to produce long molecules or (2) create molecules in which electrons can be easily redistributed. Thus, large conjugated side groups can act as suppliers of missing electron for the main chain. These can significantly reduce depth of trap in short chains or small molecules, which could connect near-by electronic devices.

The dependence of the polaron binding energy (as shown in section 6.1) on the chain length is very strong. Therefore, estimation of the actual polaron localization length is a parameter, which significantly affects absolute value of polaron binding energy and transport properties of given material. In order to estimate this property, *molecular dynamics* calculations were employed (see section 6.2). They revealed that actual localization length is about

19 monomer units for the PMPSi and 22 monomer units for the PBMSi. Irie *et.al.* (Irie & Irie, 1997) measured and Tachikawa (Tachikawa, 2007) modeled this parameter for poly(dimethylsilylene) and obtained the value of 16 monomer units. When these three results are put side by side, one can notice that the delocalization length increases with increasing size of the side group. This effect can be explained by greater steric hindering of the chain deformation. When formations of the chain are limited, then there is smaller possibility of emerging chain defects, which can limit the polaron delocalization.

Using the delocalization lengths, as calculated in section 6.2, I could estimate the polaron binding energy. For both model polymers we get approximately same value of about 0.23 eV (calculated for 20-mer).

The effect, when chain defects limits the polaron delocalization were modeled with the use of ideal polymer chain, 100 monomer units long. Results have shown that the introduction of even small imperfection can lead to significant shortening of conjugation length. Two defects are available: (1) defects which disturb conjugation, such as bond length increase, angle or dihedral angle increase. These lead to polaron localization on one of the sides of the defect. The other type (2) is imperfection which improves conjugation, such as bond length decrease, angle or dihedral angle decrease. These defects act as “magnets” for the polaron, which has tendency to be localized around them.

Since, later type (2) generates shorter polarons, it can more severely increase the polaron binding energy, and thus, hinder the transport more effectively. This kind of deformation is possible at locations where polymer chain creates sharp breaks, e.g. at the edge of micro crystalline regions. To minimize the influence of these defects, transport molecule should be stiff or contain large side groups.

Presented results confirmed that the charge carrier localizes itself on the chain. I anticipate that it is delocalized inside this conjugated region and moves according to band model. However, actual transfer over greater distances occurs via hopping model. To estimate intrachain mobility one needs to evaluate three parameters of the system: (1) polaron binding energy or reorganization energy (known from section 6.1), (2) jumping distance of the charge carrier, i.e. polaron localization length (known from results of section 6.2) and (3) electron coupling between neighboring sites (see section 6.3). All of these values were calculated and used for relative evaluation of the mobility of PMPSi and PBMSi. Results have shown that hole mobility of PBMSi is only 50% of that of PMPSi. The difference comes from the fact that values of the reorganization energy and electron coupling are smaller for PBMSi system.



Removal of an electron from the chain has also another effect, which needs to be taken into account, if polysilylenes should be used as conduction material in electronic devices. It causes weakening of the Si-Si bond which can result in chain scission and thus terminate the junction. Section 6.4 dealt with the rate of degradation and results indicated that silanes can be used in other aspects of electronic parts manufacturing; as photo-lithography resists. Theoretical and experimental data suggest that higher efficiency in the polymer degradation can be accomplished by usage of electron acceptors, which are unstable in the form of anion-radical. As additive decomposes, it produces anion and radical molecule, what has two side-effects: (1) back electron transfer is impossible and thus polymer chain cannot stabilize and is more susceptible to decomposition; and (2) emerged anion can attack positively charged silane chain and speed up the degradation.

Last section of results (6.5) investigated phthalocyanine molecules, which self assemble into 1-D stack. In this form, they can be used for gas sensing applications. As simulations and experiments revealed,  $\text{NO}_2$  molecule can significantly affect optical and electrical properties of a bulk sample. These changes can be of 2 orders of magnitude, which is sufficient for real industry applications in sensor applications.

As one can see, wide variety of properties of a single polymer chain have been explored in the chapters above. But in real applications, molecules are never isolated and always interact with its surroundings. Addition of such interactions would result in many new and practical problems and their exploration would be logical continuation of this work. Such themes would be: (a) intermolecular transfer in bulk samples; (b) interaction of polaron with additives (e.g. polar or dipolar molecules); (c) utilization of isomers for current switching; (d) interaction of polymers at interfaces; etc.

This thesis provided deep insight into charge carrier transport in model silane polymers, from theoretical point of view. Some of the results were also supported with indirect experimental methods, which measure molecular properties on bulk samples (such as TRMS method). However, contemporary experimental methods have evolved so much, that they allow direct measurement of some of the properties on single molecules (e.g. AFM conductivity measurements). It would be very interesting to confront theoretical and experimental results.



# References

- ACCELRY'S, INC. 2010. *Materials studio*. Accelrys, Inc., 10188 Telesis Court, Suite 100 San Diego, CA 92121 USA.
- ATKINS, P.W. 1994. *Physical Chemistry*. 5th ed. edn. Oxford University Press: Oxford, U.K.
- BALDINI, F., CAPOBIANCHI, A., FALAI, A., & PENNESI, G. 1998. A new sandwich-type dipthalocyanine as a potential optical transducer for NO<sub>2</sub> detection. *Sensors and Actuators B: Chemical*, **51**(1-3), 176 – 180.
- BECKE, A. D. 1988. Density-functional exchange-energy approximation with correct asymptotic behavior. *Phys. Rev. A*, **38**(6), 3098–3100.
- BECKE, AXEL D. 1992a. Density-functional thermochemistry. I. The effect of the exchange-only gradient correction. *Journal of Chemical Physics*, **96**, 2155–2161.
- BECKE, AXEL D. 1992b. Density-functional thermochemistry. II. The effect of the Perdew–Wang generalized-gradient correlation correction. *Journal of Chemical Physics*, **97**, 9173–9178.
- BECKE, AXEL D. 1993a. Density-functional thermochemistry. III. The role of exact exchange. *Journal of Chemical Physics*, **98**, 5648–5653.
- BECKE, AXEL D. 1993b. A new mixing of Hartree–Fock and local density-functional theories. *The Journal of Chemical Physics*, **98**(2), 1372–1377.
- BORTCHAGOVSKY, E. G., KAZANTSEVA, Z. I., KOSHETS, I. A., NE-SPUREK, S., & JASTRABIK, L. 2004. Optical properties of double-layer structure phthalocyanine-tetracyanoquinodimethane. *Thin Solid Films*, **460**(1-2), 269 – 273.

- BÄSSLER, H., BORSENERGER, P. M., & PERRY, R. J. 1994. Charge transport in poly(methylphenylsilane): The case for superimposed disorder and polaron effects. *Journal of Polymer Science Part B: Polymer Physics*, **32**, 1677 – 1685.
- CAPOBIANCHI, A., PAOLETTI, A. M., PENNESI, G., & ROSSI, G. 1998. Effect of nitrogen dioxide on titanium bisphthalocyaninato thin films. *Sensors and Actuators B: Chemical*, **48**(1-3), 333 – 338.
- FARAG, A. A.M. 2007. Optical absorption studies of copper phthalocyanine thin films. *Optics & Laser Technology*, **39**(4), 728 – 732.
- FERNANDES, A.N., & RICHARDSON, T.H. 2006. Characterisation and gas sensing properties of tert-butyl silicon-[bis ethyloxy]-phthalocyanine LB films. *Colloids and Surfaces A: Physicochemical and Engineering Aspects*, **284-285**, 335 – 338. A selection of papers from the 11th International Conference on Organized Molecular Films (LB11), June 26-30, 2005, Sapporo.
- FRISCH, M. J., TRUCKS, G. W., & SCHLEGEL, H. B. 2003. *Gaussian 03*. Gaussian, Inc., Pittsburgh PA.
- FRISCH, M. J., TRUCKS, G. W., & SCHLEGEL, H. B. 2009. *Gaussian 09*. Gaussian, Inc, Wallingford CT.
- HARRAH, L. A., & ZEIGLER, J. M. 1987. Electronic spectra of polysilanes. *Macromolecules*, **20**(3), 601–608.
- HAYASE, SHUZI. 2003. Polysilanes for semiconductor fabrication. *Progress in Polymer Science*, **28**(3), 359 – 381.
- HOFFMANN, ROALD. 1963. An Extended Huckel Theory. I. Hydrocarbons. *The Journal of Chemical Physics*, **39**(6), 1397–1412.
- HWANG, M. J., STOCKFISCH, T. P., & HAGLER, A. T. 1994. Derivation of Class II Force Fields. 2. Derivation and Characterization of a Class II Force Field, CFF93, for the Alkyl Functional Group and Alkane Molecules. *Journal of the American Chemical Society*, **116**(6), 2515–2525.
- IRIE, SETSUKO, & IRIE, MASAHIRO. 1997. Absorption Spectra of Radical Ions of Low Molecular Weight Poly(methyl-n-propylsilane)sChain Length Dependence. *Macromolecules*, **30**, 7906–7909.

- KANI, RIKAKO, NAKANO, YOSHIHIKO, YOSHIDA, HIROSHI, & HAYASE, SHUZI. 1998. Photosensitization of Base-Developable Poly(phenylhydrosilane) with 3,3',4,4'-Tetra(tert-butylperoxycarbonyl)benzophenone. Mechanism of the Drastic Photosensitization in Terms of Photoinduced Electron Transfer. *Macromolecules*, **31**, 8794–8801.
- KEPLER, R. G., ZEIGLER, J. M., HARRAH, L. A., & KURTZ, S. R. 1987. Photocarrier generation and transport in sigma-bonded polysilanes. *Phys. Rev. B*, **35**(6), 2818–2822.
- KING, HARRY F., STANTON, RICHARD E., KIM, HOJING, WYATT, ROBERT E., & G., PARR. ROBERT. 1967. Corresponding Orbitals and the Nonorthogonality Problem in Molecular Quantum Mechanics. *The Journal of Chemical Physics*, **47**(6), 1936–1941.
- KOCHALSKA, ANNA, NOŽÁR, JURAJ, NEŠPŮREK, STANISLAV, & PETER, JAKUB. 2010. Photodegradation of Poly[methyl(phenyl)silylene] in the Presence of Modifying Substances. *Macromolecular Symposia*, **295**, 71–76.
- KRICHELDORF, HANS RYTGER, KREUZER, F., BURGER, C., HERTLER, W. R., & KOCHS, P. 1996. *Silicon in Polymer Synthesis*. Springer-Verlag New York, LLC.
- KUBO, RYOGO. 1957. Statistical-Mechanical Theory of Irreversible Processes. I. General Theory and Simple Applications to Magnetic and Conduction Problems. *Journal of the Physical Society of Japan*, **12**(6), 570–586.
- KUMAR, G.A., THOMAS, J., GEORGE, N., KUMAR, B.A., RADHAKRISHNAN, P., NAMPOORI, V.P.N., VALLABHAN, C.P.G., & UNNIKRISHNAN, N.V. 2000. Optical absorption studies of free (H2Pc) and rare earth (RePc) phthalocyanine doped borate glasses. *Physics and Chemistry of Glasses*, **41**, 89–93.
- LEE, CHENGTEH, YANG, WEITAO, & PARR, ROBERT G. 1988. Development of the Colle-Salvetti correlation-energy formula into a functional of the electron density. *Phys. Rev. B*, **37**(2), 785–789.
- LEE, YUH-LANG, & CHANG, CHI-HSIU. 2006. NO<sub>2</sub> sensing characteristics of copper phthalocyanine films: Effects of low temperature annealing and doping time. *Sensors and Actuators B: Chemical*, **119**(1), 174 – 179.

- LEMAUR, VINCENT, STEEL, MICHELLE, BELJONNE, DAVID, BRÉDAS, JEAN-LUC, & CORNIL, JÉRÔME. 2005. Photoinduced Charge Generation and Recombination Dynamics in Model Donor/Acceptor Pairs for Organic Solar Cell Applications: A Full Quantum-Chemical Treatment. *Journal of the American Chemical Society*, **127**(16), 6077–6086. PMID: 15839709.
- LUJUN, PAN, MEI, ZHANG, & YOSHIKAZU, NAKAYAMA. 1999. Effect of residual solvent on carrier transport in polysilane. *J. Chem. Phys.*, **110**, 10509–10514.
- MAGGIONI, G., CARTURAN, S., TONEZZER, M., QUARANTA, A., & MEA, G. DELLA. 2008. Plasma-deposited copper phthalocyanine: A single gas-sensing material with multiple responses. *Sensors and Actuators B: Chemical*, **131**(2), 496 – 503.
- MAGGIONI, GIANLUIGI, CARTURAN, SARA, TONEZZER, MICHELE, BONAFINI, MARCO, VOMIERO, ALBERTO, QUARANTA, ALBERTO, MAURIZIO, CHIARA, GIANNICI, FRANCESCO, SCANDURRA, ANTONINO, D'ACAPITO, FRANCESCO, DELLA MEA, GIANANTONIO, & PUGLISI, ORAZIO. 2006. Effects of Heat Treatments on the Properties of Copper Phthalocyanine Films Deposited by Glow-Discharge-Induced Sublimation. *Chemistry of Materials*, **18**(17), 4195–4204.
- MAPLE, J. R., HWANG, M.-J., STOCKFISCH, T. P., DINUR, U., WALDMAN, M., EWIG, C. S., & HAGLER, A. T. 1994. Derivation of class II force fields. I. Methodology and quantum force field for the alkyl functional group and alkane molecules. *Journal of Computational Chemistry*, **15**, 162–182.
- MARCUS, RUDOLPH A. 1993. Electron transfer reactions in chemistry. Theory and experiment. *Rev. Mod. Phys.*, **65**(3), 599–610.
- MESZÁROŠ, O., SCHMIDT, P., POSPÍŠIL, J., & NEŠPŮREK, S. 2003. Phototriggered atmospheric degradation of poly[methyl(phenyl)silanediy] in the presence of ultraviolet absorbers. *Journal of Polymer Science Part A: Polymer Chemistry*, **42**, 714 – 721.
- MILLER, ROBERT D., & MICHL, JOSEF. 1989. Polysilane High Polymers. *Chem.Rev.*, **89**, 1359–1410. general article about polysilanes, their chemistry and physical properties. spectra, electrochemistry,...
- NAITO, HIROYOSHI. 2002. Photoinduced Metastable States in Amorphous Organic Polysilanes

- Studied by the Transient Photocurrent Technique. *Japanese Journal of Applied Physics*, **41**(Part 1, No. 9), 5523–5528.
- NAVRATIL, K, SIK, J, HUMLICEK, J, & NESPUREK, S. 1999. Optical properties of thin films of poly(methyl-phenylsilylene). *Optical Materials*, **12**(1), 105–113.
- NESPUREK, S, & ECKHARDT, A. 2001. Poly(silylene)s: Charge carrier photogeneration and transport. *Polymers for Advanced Technologies*, **12**, 427–440.
- NESPUREK, S., HERDEN, V., KUNST, M., & SCHNABEL, W. 2000. Microwave photoconductivity and polaron formation in poly[methyl(phenyl)silylene]. *Synthetic Metals*, **109**, 309–313.
- NESPUREK, S., VALERIAN, H., ECKHARDT, A., HERDEN, V., & SCHNABEL, W. 2001. Charge carrier transport in poly[methyl(phenyl)silylene]: the effect of additives. *Polymers for Advanced Technologies*, **12**, 306 – 318.
- NĚMEC, HYNEK, KRATOCHVÍLOVÁ, IRENA, ŠEBERA, JAKUB, KOCHALSKA, ANNA, NOŽÁR, JURAJ, & NEŠPŮREK, STANISLAV. 2010. Charge carrier mobility in poly[methyl(phenyl)silylene] studied by time-resolved terahertz spectroscopy and density functional theory. *Physical Chemistry Chemical Physics*.
- PERDEW, JOHN P. 1986. Density-functional approximation for the correlation energy of the inhomogeneous electron gas. *Phys. Rev. B*, **33**(12), 8822–8824.
- PERDEW, JOHN P., ERNZERHOF, MATTHIAS, & BURKE, KIERON. 1996. Rationale for mixing exact exchange with density functional approximations. *The Journal of Chemical Physics*, **105**(22), 9982–9985.
- RIGBY, DAVID, SUN, HUAI, & EICHINGER, B. E. 1997. Computer simulations of poly(ethylene oxide): force field, pvt diagram and cyclization behaviour. *Polymer International*, **44**, 311–330.
- SCHER, H., & LAX, M. 1973. Stochastic Transport in a Disordered Solid. I. Theory. *Phys. Rev. B*, **7**(10), 4491–4502.
- SHARMA, ASHA, KATIYAR, MONICA, DEEPAK, SHUKLA, SANJEEV K., & SEKI, SHU. 2007. Effect of ambient, excitation intensity and wavelength, and chemical structure on photodegradation in polysilanes. *Journal of Applied Physics*, **102**(10), 104902.

- SILINSH, E. A. 1980. *Organic Molecular Crystals: Their Electronic States*. Berlin: Springer-Verlag.
- SILINSH, E. A., & CAPEK, V. 1994. *Organic Molecular Crystals: Interaction, Localization, and Transport Phenomena*. N.Y: AIP Press.
- SKALA, LUBOMIR. 1994. *Kvantova teorie molekul*. Karolinum.
- STRAATSMA, T.P., APRA, E., WINDUS, T.L., BYLASKA, E.J., DE JONG, W., HIRATA, S., VALIEV, M., HACKLER, M., POLLACK, L., HARRISON, R., DUPUIS, M., SMITH, D.M.A, NIEPLOCHA, J., V., TIPPARAJU, KRISHNAN, M., AUER, A.A., BROWN, E., CISNEROS, G., FANN, G., FRÜCHTL, H., GARZA, J., HIRAO, K., KENDALL, R., NICHOLS, J., TSEMEKHMEN, K., WOLINSKI, K., ANCHELL, J., BERNHOLDT, D., BOROWSKI, P., CLARK, T., CLERC, D., DACHSEL, H., DEEGAN, M., DYALL, K., ELWOOD, D., GLENDENING, E., GUTOWSKI, M., HESS, A., JAFFE, J., JOHNSON, B., JU, J., KOBAYASHI, R., KUTTEH, R., LIN, Z., LITTLEFIELD, R., LONG, X., MENG, B., NAKAJIMA, T., NIU, S., ROSING, M., SANDRONE, G., STAVE, M., TAYLOR, H., THOMAS, G., VAN LENTHE, J., WONG, A., & ZHANG, Z. 2009. *NWChem, A Computational Chemistry Package for Parallel Computers*. 5.0 edn. Pacific Northwest National Laboratory, Richland, Washington 99352-0999, USA.
- SUN, H. 1998. COMPASS: An ab Initio Force-Field Optimized for Condensed-Phase Applications Overview with Details on Alkane and Benzene Compounds. *The Journal of Physical Chemistry B*, **102**(38), 7338–7364.
- SUN, H., REN, P., & FRIED, J. R. 1998. The COMPASS force field: parameterization and validation for phosphazenes. *Computational and Theoretical Polymer Science*, **8**(1-2), 229 – 246.
- SUN, HUAI, & RIGBY, DAVID. 1997. Polysiloxanes: ab initio force field and structural, conformational and thermophysical properties. *Spectrochimica Acta Part A: Molecular and Biomolecular Spectroscopy*, **53**(8), 1301 – 1323. Ab Initio and Ab Initio Derived Force Fields: State of the Science.
- SUN, HUAI, MUMBY, STEPHEN J., MAPLE, JON R., & HAGLER, ARNOLD T. 1994. An ab Initio CFF93 All-Atom Force Field for Polycarbonates. *Journal of the American Chemical Society*, **116**(7), 2978–2987.



- TACHIKAWA, HIROTO. 2007. Mechanism of Electron and Hole Localization in Poly(dimethylsilane) Radical Ions. *J. Phys. Chem. A*, **111**, 10134–10138.
- TAKEDA, KYOZABURO, SHIRAISHI, KENJI, FUJIKI, MICHIIYA, KONDO, MICHIO, & MORIGAKI, KAZUO. 1994. Photocreated metastable states in polysilanes. *Phys. Rev. B*, **50**(8), 5171–5179.
- TERAMAE, HIROYUKI, & TAKEDA, KYOZABURO. 1989. Ab initio studies on silicon compounds. Part II. The gauche structure of the parent polysilane. *J. Am. Chem. Soc.*, **111**, 1281–1285.
- TOMAN, P., NEŠPŮREK, S., JANG, J. W., & LEE, C. E. 2002. Conformation changes of polysilanes during the polaron formation. *Current Applied Physics*, **2**, 327–330.
- TOMAN, PETR. 2000. Quasiparticles in sigma-conjugated polymers. *Synthetic Metals*, **109**, 259–261.
- TOMAN, PETR, NEŠPŮREK, STANISLAV, WEITERM, MARTIN, VALA, MARTIN, SWORAKOWSKI, JULIUSZ, BARTKOWIAK, WOJCIECH, & MENŠÍK, MIROSLAV. 2006. Influence of dipolar species on charge transport in poly[2-methoxy-5-(2-ethylhexyloxy)-p-phenylene vinylene]. *Polymers for Advanced Technologies*, **17**, 673–678.
- TOMAN, PETR, NEŠPŮREK, STANISLAV, WEITER, MARTIN, VALA, MARTIN, SWORAKOWSKI, JULIUSZ, BARTKOWIAK, WOJCIECH, & MENŠÍK, MIROSLAV. 2009. Model of the influence of energetic disorder on inter-chain charge carrier mobility in poly[2-methoxy-5-(20-ethylhexyloxy)-p-phenylene vinylene]. *Polym. Adv. Technol.*, **20**, 263–267.
- VENKATARAMAN, LATHA, KLARE, JENNIFER E., NUCKOLLS, COLIN, HYBERTSEN, MARK S., & STEIGERWALD, MICHAEL L. 2006. Dependence of single-molecule junction conductance on molecular conformation. *Nature*, **442**, 904–907.
- WENG, SHOU-ZHENG, SHUKLA, PARITOSH, KUO, MING-YU, CHANG, YU-CHANG, SHEU, HWO-SHUENN, CHAO, ITO, & TAO, YU-TAI. 2009. Diazapentacene Derivatives as Thin-Film Transistor Materials: Morphology Control in Realizing High-Field-Effect Mobility. *App. Mater. Interfaces*, **1**, 2071–2079.

- WOITELLIER, S., LAUNAY, J. P., & JOACHIM, C. 1989. The possibility of molecular switching: Theoretical study of  $[(\text{NH}_3)_5\text{Ru}-4,4'\text{-bipy-Ru}(\text{NH}_3)_5]^{5+}$ . *Chemical Physics*, **131**, 481–488.
- YANAI, TAKESHI, TEW, DAVID P., & HANDY, NICHOLAS C. 2004. A new hybrid exchange–correlation functional using the Coulomb-attenuating method (CAM-B3LYP). *Chemical Physics Letters*, **393**, 51–57.
- ZHANG, XING-HUA, & WEST, ROBER. 1984. Organosilane polymers: Formable copolymers containing dimethylsilylene units. *Journal of Polymer Science: Polymer Chemistry Edition*, **22**, 159 – 170.
- ZHAO, YAN, SCHULTZ, NATHAN E., & TRUHLAR, D. G. 2005. Exchange-correlation functional with broad accuracy for metallic and nonmetallic compounds, kinetics, and noncovalent interactions. *The Journal of Chemical Physics*, **123**(16), 161103.

# List of Tables

|     |  |    |
|-----|--|----|
| 4.1 | Ideal parameters used for initial geometries of the MD calculations. . . . .   | 58 |
| 5.1 | Optimized parameters of <i>neutral</i> PMPSi. Values were obtained from optimized geometries of MPSi-16-mer, from its central part. . . . .  | 67 |
| 5.2 | Optimized parameters of <i>relaxed</i> PMPSi. Values were obtained from optimized geometries of MPSi-16-mer, from its central part. . . . .  | 67 |
| 5.3 | Data of experimental spectrum of PMPSi and theoretical spectra of MPSi-8-mer for basis sets 6-31G* and STO-3G* (method B3LYP). For both basis sets the <i>raw</i> calculated values are shown, from which the average scaling factor is calculated, which is then used to calculate values in column <i>scaled</i> . . . .                             | 68 |
| 5.4 | Optimized parameters of neutral PBMSi. Values were obtained from optimized geometries of BMSi-10-mer, of its central part. . . . .   | 76 |
| 5.5 | Optimized parameters of positive PBMSi. Values were obtained from optimized geometries of BMSi-10-mer, of its central part. . . . .  | 76 |
| 6.1 | Calculated values of the deformation energy, $E_{def}$ , of PMPSi oligomers of different lengths and for all employed levels of theory. Values marked as n/a were not calculated due to excessive computer requirements. Numbers have following meaning: (1) B3LYP/6-31G*, (2) B3LYP/STO-3G*, (3) CAM-B3LYP/6-31G* and (4) CAM-B3LYP/STO-3G* . . . . . | 87 |

|      |   |     |
|------|---|-----|
| 6.2  | Calculated values of the electron-phonon term, $E_{e-ph}$ , of PMPSi oligomers of different lengths and for all employed levels of theory. Values marked as n/a were not calculated. (1) B3LYP/6-31G*, (2) B3LYP/STO-3G*, (3) CAM-B3LYP/6-31G* and (4) CAM-B3LYP/STO-3G* . . . . .  | 88  |
| 6.3  | Calculated values of the deformation energy, $E_{def}$ , of PBMSi oligomers of different lengths and for all employed levels of theory. Values marked as n/a were not calculated due to excessive computer requirements. Numbers have following meaning: (1) B3LYP/6-31G*, (2) B3LYP/STO-3G*, (3) CAM-B3LYP/6-31G* and (4) CAM-B3LYP/STO-3G* . . . . .    | 91  |
| 6.4  | Calculated values of the electron-phonon term, $E_{e-ph}$ , of PBMSi oligomers of different lengths and for all employed levels of theory. Values marked as n/a were not calculated due to extensive computer requirements. Numbers have following meaning: (1) B3LYP/6-31G*, (2) B3LYP/STO-3G*, (3) CAM-B3LYP/6-31G* and (4) CAM-B3LYP/STO-3G* . . . . . | 92  |
| 6.5  | Ideal parameters used for demonstration of the impact of geometry nuances on the polaron delocalization length in PMPSi and PBMSi . . . . .   | 95  |
| 6.6  | FWHM of the distributions of silicon backbone properties. Values were obtained as average from 10 optimized geometries from MD trajectory. . . . .  | 104 |
| 6.7  | Comparison of the hole mobility in the PMPSi and PBMSi. Values are given as average ratio (over the chain lengths equal or greater the 8 monomer units). Level of theory numbers have following meaning: (1) B3LYP/6-31G*, (2) B3LYP/STO-3G*, (3) CAM-B3LYP/6-31G* and (4) CAM-B3LYP/STO-3G* . . . . .  | 107 |
| 6.8  | Blue-shift of the absorption maximum $\Delta\lambda$ and absorbance change $x_i$ of the absorption maximum of PMPSi with different additives (in solution) after 40 min of UV illumination (reference to the degradation of neat PMPSi) . . . . .   | 116 |
|      | 122table.caption.110  |     |
| 6.10 | HOMO and LUMO orbitals of the ZnPcSu $\cdots$ NO <sub>2</sub> complex. . . . .  | 125 |
| 6.11 | Calculated stabilization energy of the systems H <sub>2</sub> PcSu $\cdots$ NO <sub>2</sub> . M05/6-31G* level of theory. Here $E_{stab}$ is the stabilization energy of the complex; $E_{stab}[BSSE]$ is the value of energy after BSSE correction. . . . .  | 127 |

# Nomenclature

|                   |   |
|-------------------|---|
| $\Delta E_{e-ph}$ | Energy required to move cloud of vibronic variances from one site to another.                           |
| $\hbar$           | Reduced Planck constant. $\hbar = 6.62606810^{-34}m^2kg/s$  |
| $e^-$             | Denotes electron in figures.  |
| $E_p$             | Polaron binding energy  |
| $E_{def}$         | Energy difference between <i>hot</i> and <i>relaxed</i> state of a molecule                             |
| $E_{e-ph}$        | Electron-phonon coupling term   |
| $h^+$             | Denotes hole in figures. Empty electron state in the valence band after electron removal or excitation. |
| $k_B$             | Boltzmann constant. $k_B = 1.30810^{-23}JK^{-1}$  |
| AO                | Atomic orbital  |
| BSSE              | Basis-set superposition error   |
| CTC               | Charge-transfer complex   |
| DFT               | Density functional theory   |
| DOS               | Density of states   |
| e                 | Elementary charge, $e = 1.6021764610^{-19}C$  |
| EA                | Electron acceptor   |
| eV                | Electronvolt. Unit of energy. $1eV = 1.60217653(14)10^{-19}J$   |
| FF                | Force field - empirical fit of the potential energy surface for the nuclei motion                       |

|       |   |
|-------|---|
| GTO   | Gaussian type orbitals  |
| HOMO  | Highest occupied molecular orbital  |
| LCAO  | Linear combination of atomic orbitals   |
| LUMO  | Lowest unoccupied molecular orbital   |
| MM    | Molecular mechanics   |
| MO    | Molecular orbital   |
| MP    | Molecular polaron. Polaron model introduced by (Silinsh & Capek, 1994)                                  |
| PBMSi | Poly[biphenyl(methyl)silylene], sigma conjugated silylene polymer (see section 5.1.2 for details)       |
| Pcs   | Phthalocyanines   |
| PES   | Potential energy surface. Dependence of molecules energy on an atomic variable.                         |
| PMPSi | Poly[methyl(phenyl)silylene], sigma conjugated silylene polymer (see part 5.1.1 for details)            |
| SPE   | Single-point energy. Potential energy of a molecule for given arrangement of the atoms in the molecule. |
| STO   | Slater type orbitals  |

# List of publications and conference contributions

## List of publications in peer reviewed journals

1. S. Nešpůrek, A. Kochalska, J. Nožár, A. Kadashchuk, I. I. Fishchuk, J. Sworakowski, F. Kajzar; *Molecular Crystals and Liquid Crystals*; 2010, 521 (72-83), *Feature of Polaronic Charge Carriers in Polysilanes: Experimental and Theoretical Approach*
2. Kochalska, Anna; Nožár, Juraj; Nešpůrek, Stanislav; Peter, Jakub; *Macromolecular Symposia*; 2010, 295, (71-76), *Photodegradation of Poly [methyl(phenyl)silylene] in the Presence of Modifying Substances*
3. Němec, Hynek; Kratochvílová, Irena; Šebera, Jakub; Kochalska, Anna; Nožár, Juraj; Nešpůrek, Stanislav; *Physical Chemistry Chemical Physics*; 2010, *Charge carrier mobility in poly[methyl(phenyl)silylene] studied by time-resolved terahertz spectroscopy and density functional theory*
4. Pochekailov, Sergii; Nožár, Juraj; Nešpůrek, Stanislav; Rakušan, Jan; Karásková, Marie; *Sensors Actuators: B; Nitrogen dioxide sensor based on sulfonamide-substituted phthalocyanines: An optical detection and mechanism*(Submitted article)
5. Nožár, Juraj; Nešpůrek, Stanislav; Šebera, Jakub; *Journal of Molecular Modeling*; *Polaron binding energy in polymers: poly[methyl(phenyl)silylene]* (submitted article)
6. Nešpůrek, Stanislav; Nožár, Juraj; Šebera, Jakub; *Materials Research Innovations*; *Polaron Dynamics in Molecular Polysilane Wires* (submitted article)
7. Nešpůrek, Stanislav; Nožár, Juraj; Rais, David; Pochekaylov, Sergii; Šebera, Jakub; Kochalska, Anna; *Journal of Physics: Conference Series* 253; 210, 1-10, *Charge transfer in some physical processes*

## List of contributions at the international conferences

1. 4<sup>th</sup> Conference International Dielectric Society, 9<sup>th</sup> International Conference Dielectric and Related Phenomena, IDS & DRP 2006, September 3.-7., 2006, Poznan, Poland, Nešpůrek S., Nožár J., Toman P., Kadashchuk A., Fishchuk I.I., *Polarons in wide band-gap: polysilylenes*.
2. 14<sup>th</sup> International School on Condensated Matter Physics. Advances in the Micro and Nano Physics of Solid and Soft Matter. September 17.-22., 2006, Varna, Bulgaria. Nešpůrek S., Nožár J., Toman P., Menšík M., Kratochvílová I., Sworakovski J., *Charge carrier transport in molecular materials: From molecular wire to 3D systems*.
3. 15<sup>th</sup> International School on Condensed Matter Physics, Varna, Bulharsko, 31.8. - 5.9.2008, Institute of Solid State Physics - Bulgaria Academy of Sciences, Authors: Nešpůrek S., Toman P., Nožár J., Sworakowski J., *Optoelectronic processes in molecular wires and stacks: Model experiments and theoretical approach*
4. 73<sup>rd</sup> Prague Meeting on Macromolecules: New Frontiers in Macromolecular Science: From Macromolecular Concepts of Living Matter to Polymers for Better Quality of Life, Authors: Nožár J., Nešpůrek S., Prague, Czech rep., July 5 - 9, 2009, Institute of Macromolecular Chemistry, Academy of Sciences of the Czech Republic, *Polarons in Polymers, Determination its Dynamical Properties*
5. 3<sup>rd</sup> International Conference on Functional Materials and Devices (ICFMD), Authors: Nešpůrek S., Šebera J., Nožár J., Kochalska A., Kuala Terengganu, Malaysia, June 14-17, 2010, *Molecular polysilane wire*
6. 18<sup>th</sup> International Conference on Composites or Nano Engineering (ICCE-18), Authors: Nešpůrek S., Nožár J., Šebera J., Kochalska A., Anchorage, Alaska, USA, July 4-10, 2010, *Influence of dipolar additives on polar binding energy in polysilane composite*
7. 16<sup>th</sup> International School on Condensed Matter Physics: Progress in Solid State and Molecular Electronics, Ionics and Photonics, Authors: Nešpůrek S., Rais D., Nožár J., Šebera J., Kochalska A., Varna, Bulgaria, August 29-September 4, 2010, *Influence of charge transfer on photoorientation and photodegradation in polymers*



## List of oral lectures

1. Institute of Macromolecular Chemistry of Academy of Sciences, Czech Republic, Prague, 12.11.2006; *Creation of polarons in polymers*.
2. Week of Doctoral Students'07, Faculty of Mathematics and Physics, Charles University in Prague, Prague; 7.6.2005; *Polarons in polymers, estimating their dynamical properties*.
3. Institute of Macromolecular Chemistry of Academy of Sciences, Czech Republic, Prague, Kolokvium 2009, 16.2.2009; *Photodegradation of polysilane – theoretical modeling*.
4. Seminar of BIMORE Inter-Project Transfer of Knowledge Activities, Szklarska Poreba, Poland, February 22-24, 2009, Szklarska Poreba, Poland



# Chapter 7

## Appendices

This chapter contains support information and examples of input files for calculations.

### 7.1 Dynamic electron-phonon term

This term is derived from the perturbation theory for harmonic oscillator. In the moment of the charge carrier jump from one site to another, both sites undergo relaxation of opposite directions. The first one relaxes from the *relaxed* to *neutral* state (see part 4.1.3 for term explanations) and the second in the opposite way. This process of transfer between two molecules of the same kind can be described (for a single vibration mode):

$$\Delta E_0 + \Delta E_p = \frac{1}{2} \left( n_0 + \frac{1}{2} \right) \hbar \omega_0 \left[ \frac{\omega_p^2 - \omega_0^2}{\omega_0^2} \right] + \frac{1}{2} \left( n_p + \frac{1}{2} \right) \hbar \omega_p \left[ \frac{\omega_0^2 - \omega_p^2}{\omega_p^2} \right], \quad (7.1)$$

where  $\Delta E_0$  is energy change on the molecule onto which the charge carrier jumps,  $\Delta E_p$  is the energy change on the molecule from which the charge carrier jumps,  $\omega$  is the angular frequency of given vibration mode and  $n$  is the number of phonons in the given vibration mode, which can be calculated according to Eq. 7.2:

$$n = \frac{1}{\frac{\hbar \omega}{e k_B T} - 1}, \quad (7.2)$$

where  $k_B$  is the Boltzmann constant and  $T$  is absolute temperature. By simple rearranging Eq. 7.1 using expressions:

$$\omega_p^2 - \omega_0^2 = 2\omega_p\omega_0 - 2\omega_p\omega_0 + \omega_0^2 - \omega_0^2 + \omega_p^2 - \omega_0^2 \quad (7.3)$$

$$\omega_p^2 - 2\omega_p\omega_0 + \omega_0^2 = (\omega_p - \omega_0)^2 \quad (7.4)$$

$$\Delta\omega = \omega_p - \omega_0 \quad (7.5)$$

we get

$$\begin{aligned} \Delta E_0 + \Delta E_p &= \left(n_0 + \frac{1}{2}\right) \left[ \hbar\Delta\omega + \frac{(\Delta\omega)^2}{2\omega_0}\hbar \right] \\ &+ \left(n_p + \frac{1}{2}\right) \left[ -\hbar\Delta\omega + \frac{(\Delta\omega)^2}{2\omega_p}\hbar \right] \end{aligned} \quad (7.6)$$

or after further rearrangements

$$\begin{aligned} \Delta E_0 + \Delta E_p &= (n_0 - n_p)\hbar\Delta\omega \\ &+ \frac{1}{2} \left[ \left(n_0 + \frac{1}{2}\right) \hbar \frac{(\Delta\omega)^2}{\omega_0} + \left(n_p + \frac{1}{2}\right) \hbar \frac{(\Delta\omega)^2}{\omega_p} \right] \end{aligned} \quad (7.7)$$

High temperature approximation of this term can be obtained by expansion to Taylor series of the  $(n_0 - n_p)$  expression. Only first (its value is zero, see Eq. 7.10) and second member of the Taylor series are used.

$$n_0 - n_p = \frac{1}{\frac{\hbar\omega_0}{e^{k_B T}} - 1} - \frac{1}{\frac{\hbar\omega_p}{e^{k_B T}} - 1} = f(\omega_p) \quad (7.8)$$

$$f(\omega_p) = f(\omega_0) + \frac{f'(\omega_0)}{1!} \Delta\omega \quad (7.9)$$

$$f(\omega_0) = \frac{1}{\frac{\hbar\omega_0}{e^{k_B T}} - 1} - \frac{1}{\frac{\hbar\omega_0}{e^{k_B T}} - 1} = 0 \quad (7.10)$$

$$f'(\omega_p) = \left[ \frac{\left( \frac{\hbar\omega_p}{e^{k_B T}} - 1 \right) - \left( \frac{\hbar\omega_0}{e^{k_B T}} - 1 \right)}{\left( \frac{\hbar\omega_p}{e^{k_B T}} - 1 \right) \left( \frac{\hbar\omega_0}{e^{k_B T}} - 1 \right)} \right]' \quad (7.11)$$

$$f'(\omega_p) = \frac{\left(\frac{\hbar\omega_0}{e k_B T} - 1\right) \left[ \left(\frac{\hbar\omega_p}{e k_B T} - 1\right) - \left(\frac{\hbar\omega_p}{e k_B T} - \frac{\hbar\omega_0}{e k_B T}\right) \right] \frac{\hbar}{k_B T} e^{\frac{\hbar\omega_p}{k_B T}}}{\left[ \left(\frac{\hbar\omega_0}{e k_B T} - 1\right) \left(\frac{\hbar\omega_p}{e k_B T} - 1\right) \right]^2} \quad (7.12)$$

$$(n_0 - n_p) = f'(\omega_0)\Delta\omega = \frac{\frac{\hbar\omega_p}{e k_B T}}{\left(\frac{\hbar\omega_p}{e k_B T} - 1\right)^2} \frac{\hbar}{k_B T} \Delta\omega \quad (7.13)$$

High temperature approximation is valid when following condition is met (i.e.  $T \geq 200K$  for polysilylenes)

$$(\hbar\Delta\omega) \ll k_B T \quad (7.14)$$

Then following assumptions can be made

$$\frac{\omega_0}{\omega_p} \approx 1 \quad (7.15)$$

$$(n_0 + n_p)/2 \approx n_0 \quad (7.16)$$

Using Eq. 7.13 and utilizing assumptions 7.15 and 7.16, the Eq. 7.7 can be modified to final form

$$\Delta E_{e-ph} = \Delta E_0 + \Delta E_p = \frac{\frac{\hbar\omega_0}{e k_B T}}{\left(\frac{\hbar\omega_0}{e k_B T} - 1\right)^2} \frac{(\hbar\Delta\omega)^2}{k_B T} + \left(\frac{1}{e^{\frac{\hbar\omega_0}{k_B T}} - 1} + \frac{1}{2}\right) \hbar \frac{(\Delta\omega)^2}{\omega_0} \quad (7.17)$$

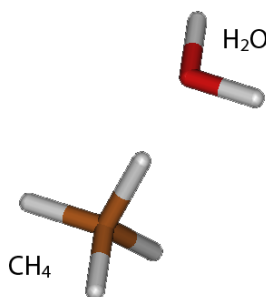


Figure 7.1: Illustrational dimer for electronic coupling calculations.

## 7.2 Electron coupling input file

Following example is an input file for NWChem 5.0 (Straatsma *et al.*, 2009), which calculates electronic coupling (see theory 2.1.3) between methane and water molecule (this system is selected as illustrative and does not have any meaning for the results in this thesis). Modeled complex is shown in Fig. 7.1.

File at first defines cartesian positions of atoms of the dimer  $\text{CH}_4 \cdots \text{H}_2\text{O}$  and coordinates of separate  $\text{CH}_4$  and  $\text{H}_2\text{O}$ <sup>1</sup>. Then basis set for each type of atom is selected. Afterwards, following calculation are stepwise performed:

1. Calculate MOs of  $\text{CH}_4$  in neutral state.
2. Calculate MOs of  $\text{CH}_4$  in cation state.
3. Calculate MOs of  $\text{H}_2\text{O}$  in neutral state.
4. Calculate MOs of  $\text{H}_2\text{O}$  in anion state.
5. Calculate MOs of dimer  $\text{CH}_4 \cdots \text{H}_2\text{O}$  (state before electron transfer; calculated from MOs from step 1. and 3.).
6. Calculate MOs of dimer  $\text{CH}_4^+ \cdots \text{H}_2\text{O}^-$  (state after electron transfer; calculated from MOs from step 2. and 4.).
7. Calculate electron transfer integral from MOs from step 5. and 6.

---

<sup>1</sup>Note, that actual positions in dimer and monomers are identical in absolute values. NWChem can estimate distance between monomers through this consistency, thus follow this rule. It is ideal to create the dimer structure, optimize it and then copy the cartesian coordinates from it and use them for the monomers unchanged.

```
#Input file for calculating electronic coupling for
#Methane-Water dimer in NWChem 5.0 program
```

```
echo
```

```
#maximum memory available for the process
memory 2500 mb
```

```
#cartesian coordinates of the dimer
geometry "ch4+h2o" units angstroms noautoz
symmetry c1
```

|   |           |           |           |
|---|-----------|-----------|-----------|
| C | 0.013537  | 0.054369  | 0.026269  |
| H | 0.104523  | 0.166648  | 1.108612  |
| H | 1.010274  | 0.054866  | -0.420358 |
| H | -0.562999 | 0.890620  | -0.376466 |
| H | -0.487401 | -0.890321 | -0.196439 |
| O | -1.626099 | -3.037033 | -0.702236 |
| H | -1.326366 | -2.750112 | -1.563606 |
| H | -2.427792 | -2.542818 | -0.564803 |

```
end
```

```
#cartesian coordinates of the monomers
geometry "ch4" units angstroms noautoz
symmetry c1
```

|   |           |           |           |
|---|-----------|-----------|-----------|
| C | 0.013537  | 0.054369  | 0.026269  |
| H | 0.104523  | 0.166648  | 1.108612  |
| H | 1.010274  | 0.054866  | -0.420358 |
| H | -0.562999 | 0.890620  | -0.376466 |
| H | -0.487401 | -0.890321 | -0.196439 |

```
end
```

```
geometry "h2o" units angstroms noautoz
symmetry c1
```

|   |           |           |           |
|---|-----------|-----------|-----------|
| O | -1.626099 | -3.037033 | -0.702236 |
| H | -1.326366 | -2.750112 | -1.563606 |
| H | -2.427792 | -2.542818 | -0.564803 |

```
end
```

```
#-----
#Basis sets used for each atom type
basis
c library 6-31G*
```

```
o library 6-31G*
h library 6-31G*
end

#-----
#calculate MOs for ch4 in neutral state
scf
maxiter 200
#convergence criterion
THRESH 1e-5
#CH4 in neutral state is singlet
SINGLET
UHF
#memory is given in 64-bit words (8bytes)
SEMIDIRECT filesize 60000000 memsize 100000000
#Calculated MOs will be stored in file named CH4n.movecs
vectors output CH4n.movecs
end

charge 0

property
mulliken
end

#set geometry which to use
set geometry "ch4"
task scf

#-----
#calculate MOs for ch4 in positive state
scf
maxiter 200
THRESH 1e-6
DOUBLET
UHF
SEMIDIRECT filesize 60000000 memsize 100000000
vectors output CH4+.movecs
end

charge 1
```



```
property
mulliken
end

#set geometry which to use
set geometry "ch4"
task scf

#-----
#calculate MOs for h2o in neutral state
scf
maxiter 200
THRESH 1e-5
SINGLET
UHF
SEMIDIRECT filesize 60000000 memsize 100000000
vectors output H2on.movecs
end

charge 0

property
mulliken
end

#set geometry to use
set geometry "h2o"
task scf

#-----
#calculate MOs for h2o in positive state
scf
maxiter 200
THRESH 1e-6
DOUBLET
UHF
SEMIDIRECT filesize 60000000 memsize 100000000
vectors output H2o-.movecs
end
```

```
charge -1

property
mulliken
end

#set geometry to use
set geometry "h2o"
task scf

#-----
#calculate MOs for ch4(neut) + h2o(neutral)
charge 0
scf
maxiter 500
THRESH 1e-5
SINGLET
UHF
SEMIDIRECT filesize 50000000 memsize 200000000
#MOs of the dimer in this state will be stored in file CH4n_H2on.movecs
vectors input fragment CH4n.movecs H2on.movecs output CH4n_H2on.movecs
end

property
mulliken
end

set geometry "ch4+h2o"
task scf

#-----
#calculate MOs for ch4(cation) + h2o(anion)
charge 0
scf
maxiter 500
THRESH 1e-5
TRIPLET
UHF
SEMIDIRECT filesize 50000000 memsize 200000000
vectors input fragment CH4+.movecs H2o-.movecs output CH4+_H2o-.movecs
end
```

```

property
mulliken
end

set geometry "ch4+h2o"
task scf

#-----
#calculate tranfer between molecules
et
#load MOs calculated in previous two steps and calculate electronic coupling
vectors reactants CH4n_H2on.movecs
vectors products CH4+_H2o-.movecs
end

property
mulliken
end

#calculate electron transfer from loaded MOs
task scf et

```

Output file of NWChem will contain resulting electron transfer coupling energy (i.e.  $t$  in Eq. 2.12 and 2.16) in the following format:

```

Electron Transfer Coupling Energy |V(RP)|  0.0869749581
                                           19088.794 cm-1
                                           2.366710 eV
                                           54.578 kcal/mol

```

## 7.3 Deformation energy input file

Example of an input which will calculate all values needed for estimation of the deformation energy  $E_{def}$  in one run for methane molecule.

```

%chk=deformationEnergy
%nproc=2
#P B3LYP/6-31G*
opt=(maxcycle=500)
nosymm

```

```
scf=(maxcycle=500, conver=7)
```

Example of an input file for Gaussian program package, which calculates all values needed for the deformation energy (for methan). This first job will optimize neutral geometry. Intermediate results are stored in checkpoint file "deformationEnergy.chk".

```
0 1
  C
  H  1.089
  H  1.089      109.0
  H  1.089      109.0      120.0
  H  1.089      109.0      120.0
```

```
--Link1--
%chk=deformationEnergy
#P B3LYP/6-31G*
SP
geom=checkpoint
```

This step will calculate single point energy of the optimized neutral geometry with charge = 1 and multiplicity = 2; i.e. energy of the hot state. Atom positions are read from the checkpoint file.

```
1 2

--Link1--
%chk=deformationEnergy
#P B3LYP/6-31G*
opt
nosymm
geom=checkpoint
scf=(maxcycle=500)
```

Optimization of the positively charged molecule. Atom positions are read from checkpoint file, thus initial geometry of optimization is the neutral geometry.

```
1 2
```

